A MID-INFRARED IMAGING SURVEY OF STAR FORMING REGIONS CONTAINING METHANOL AND WATER MASER EMISSION

By

JAMES MICHAEL DE BUIZER

A DISSERTATION PRESENTED TO THE GRADUATE SCHOOL
OF THE UNIVERSITY OF FLORIDA IN PARTIAL FULFILLMENT
OF THE REQUIREMENTS FOR THE DEGREE OF
DOCTOR OF PHILOSOPHY

UNIVERSITY OF FLORIDA

2000

To Mom, Dad, and Michele

ACKNOWLEDGMENTS

This dissertation is the fruit of three years of research during which many people have contributed, through their help, advice, or simply their friendship, to make this experience fulfilling and enjoyable. To these people I would like to express my gratitude.

First and foremost I would like to thank my advisor, Robert Piña, for his guidance and support throughout this whole project. I am most appreciative of his willingness to assist me no matter how busy he became. His knowledge and work ethic are only superceded by his enthusiasm, and I thank him for being a good role model as well as a great educator.

It has also been a pleasure to work with the Infrared Astrophysics Group. To this group I am eternally grateful, for without their unselfishness and dedicated work, none of the data presented in this dissertation would have been obtained. I would like to thank Charles Telesco for his support and knowledge, as well as for having enough confidence in my ability to make me an integral member of his observing and support staff. I would like to thank those generous members of the group that gave up personal telescope time so that I may collect data for my thesis project.

I would like to thank R. Scott Fisher and James "Rathgar" Radomski for their help in keeping me sane on those long observing runs. I value their friendship, advice, stimulating conversation, and childishness. It was a pleasure to share an office with them for three years, travel with them all over the world, and party with them in Hilo and Santiago.

I thank Jeff Julian and Kevin Hanna for keeping OSCIR purring, the secretarial staff of Carlon Ann Elton, Glenda Smith, Debra Hunter and Audrey Sims for being my mothers away from home, and fellow graduate students Veera Boonyasait and Sue Lederer for their friendship and advice.

Last but not least, I wish to thank my family and my friends outside of astronomy. I thank my parents and Michele Garnier for their love, support, and encouragement throughout my long ten year college career. I also thank Tom Kessler, Justin Winn, and Andy Kellenberger for their warm friendship.

This research was supported by the NASA Florida Space Grant Consortium grant NGT5-40025 and the University of Florida.

TABLE OF CONTENTS

page

ACKNOWLEDGMENTS iv

LIST OF TABLES x

LIST OF FIGURES xi

ABSTRACT xiv

CHAPTERS

1 MASSIVE STAR FORMATION 1

Why is the Study of Massive Stars Important? 1
Giant Molecular Clouds and Cloud Cores 2
Low and Intermediate Mass Star Formation 3
High Mass Star Formation 5
The Formation of HII Regions 8
HII Region Morphologies 10
Hot Molecular Clumps 13
Circumstellar Disks 13

2 BACKGROUND CONCEPTS IN PHYSICAL CHEMISTRY AND MASERS 15

Introduction to the Maser Phenomena 15
Hydroxyl Molecular Transitions 17
The Hydroxyl Maser 19
Water Molecular Transitions 20
The Water Maser 23
Methanol Molecular Transitions 23
The Methanol Maser 26

3 MOTIVATION AND FORMULATION OF THE DISSERTATION 27

Summary of Observations of Masers in Massive Star Forming Regions 27
Shock Fronts 28
Outflows 28
Circumstellar Disks 29
Embedded Sources 30

Pumping Considerations 31
Mid-Infrared Astronomy 32
A Case for the Present Work 35

4 DATA ACQUISITION AND REDUCTION 37

IRTF – Water Maser Observations 37
CTIO – Methanol Masers Observations 40
Data Reduction 42
Airmass Correction 42
Color Corrected Fluxes 43
Resolved sources 43
Unresolved sources with good S/N 44
Unresolved, low S/N sources 45
Luminosities 46
Sources Observed in Only One Filter 47
Visual Extinction, Bolometric Luminosity, and Spectral Types 47
Adopted Distances 48

5 METHANOL MASER SELECTED SURVEY 53

Individual Sources 54
G305.21+0.21 54
G305.20+0.21 55
G309.92+0.48 (IRAS 13471-6120) 57
G318.95-0.20 (IRAS 14567-5846) 60
G323.740-0.263 and G323.741-0.263 (IRAS 15278-5620) 62
G328.24-0.55 64
G328.25-0.53 65
G328.81+0.63 (IRAS 15520-5234) 67
G331.28-0.19 (IRAS 16076-5134) 70
G336.43-0.26 (IRAS 16306-4758) 73
G339.88-1.26 (IRAS 16484-4603) 73
G340.78-0.10 (IRAS 16465-4437) 76
G345.01+1.79 77
G345.01+1.80 79
G351.42+0.64 (NGC6334F and NGC6334F-NW) 81
G351.44+0.66 84
G351.77-0.54 (IRAS 17233-3606) 84
G9.621+0.196 and G9.619+0.193 (IRAS 18032-2032) 87
Results and Discussion 91
Summary of Mid-Infrared Sources Associated with Linearly Distributed Methanol Masers and the Circumstellar Disk Candidates 91
The Nature of Massive Stars Exhibiting Methanol Maser Emission 95
The Relationships between Mid-Infrared, IRAS and Radio Observations 101
Alternatives to the Disk Hypothesis 108

6 WATER MASER SELECTED SURVEY 111

Individual Sources 112
G00.38+0.04 (IRAS 17432-2835) 112
G00.55-0.85 (IRAS 17470-2853) 113
G10.62-0.38 (IRAS 18075-1956) 116
G12.68-0.18 119
G16.59-0.05 (IRAS 18182-1433) 121
G19.61-0.23 (IRAS 18248-1158) 122
G28.86+0.07 (IRAS 18411-0338) 125
G34.26+0.15 (IRAS 18507+0110) 126
G35.20-0.74 (IRAS 18556+0136) 129
G35.20-1.74 (IRAS 19592+0108) 133
G35.58-0.03 (IRAS 18538+0216) 135
G40.62-0.14 (IRAS 19035+0641) 137
G43.80-0.13 (IRAS 19095+0930) 138
G45.07+0.13 140
G45.47+0.05 142
G48.61+0.02 (IRAS 19181+1349) 145
G49.49-0.39 146
Results and Discussion 148
The Search for Embedded Sources and Outflows 150
The Nature of Sources with Water Maser Emission 155
The Relationship Between Mid-Infrared , IRAS and Radio Observations 159

7 CONCLUSIONS 163

Conclusions from the Methanol Selected Survey 163
Conclusions from the Water Selected Survey 164
General Conclusions 166
Suggestions for Future Work 167

APPENDICES

A OSCIR 170

Overview 170
The Journey of a Mid-Infrared Photon 171
Extracting the Source Signal 175
The Standard Chop-Nod Technique 176
The Detector 179

B DERIVATIONS OF IMPORTANT RELATIONSHIPS 181

Color Correction Factor 181
Resolution Limiting Size 183
Radio Flux Density as a Function of Lyman Continuum Photon Rate 184

LIST OF REFERENCES 188

BIOGRAPHICAL SKETCH 197

LIST OF TABLES

Title	Page
4-1. Positions of H_2O maser reference features and mid-infrared detections.....	39
4-2. Positions of methanol maser reference features and mid-infrared detections....	41
5-1. Physical parameters derived from the mid-infrared observations.....	92
5-2. The nature of the sources associated with methanol masers.....	97
5-3. Total integrated flux density observed in the OSCIR field of view and corresponding IRAS flux density measurements.....	102
6-1. Observed and derived parameters for the mid-infrared sources.....	149
6-2. Total integrated flux density observed in the OSCIR field of view and corresponding IRAS flux density measurements.....	160
6-3. Radio continuum flux and derived spectral types.....	161

LIST OF FIGURES

Title	Page
1-1. The four stages of intermediate mass star formation	4
1-2. The evolutionary scheme of an expanding HII region	8
1-3. Ionizing photon rate vs. diamter for compact and ultracompact HII regions	11
1-4. A schematic of the basic UCHII region morphologies	12
2-1. The OH molecule	18
2-2. The H_2O molecule	21
2-3. The CH_3OH molecule	25
3-1. Infrared radiation and dust	34
5-1. A three-panel plot for G305.20+0.21	56
5-2. A four-panel plot of G309.92+0.48	58
5-3. A possible mode of G309.92+0.48	59
5-4. G318.95-0.20	61
5-5. G323.74-0.26	63
5-6. G328.25-0.53	66
5-7. G328.81+0.63	68
5-8. G331.28-0.19	71
5-9. G339.88-1.26	75
5-10. G345.01+1.79	78
5-11. G345.01+1.80	80

5-12. G351.42+0.64..... 82

5-13. G351.77-0.54..... 85

5-14. G9.62+0.19..... 88

5-15. Spectral energy distributions for six sources..... 100

5-16. Methanol maser distribution size versus physical IHW18 extent..... 105

5-17. Methanol maser distribution size for sources with and without UCHII regions..... 107

6-1. G00.38+0.04..... 113

6-2. G00.55-0.85..... 114

6-3. G10.62-0.38..... 117

6-4. G12.68-0.18..... 120

6-5. G16.59-0.05..... 122

6-6. G19.61-0.23..... 124

6-7. G28.86+0.07..... 126

6-8. G34.26+0.15..... 128

6-9. G35.20-0.74..... 132

6-10. G35.20-1.74..... 135

6-11. G35.58-0.03..... 136

6-12. G40.62-0.14..... 138

6-13. G43.80-0.13..... 140

6-14. G45.07+0.13..... 142

6-15. G45.47+0.05..... 144

6-16. G48.61+0.02..... 146

6-17. G49.49-0.39..... 148

6-18. Separations between masers and mid-infrared and UCHII region source peaks..... 158

A-1. Atmospheric transmission..... 172

A-2. A cut-away view of OSCIR..... 173

A-3. OSCIR broadband filters..... 175

A-4. A schematic of the chop-nod technique..... 177

A-5. Image of OSCIR detector under uniform N-band illumination..... 180

Abstract of Dissertation Presented to the Graduate School
of the University of Florida in Partial Fulfillment of the
Requirements for the Degree of Doctor of Philosophy

A MID-INFRARED IMAGING SURVEY OF
STAR FORMING REGIONS CONTAINING
METHANOL AND WATER MASER EMISSION

By

James Michael De Buizer

August 2000

Chairman: Robert Piña
Major Department: Astronomy

This thesis presents the first mid-infrared imaging surveys towards massive star forming regions. The first of the two surveys presented here is of 21 sites of massive star formation associated with methanol masers. Recent radio observations of young massive stars revealed that methanol masers tend to exist in linear arrangements. It has been argued that these methanol masers exist in, and delineate, edge-on circumstellar disks. In the mid-infrared survey conducted here, three sources were observed that are elongated at the same position angle as their linear methanol maser distributions. It is believed that these elongated mid-infrared objects are indeed circumstellar disks. Furthermore, for the first time direct evidence has been found showing methanol masers arise inside the mid-infrared emitting regions of young stellar objects, indicating that they may be pumped by mid-infrared photons.

The second mid-infrared imaging survey presented here is directed towards 21 star formation regions associated with water maser emission. Water masers are generally believed to be associated with shocks in outflow from young massive stars, however new ammonia images have revealed the presence of 'molecular clumps' directly coincident with water maser emission. It is believed that these clumps are extremely young embedded stellar sources. The mid-infrared water maser survey presented here reveals the detection of 5 possible embedded sources associated with water maser emission.

Though it is generally believed that masers are associated with massive stars, radio studies have shown many sites of maser emission have no UCHII regions. The most popular explanation for this is that the associated stars are too young to have ionized their surroundings. For the stellar sources associated with methanol masers it was found that this is most likely because they are in general lower mass, non-ionizing stars, rather than being young. The detection of embedded sources in the water maser survey indicates, in the case of water masers, stellar youth plays a role. Furthermore, a better coincidence was found between water masers and mid-infrared sources, than radio continuum or near-infrared sources.

Combined, these two surveys provide new insight into the roles masers play in the development of massive stars, as well as provide much needed data concerning the formation of massive stars in general.

CHAPTER 1
MASSIVE STAR FORMATION

Why is the Study of Massive Stars Important?

Massive stars are extremely important astronomical objects on both the smallest and largest scales. From the moment they form photospheres, massive stars are violently changing their environment. They produce copious amounts of UV photons which ionize the interstellar gas around them. They can heat material out to large distances in the clouds from which they formed, and in the process enrich the interstellar medium with molecules through evaporation of dust grain mantles. They may have powerful outflows which shock and churn the interstellar medium. Massive stars live fast and furious, and end their lives just as spectacularly. They explode as supernovae, releasing as much energy in the process as they had produced over their entire lives. Supernovae are invaluable alchemists. They produce the heavy elements that are otherwise impossible to create by normal stellar fusion processes. The force of their explosions spread these heavy elements throughout large distances in a galaxy, enriching the interstellar medium and thereby affecting later generations of stellar chemistry. These supernovae generate disruptive shock waves, which may in turn spark the formation of the next generation of stars. In this way, massive stars are responsible for the creation and distribution of elements in a galaxy, and are therefore ultimately responsible for the chemical building blocks necessary for the creation of other stars, planets, and life as we know it.

Giant Molecular Clouds and Cloud Cores

Star formation is known to exist in association with giant molecular clouds in our galactic plane. Observations of giant molecular clouds (GMCs) have been performed, mostly by tracing their CO radio emission (Blitz 1991). Comparisons of observed CO emission of Dame et al. (1987) and FIR-selected potentially embedded O stars from Wood and Churchwell (1989b) show that there are no locations of star formation in the Galaxy where CO emission is absent (Churchwell 1991). It has been therefore plausibly argued that stars must form out of condensations of interstellar matter within giant molecular clouds.

The process by which the material in GMCs collapse into star forming regions is largely thought to be governed by gravitation. A density enhancement in the GMC, caused perhaps by the passage of a spiral density wave, gravitationally attracts surrounding material. The gravitational attraction does not take place without resistance. Shearing forces due to the rotation of the galactic disk about the center of the Galaxy try to rip the cloud asunder. Thermal pressure in the gas and centrifugal forces due to rotation of the coalescing material push outward. Magnetic field strength of the material amplifies during collapse, and could become strong enough to halt contraction as well. Ambipolar diffusion, a process by which neutral material slips past field lines in a lightly ionized medium, has been widely recognized as a way to alleviate built up magnetic stresses. While this may help in the earliest stages of collapse, it is not known exactly how a highly magnetized gas will behave as stellar densities are approached. Even though it is not exactly known how this build up is halted, it is believed that this and all of the other competing internal pressure forces are not strong enough to combat the gravitational attraction of the infalling material if the cloud has a sufficiently large mass.

Low and Intermediate Mass Star Formation

A scenario by which stars form can now be pieced together. Observations have been well matched to the 4-stage low and intermediate star formation paradigm developed by Shu et al. (1987). In this scenario, the first stage involves the formation of a slowly rotating molecular clump from the molecular cloud in which it resides, as described above (Shu et al. 1987; Figure 1-1a). Since the inner regions of the clump must support the weight of the outer layers, thermal (and magnetic) pressure increases towards the center. The density therefore increases in the center as well. Once this clump becomes sufficiently centrally concentrated, the thermal support in the dense interior eventually fails. A consequence of this density configuration is that this interior region of the cloud begins to collapse before the outer regions. It is therefore said that stars are formed via an 'inside-out' collapse (Shu 1977). The collapse occurs at the free-fall speed, and within the boundary of an expanding rarefaction wave, which spreads outward at the local sound speed. Initially, the material within this rarefaction wave has very little angular momentum, and so the material falls directly onto the growing core. However, as this boundary moves outward, material with much higher angular momentum from the rotating cloud's equatorial region begins to fall towards the core. This material has enough angular momentum that it misses the core, and instead reaches the core by assuming a spiraling orbit. As more high angular momentum material becomes involved, more material enters in an orbit around the growing protostellar core, creating a circumstellar accretion disk. This is the second stage (Figure 1-1b) in the scenario of Shu et al. (1987). This stage is characterized by the formation of the protostellar object at the

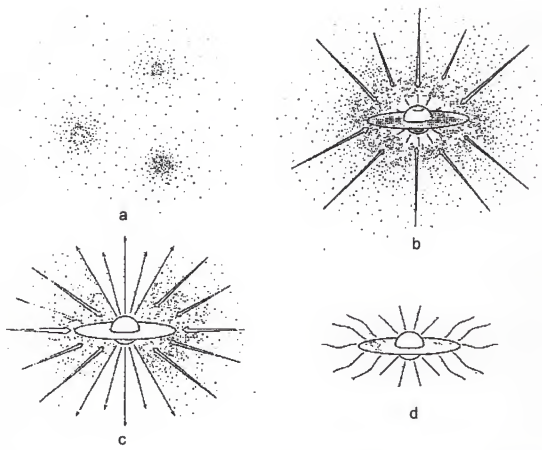

Figure 1-1: The four stage of low and intermediate mass star formation (from Shu et al 1987). (a) Cores form within a molecular cloud. (b) A protostar with a surrounding accretion disk forms at the center of a cloud core that has undergone inside-out collapse. (c) A stellar wind breaks out along the rotational axis of the system, creating a bipolar outflow. (d) The infall terminates, revealing a newly formed star with a circumstellar disk.

center with a circumstellar disk, both deeply embedded in an infalling envelope of dust and gas.

The accretion disk continues to feed the protostar causing it to increase in mass as well as luminosity. Accretion continues until a stage is reached where the protostar begins to develop a stellar wind. The stellar wind cannot break out in all direction from the protostellar surface because of the pressure from material infalling directly onto the

protostar suppress this breakout. However, once material begins to preferentially infall to the disk, rather than directly on the protostellar surface, stellar winds can break out at the rotational poles. This creates what is called a 'bipolar outflow', which signals the third stage of stellar evolution in the low-mass star formation paradigm (Figure 1-1c). The material accreting from the disk prevents the stellar wind from breaking out in the protostar's equatorial regions. Furthermore, this accretion disk causes the stellar wind to be well collimated initially. Eventually, the angular extent of the outflow increases, and as a consequence of clearing away the material nearby, the extinction to the central source decreases. The final stage is now at hand, as the infall terminates and the central protostar and its circumstellar disk are exposed (Figure 1-1d). This is referred to as the T-Tauri phase of stellar evolution. From this point, the protostar proceeds along its pre-main sequence (PMS) track in the Hertzsprung-Russell diagram toward the zero age main sequence (ZAMS).

High Mass Star Formation

The formation of massive stars is thought to be similar to that for low-mass stars as described by the scenario of Shu et al. (1987). If massive stars form via accretion, as described in the last section, then it is a requirement that the accreting molecular material be in rotation. Once a protostar reaches a mass >10 M_{sun}, it would generate such a large radiation pressure, that it would halt the collapse and reverse the infall (Garay and Lizano 1999). The only way to circumvent this is if the infalling material at this stage is in an accretion disk so that this pressure may be released through the poles. Furthermore, the accretion rate must be very high, with $dM/dt > 10^{-3}$ M_{sun}/yr, about 100 times higher than

that for low-mass stars. Only at these large accretion rates can the material create enough ram pressure to overcome the radiative pressure on the dust and allow continuous accretion onto the protostar. Hence if the scenario for low-mass star formation is to hold in the high mass case, the massive protostars *must* have circumstellar disks.

Until recently, evidence for circumstellar disks around massive stars did not exist. The evidence to date is still somewhat inconclusive. Lienert (1986) detected a ~100 AU elongated dust feature at near-infrared wavelengths around the massive star MWC 349A. Molecular disks have been found by Zhang et al. (1998) around the high mass star IRAS 20126+4104, and G35.2N by Brebner et al. (1987). G35.2N is thought to be one of the clearest examples of a bipolar molecular outflow surrounded by a molecular circumstellar disk[1]. There are a few other candidates as well, but the main point is that evidence is still weak, and there is, as yet, no conclusive observational evidence that massive stars form circumstellar disks.

This lack of observational evidence is mostly caused by another facet of massive star formation that is different from low-mass star formation. In the low mass star formation paradigm, the infall terminates and the star can be seen in its T-Tauri phase as it moves through the pre-main sequence (PMS) stage of its life. Massive stars, however, spend their entire PMS lifetime, which is very short, still embedded in their circumstellar dust and gas. It is very difficult to observe massive stars at this stage of formation because of this. They enter the main sequence as actively accreting protostars (Yorke 1993).

[1] As will be seen for this source, which is in the survey presented here, the molecular disk may not be a disk at all (see page 132).

It is also possible that massive stars may not form via accretion, or at least not via accretion alone. If the molecular cloud is composed of many molecular clumps, a clump may gain mass through coagulation with other clumps (Larson 1992). It is believed that massive stars form in close proximity with other massive stars, and in regions of exceptionally high density at the centers of giant molecular clouds, along with less massive stars. Interactions may exist between these dense pre-stellar clumps and accreting protostars. Massive stars may also form via the merging of two already formed less massive stars (Bonnell, Bate, and Zinnecker 1998; Stahler et al. 2000). In this case, it is not known if circumstellar disks would survive or reform around the massive stellar product. This is in stark contrast to the accretion paradigm of Shu et al. (1987) which, as was stated, would *require* the existence of a circumstellar disk.

There could also be a two-stage process to massive star formation. A first stage whereby dense cores or accreting protostars coalesce through mergers, and a second whereby the massive stellar product accretes the material from its surroundings to reach its final mass (Garay and Lizano 1999). In this two-stage process one would again expect a circumstellar accretion disk to form.

During the pre-main sequence phase of massive stellar evolution, massive stars, whether they formed via accretion, mergers or both, are surrounded by compact regions of ionized hydrogen. This is the case for two reasons. The first is because massive stars produce copious amounts of Lyman continuum (UV) photons. The second is that high mass stars form in dense regions in molecular clouds that provide plenty of molecular hydrogen that they can ionize. This is another unique feature of the high mass star

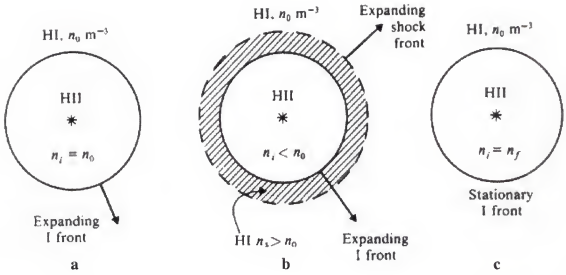

Figure 1-2: The evolutionary scheme of an expanding HII region (from Dyson and Williams 1980). (a) The initial stages of the expansion of the ionization front. This stage proceeds rapidly and thus the density of the ionized material, n_i is about the same as that in the surrounding ambient medium, n_o. (b) The ionization front continues to expand, however the hot ionized gas begins to expand as well, creating a shock front that moves out through the ambient medium. There is density enhancement in the shocked region, i.e. $n_s > n_o$. (c) The final stage where there is pressure equilibrium between the ionized region and the ambient medium.

formation process that is not found in the low mass star formation paradigm of Shu et al. (1987).

The Formation of HII Regions

When hydrogen burning begins in the core of a massive star, energetic photons are created which ionize the molecular gas surrounding the star. These ionized regions are also known as HII regions. The classical analysis of HII regions can be found in Spitzer (1978) and Dyson and Williams (1980). In these analyses, the surrounding molecular gas is assumed to be uniform in density and temperature, and one neglects the

effects of stellar winds. The energetic UV photons emitted by the star create an ionization front that expands supersonically through the surrounding ambient medium, ionizing the medium, but otherwise leaving it undisturbed. The expansion of the ionization front ends when the total number of photoionizations in the ionized region equals the total number of recombinations. At this point, the HII region has reached what is called the 'initial' Strogren radius, R_S

$$R_S = 0.032 \cdot \left(\frac{N_{uv}}{10^{49} \cdot s^{-1}} \right)^{\frac{1}{3}} \cdot \left(\frac{10^5 \cdot cm^{-3}}{n_o} \right)^{\frac{2}{3}} \quad \text{parsec}$$

as given by Stromgren (1939), where N_{uv} is the rate of ionizing photons emitted by the star, and n_o is the initial density of the ionized gas.

The heated gas in this region will begin to expand and form a shock front which moves out through the neutral gas. Spitzer (1978) show that the rate of expansion of the HII region is largely governed by the interaction between the shock and ionization fronts. The radius, R_I, of the HII region increases as

$$R_I = R_S \cdot \left[\frac{(1 + 7 c_I t)}{4 \cdot R_S} \right]^{\frac{4}{7}}$$

where c_I is the speed of sound in the ionized region, and t is time. This expansion ends when the thermal pressure of the region reaches an equilibrium with the surrounding cool ambient medium. This is given by the final radius of the HII region, R_F

$$R_F = \left(2 \frac{T_e}{T_o} \right)^{\frac{2}{3}} \cdot R_S$$

where T_e in the kinetic temperature of the ionized gas and T_o is the temperature of the ambient gas (Dyson and Williams 1980, Figure 1-2).

HII Region Morphologies

HII regions come in a variety of shapes and sizes. They are grouped into classifications based upon their angular sizes (Habing and Isreal 1979). 'Ultracompact' HII (or UCHII) regions are the smallest class, with typical sizes of about 0.1 pc or less, and are characterized by very high electron densities on the order of 10^4-10^5 cm $^{-3}$. The next class is the 'compact' HII region, which has typical sizes ranging from 0.1 to a few pc, with electron densities around 10^3 cm^{-3}. Though UCHII regions are thought of as the earliest stages of the HII region, and in some cases they most certainly are, on average the stars that excite UCHII regions are lower luminosity than those that excite compact HII regions (Garay and Lizano 1999; Figure 1-3). In other words, just because a HII region is small does not necessarily mean that it is extremely young. Finally, some HII regions are very extended (many pc in size) and do denote a mature stage of HII evolution. This class is referred to as 'extended' or 'classical' HII regions.

Compact and ultracompact HII regions do not always expand as perfect Stromgren spheres. Wood and Churchwell (1989a) performed a radio continuum survey of 75 regions of UC and compact HII regions and found that 20% of them have cometary shapes, 16% have a core-halo morphology, 4% have a shell structure, 17% are irregular or have multiple peaks, and 43% are spherical or unresolved (Figure 1-4). As can be see in Figure 1-4 taken from Wood and Churchwell (1989a), often the term 'UCHII region'

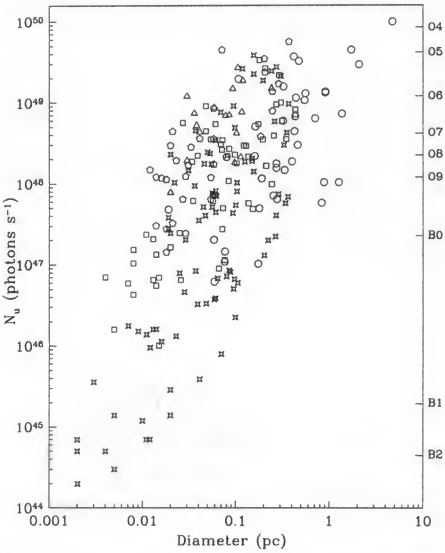

Figure 1-3: Ionizing photon rate vs. diameter for compact and ultracompact HII regions (from Garay et al. 1999). On the right axis is the number of ionizing photons emitted by ZAMS stars with spectral types from B2 to O4. There is a general trend showing that more compact radio sources come from less luminous stars.

and 'compact HII region' are simply referred to collectively as UCHII regions. This nomenclature will be adopted throughout this work.

The morphology which has gained the most attention is the 'cometary' UCHII region, which is identified as having a bright compact head and a diffuse extended tail. There are two major hypotheses that are considered to explain the cometary morphology

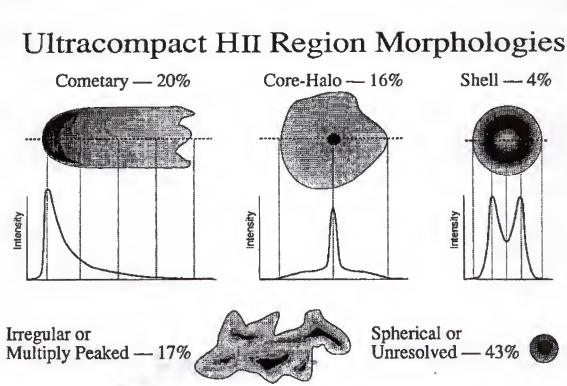

Figure 1-4: A schematic of the basic UCHII region morphologies (as seen in high resolution VLA observations of Wood Churchwell 1989a). The spatial resolution of the survey was 0.4 arcseconds.

of a UCHII region: champagne flow and bow-shock. Champagne flow or 'blister' models assume the HII regions evolve in a media with a strong density gradient (Tenorio-Tagle 1979; Bodenhemer, Tenorio-Tagle, and Yorke 1979; Tenorio-Tagle, Yorke, and Bodenhemer 1979; Bedijn and Tenorio-Tagle 1981; and Yorke, Tenorio-Tagle, and Bodenheimer 1983). In this scenario the HII region expands preferentially towards the lower density regions, and is ionization bounded on the high-density side and density bounded on the low-density side, giving a cometary appearance. The bow-shock model is one in which the star that excites the HII region is moving supersonically through the molecular cloud in which it was formed. In this way the head of the cometary HII region appears compressed due to the motion through the surrounding medium, and the tail is

diffuse and trails behind. Neither scenario has been able to explain all cometary HII regions, but there are cases where one or the other scenario best fit the observations.

Hot Molecular Clumps

As previously discussed, massive stars are thought to be gregarious by nature, and are often observed to form in associations. It has also been observed (e.g. Blaauw 1991) that sites of massive star formation contain sources in various stages of development. For instance, Cesaroni et al. (1994) observed four sites of UCHII regions in molecular transitions of NH_3. They found small structures (~0.1 pc), with kinetic temperatures greater than 50 and up to 200 K, densities approximating 10^7 cm^{-3}, and masses of a couple hundred solar masses. These hot molecular clumps are believed to be the precursors to massive stars. They lie within larger and less dense structures of molecular material, and are observed via molecular line transitions. While they are found near UCHII regions, not all UCHII regions have associated molecular clumps.

Circumstellar Disks

There are two types of phenomena most often associated with the name 'circumstellar disk'. The first can be lumped into the category 'debris disks'. These objects include the disks around Fomalhaut, Vega, Beta Pictoris, Epsilon Eridani, and HR4796A. These debris disks are around main sequence (A type) stars and have comparable extents of ~ 500 AU in diameter as seen in the submillimeter. The typical dust mass in these disks is a few times the mass of the Moon (~10^{23} kg, Chandler and Richer 1999). Another property of debris disks is that they are depleted of gas.

The other familiar circumstellar disk type are those found around pre-main sequence, solar mass (so called 'T Tauri') stars and around low-mass protostars. These types of disks can be grouped into a category called 'accretion disks'. These disks have typical diameters around a few hundred AU as seen in the submillimeter (Chandler and Richer 1999). Typical masses for these disks are on the order of a few $\times$ 0.01 M_{sun} ($\sim 10^{28}$ kg, e.g. Beckwith et al. 1990, Osterloh and Beckwith 1995).

The disks that are of concern to this work are of the accretion disk variety. However, if massive stars have circumstellar accretion disks, there would be major differences between the disks around massive stars and those around solar mass stars. First, dust disk sizes will be (as we will see with the results of this work) much larger than their T-Tauri counterparts (~ few thousand AU in diameter). This is a consequence of the large increase in mass and luminosity between, say, a T Tauri star of spectral type K and the early B type stars in this work. Rotating molecular disks have been found around massive protostars stars with sizes ranging up to 10,000 AU in diameter (Cesaroni et al. 1999, Zhang et al. 1998).

CHAPTER 2
BACKGROUND CONCEPTS IN PHYSICAL CHEMISTRY AND MASERS

Introduction to the Maser Phenomena

The word 'maser' is an acronym for microwave amplification by stimulated emission of radiation. The predecessor to the laser, the first laboratory maser device was constructed by Charles Townes in the 1954 (Gordon, Zeiger and Townes 1955). As the name suggests, amplification of microwave radiation can be caused by stimulated emission from excited molecules. Terrestrially, however, most molecules exist in their ground state, and radiation striking them is usually absorbed, not amplified. The fundamental feature of the maser is that in order to achieve this amplification, a majority of the population of molecules involved must be in an excited state. This is what is referred to as a *population inversion*. In more physical terms, the absorption coefficient is expressed as

$$\kappa_\nu = (N_i h\nu B_{ij}/\rho)(1 - g_i/g_j N_j/N_i)$$

and masering occurs if this is negative (more precisely if $g_i/g_j N_j/N_i > 1$). Negative absorption means negative optical depth and a negative source function since the emission coefficient is always positive. In cases of positive absorption coefficients, strong spectral lines become saturated. In this case, the negative absorption coefficients lead to strong lines which grow in strength rapidly as optical d epth increases. This leads

to very high surface brightnesses at the line frequencies and large luminosities from small volumes.

Population inversions are definitely not a situation where local thermodynamic equilibrium (LTE) is involved. But as is commonly observed, non-LTE situations are the norm in interstellar clouds. Because the low densities and large dimensions in the interstellar environment, line thermalization is rarely observed. However, to produce a population inversion, some kind of mechanism is needed which has the net effect of transferring molecules from their lower energy state to an upper metastable energy state. These mechanisms are usually referred to as *pumps*.

Strong amplification through stimulated emission of radiation occurs naturally in space as radiation propagates through an inverted medium. Maser gain is directly related to column density. In other words, to get large maser gains, large column densities are required. However, as was just discussed, interstellar volume densities are small. The way in which this dilemma is reconciled is to have small density but large path length. This creates another small problem. Because amplification is achieved by induced emission, maser photons will only interact with molecules whose transition frequency has not been Doppler shifted outside the linewidth. As observed through the large linewidths of molecular lines, interstellar clouds exhibit quite a bit of internal motion. Therefore, maser photons must seek a path through the interstellar cloud such that there is good line-of-sight velocity coherence in order to achieve large gains.

Basic properties of all interstellar masers are: 1) maser lines are much narrower and stronger than ordinary thermal lines, 2) interferometric observations show that maser sources are comprised of many individual *maser spots,* each with its own well-defined

velocity, and 3) dimensions of maser spots are of the order of ~10^{13} cm for masers in star-forming regions.

Hydroxyl Molecular Transitions

The hydroxyl radical was the first molecule found in space in 1963 by Weinreb et al. It also happens to be the first observed astronomical maser (Weaver et al. 1965). Hydroxyl masers are frequently found with methanol and water masers. Almost every source in this work has associated hydroxyl masers, so it is worthwhile to embark on a discussion of the molecule in this work. It also is also a simpler molecule than water or methanol, so it will be discussed first.

Even though hydroxyl is a simple diatomic molecule (Figure 2-1), it has an unfilled electron shell and various internal spins, resulting in a complex energy level structure. For background, we will depart into a discussion of the rotational spectra of diatomic molecules. A diatomic molecule is symmetric around the inter-nuclei axis. Because quantities are conserved around this axis, it has been given the convention of being the z-axis. For instance, projections of the total orbital angular momentum ($\boldsymbol{L}$) onto this axis are conserved, and these projections are designated by L_z or Λ. The molecule has defined states given by the quantized value of the projected angular momentum onto this axis. If $\Lambda = 0$, the state is referred to as a Σ-state. If $\Lambda = 1$ it is a Π-state, and if $\Lambda = 2$ it is called a Δ-state. The ground electronic state of OH has a $L_z = 1$, so is therefore a Π-state.

The *total* angular momentum $\boldsymbol{J}$ of any molecule excluding nuclear spin, is comprised of the molecule end-over-end rotation $\boldsymbol{K}$, the orbital angular momentum $\boldsymbol{L}$, and the electronic spin $\boldsymbol{S}$. For a diatomic molecule, rotation is about the inter-nuclei axis and

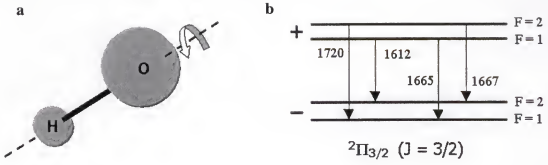

Figure 2-1: The OH molecule. (a) Model of the diatomic OH radical. The axis of symmetry is shown (z-axis) by the dashed line. (b) Ground-state rotation levels for OH. Shown are the four transitions of ground state OH that exhibit masing. The + and – show the two levels comprising the Λ doublet. Each doublet is split into two hyperfine levels as well.

therefore one is not concerned with the end-over-end rotation, meaning that $K_z = 0$. The value of the projected orbital angular momentum in the ground state is $\Lambda = 1$, so therefore $L_z = 1$. Finally, the electronic spin for OH has a value of $S_z = \pm ½$, where the signs can refer to an "up" or "down" spin. Therefore, the total angular momentum excluding nuclear spin for OH projected onto the z-axis is $J_z = 1 \pm ½$. The ±-sign therefore allows there to be two rotation ladders in the ground electronic state: $^2\Pi_{1/2}$ and $^2\Pi_{3/2}$. The subscripts denote the value of J_z and the superscript denotes the two possible electronic spin orientations.

The projection of $\boldsymbol{L}$ onto the z-axis can have a positive or negative sign for a given Λ if $\Lambda > 0$. These two projections have nearly the same energy (to a first approximation), so each Λ state is doubly degenerate. Quantum mechanically there are two states, $-J_z$ and $+J_z$, which represent the symmetric and anti-symmetric combinations of the two projections. Interactions between the orbital angular momentum $\boldsymbol{L}$ and the rotation of the nuclei $\boldsymbol{N}$ in the molecule leads to an energy difference between the $-J_z$ and

$+J_z$ states, thus splitting each energy level in two. This is referred to as Λ-doubling. The upper and lower levels of the doublet are distinguished by their different parities, either + or −. Because of the parity difference, radiative transitions between the Λ-doubled sublevels of a given J level are permitted.

The picture is further complicated by the effects of the nuclear spin $\boldsymbol{I}$, which creates a hyperfine energy level structure. The nuclear spin $\boldsymbol{I}$ adds vectorally with the total angular momentum without nuclear spin $\boldsymbol{J}$ to give the final overall angular momentum $\boldsymbol{F}$ ($\boldsymbol{F}=\boldsymbol{J}+\boldsymbol{I}$). A very weak splitting of levels is produced due to magnetic effects caused by the nuclear spin. The nuclear spin on a diatomic molecule is given by $I_z = \pm ½$, so therefore $F_z = J_z + I_z$, or $F_z = (1 \pm ½) \pm ½$. Therefore each rotation state of OH is split into *four* levels.

The allowed transitions are that $\Delta F = 0, \pm 1$. For the $^2\Pi_{3/2}$ state there are 4 spectral lines: two "main" lines with $\Delta F = 0$, and two "satellite" lines with $\Delta F = \pm 1$ (Figure 2-1). However $F = 0$ to $F = 0$ is forbidden. These four transitions are the most extensively observed astronomical maser transitions of the OH radical at around the 18 cm wavelength. The main line frequencies are 1667 MHz ($F = 2$ (upper) to $F = 2$(lower)) and 1665 MHz (F=1 (upper) to F=1 (lower)). The satellite lines are at 1720 MHz ($F = 2$ (upper) to $F = 1$ (lower)) and 1612 MHz ($F = 1$ (upper) to $F = 2$ (lower)).

The Hydroxyl Maser

The maser transition most observed in this survey is the 1665 MHz ($\lambda = 18$ cm) main line transition. The inversion occurs between the upper and lower levels of the Λ-doublet. Unfortunately, the exact pumping mechanism of OH masers in star-forming

regions is not clear. Explanations through the use of both radiative and collisional pumping mechanisms have proved to be problematic. For radiatively pumped sources, the pump photon emission rate must exceed the maser photon emission rate. Observations in the ultraviolet by Holtz (1968) and near-IR by Wynn-Williams et al. (1972) proved that the central stars studied emitted far too few photons of these wavelengths to explain the pumping. Far-IR photon emission rates, as derived from IRAS (Infrared Astronomical Satellite), show that there are enough far-IR photons, but they are from the cool dust that lies far away from the maser and central star. The region of far-IR emission is very large and the resolution of IRAS so poor, that it is likely that the far-IR photon rate at the maser region itself is smaller than the OH photon emission rate. Collisional pumping is also problematic because in order to achieve the strong maser emission observed by OH masers, densities would have to be so large that thermalization of the levels of OH would occur, quenching the maser inversion. Pumping due to mid-IR radiation has not been investigated fully. To date there is no final answer.

The most widely held belief is that the OH masers are situated in the enhanced density environment around an HII region. This environment is located between the shock and ionization fronts forming a compressed shell. This compressed shell is expanding outward allowing for systemic motions of the OH molecules, and producing the coherence needed for masing.

Water Molecular Transitions

Discovered in interstellar space by Cheung et al. (1969), water is a planar molecule with an axis of symmetry (Figure 2-2). However, it has three different moments

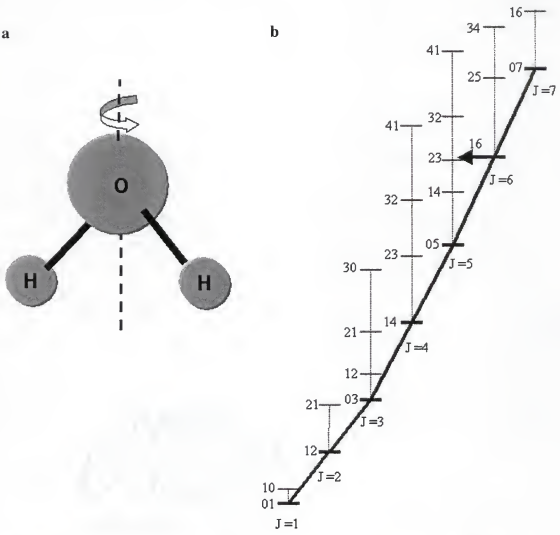

Figure 2-2: The H_2O molecule. (a) Model of the asymmetric top water (H_2O) molecule. The axis of symmetry is shown (z-axis) by the dashed line. (b) H_2O energy level J ladders. Levels are marked with $K+K-$. The "backbone" and its transitions are heavily marked. The 22 GHz maser transition at $6_{16}\rightarrow5_{23}$ is shown by the dark arrow. This ladder pertains to *ortho*-H_2O only (from Emerson, 1996).

of inertia for any set of axes chosen, and is therefore an asymmetric top rotor with a complex level structure.

For background, a *symmetric top* rotor has the same moment of inertia about two principal axes. The three moments of inertia about these three principal axes are labeled I_a, I_b and I_c, with the convention that $I_c \geq I_b \geq I_a$. A symmetric top can have the two larger

moments of inertia equal ($I_c = I_b > I_a$), which is called a *prolate* rotor, or it can have the two smallest moments of inertia equal ($I_c > I_b = I_a$), which is called an *oblate* rotor.

Molecules with three different moments of inertia, like water, are *asymmetric top* rotors. Nonetheless, it is quite often that the moments of inertia about two axes are close in value and can be assumed to be a symmetric top rotor to a first order, with its levels split to remove the remaining degeneracy. Each level of the rotational quantum number J of an asymmetric rotor are split into $2J+1$ levels which are specified by the quantum numbers $K-$ and $K+$. The value $K-$ represents the projection of the angular momentum on the symmetry axis if the molecule was a prolate symmetric top rotor. The value $K+$ represents the projection of the angular momentum on the symmetry axis if the molecule was a oblate symmetric top rotor. In this way, the levels of an asymmetric rotor are labeled as J_{K-K+}. The radiative selection rules for these molecules require $\Delta J = 0$ or ± 1, and that $K-$ and $K+$ must change their evenness.

To further complicate things in the case of the water molecule, the two hydrogen atoms both carry a nuclear spin which can combine to give a total nuclear spin of $I = 0$ or $I = 1$. This leads to two distinct species of water molecules: *ortho*-H_2O for $I = 1$ and ($K-$, $K+$) = (odd, even) or (even, odd), and *para*-H_2O for $I = 0$ and ($K-$, $K+$) = (odd, odd) or (even, even). These are treated as two distinctly separate species since they are unconnected by radiative transitions.

The water masers observed in the survey presented in this work are the *ortho*-H_2O $6_{16} \rightarrow 5_{23}$ rotational transition, which is the most commonly observed transition and whose frequency is 22 GHz (λ = 1.35 cm). This happens to be the transition first discovered by Cheung et al. (1969).

The Water Maser

In the case of *ortho*-H_2O, transitions are permitted between adjacent levels within a ladder and neighboring ladders. In some cases, the energy levels of neighboring ladders are nearly equal in energy, and selection rules concerning a change of evenness in the K quantum numbers can be obeyed, so a transition can occur. This is how the *ortho*-H_2O $6_{16} \rightarrow 5_{23}$ transition is believed to work.

The inversion process of this transition was first identified by de Jong in 1973. He concluded that the bottom levels of each rotational ladder (1_{01}, 2_{12}, 3_{03}, 4_{14}, 5_{05}, 6_{06}, etc.) formed what he called a "backbone" (Figure 2-2), which were connected through strong radiative transitions which will therefore tend to be optically thick. In a single rotation ladder, there will tend to be cascades down to the backbone level. In this way a backbone level like the 6_{16} level tends to have a higher population than the off-backbone level 5_{23}, which is actually slightly lower in energy, thus producing the population inversion.

Like OH masers, the H_2O maser pump mechanism is just as elusive. The most widely-held belief is that H_2O masers are created and pumped by shocks. One such popular scenario is that water masers could be locally created and collisionally pumped by the interaction of highly supersonic outflows from a central young star with clumps or inhomogeneities in the surrounding cloud (Elitzur 1992a and Elitzur et al. 1989).

Methanol Molecular Transitions

Methanol was first detected in interstellar space during observations of the Galactic center by Ball et al. in 1970. Over 200 spectral lines have been discovered to

date, lying in the frequency range between 834 MHz and 350 GHz. Of these, over twenty are known to display maser emission and have been observed in regions of star formation. The transitions of methanol are quite a bit more complex than OH or water.

It is an asymmetric top rotor, where the tetrahedron defined by the CH_3 group can rotate relative to the OH bond (Figure 2-3). However, this internal rotation is hindered by mutual interactions between the CH_3 group and the OH bond, thus creating a torsional oscillation. This torsional oscillation produces an angular momentum about the internal rotation axis defined by the CH_3 tetrahedron. This angular momentum becomes strongly coupled to the over-all angular momentum, and results in two torsional symmetry states. These are labeled *A* and *E*.

One can consider *A*- and *E*-type methanol as two distinct molecular species since selection rules require that transitions from one *A*-level can only be to another *A*-level, and transitions from an *E*-level can only be to another *E*-level. Maser emission can occur in either species. Rotation states in each of the two types are characterized by J_K. Here again J is the total angular momentum of the molecule, but in this case K is the component of the angular momentum on the molecular symmetry axis. For the *E*-type methanol, one uses $K = (\pm)k$ to designate the levels, where the quantum number k can carry a positive or negative value. This is because the *E*-levels of methanol are doubly degenerate. For *A*-type methanol, one uses $K = |k|$ to designate the levels. This is because the $+K$ and $-K$ *A*-levels are *torsionally* degenerate, splitting the K levels (except $K = 0$) into degenerate pairs labeled A^+ and A^-.

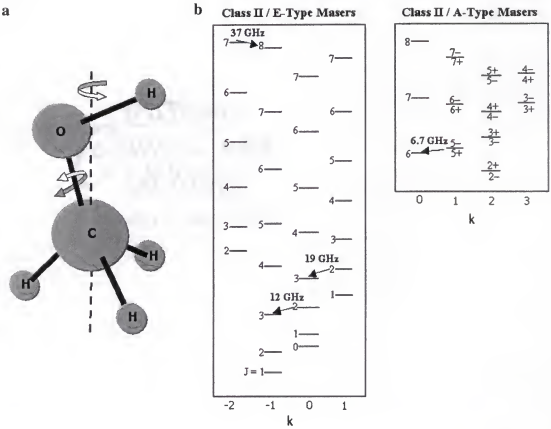

Figure 2-3: The CH_3OH molecule. (a) Model of the asymmetric top methanol (CH_3OH) molecule. Axis of symmetry is shown by the dashed line. This axis is defined by the symmetry of the CH_3 group. The CO bond is offset from this symmetry axis. The axis of the hindered internal rotation by the OH group is shown with the double-headed arrow. (b) Energy level diagrams for *E*-type (left) and *A*-type (right) methanol. Arrows indicate the more important maser transitions of the Class II masers. The *A*-type methanol levels are split into doublets too small to be shown here. Instead + and − symbols are used to show the doublet.

Strong methanol maser emission was first discovered toward the Orion-KL region by Barrett et al. (1971) in the series of $J_{k=2} \rightarrow J_{k=1}$ *E* transitions (J = 2,3,4,...) near 25 GHz. This work mostly concerns the 12 GHz $2_0 \rightarrow 3_{-1}$ *E* transitions of methanol which were first discovered by Batrla et al. (1987) toward W3(OH) and several other regions, as

well as the 6.7 GHz $5_1 \rightarrow 6_0$ A^+ transition first discovered by Menten (1991) toward several star-forming regions.

The Methanol Maser

There are certain characteristics peculiar to methanol masers which led to the division of them into two distinct classes. The classification scheme was first put forth by Batrla et al. (1987). It was observed that sites with maser emission from *E* transitions at 25, 36 and 84 GHz and *A* transitions at 44 and 95 GHz showed enhanced *absorption* at 12 GHz. These are now referred to as Class I sources. In contrast, other sites with maser action from *E* transitions at 19 and 37 GHz and *A* transitions at 6.7 and 23 GHz showed intense *maser emission* at 12 GHz. These are called Class II sources. Another fundamental difference between Class I and Class II methanol masers is that the latter ones are coincident with ultracompact HII/OH star-forming regions, while Class I masers seem to be located further away at distances of the order of 1 pc from the UCHII region. The methanol maser emission of interest in this work is obviously Class II. Methanol masers, though frequently correlated with OH masers, are suspected to originate within disks of material surrounding young stars (Norris et al. 1993).

Exactly how Class I masers are pumped and inverted is thought to be understood, however Class II masers pumping and inversion remains a mystery. Whatever mechanisms are devised must work in a way that suppresses Class I maser emission since Class I and Class II maser are never found toward the same location.

CHAPTER 3
MOTIVATION AND FORMULATION OF THE DISSERTATION

Summary of Observations of Masers in Massive Star Forming Regions

As was discussed in the last chapter, maser emission is closely related to massive star forming regions. In fact, it is commonly assumed that masers trace young massive stars. However, advances in higher resolution imaging and accurate astrometry in recent years has led to observations that show masers are often *not* directly coincident with massive stars. So the question remains*: If masers do not trace massive stars, what do they trace?*

The last chapter reviewed the current ideas on how each maser species was thought to be excited, and gave the most popular scenario for each. The situation is not that simple however. For each maser species, OH, water, or methanol, there are observations that do not fit the scenarios given in the last chapter. In fact, recent observations (and the work to be presented here) are teaching us that masers of each species can be excited in a variety of ways.

The following subsections will review the objects and processes believed to be associated with maser emission, and will give examples of each from the literature.

Shock Fronts

As discussed in Chapter 1, compact HII regions grow via ionization and shock fronts. It has been suggested (e.g. Elitzur 1992b) that the cool, dense layer of gas between the ionization and shock fronts provide a habitable zone for masers (OH masers, in particular). Velocity coherence for the masing material would be provided by the bulk motion of the expansion. Elitzur and de Jong (1978) modelled the chemistry that would occur in the regions between ionization and shock fronts. They found that water exists in large quantities there, and that photodissociation of water molecules closer to the central star would release oxygen which, in turn, would be efficiently channeled into OH.

The idea that masers can exist in a compressed shell around UCHII regions was confirmed by observations showing a close association of OH masers with the outer edges of several compact HII regions (Ho et al. 1983; Baart and Cohen 1985; Garay, Reid, and Moran 1985; and Gaume and Mutel 1987). One source that Elitzur (1992b) presents as an example of this situation is the object W3(OH). Furthermore, observations by Menten et al. (1988) showed that methanol and OH masers are found occupying the same outlying regions of W3(OH).

It seems reasonable that masers can indeed exist in shock fronts. They may display linear or arc-like arrangements if this is the case.

Outflows

The bulk motion and relatively high density of molecular material caught up in a well-collimated bipolar outflow from a young star may, in principle, be a good location for maser emission. The masers taking part in the outflow will be distributed in linear distributions pointing radially away from the parent star or UCHII region. Furthermore,

well-collimated outflows are generally high-velocity outflows. Therefore the masers would have velocities similar to those found for other material taking part in outflows (~100 km/sec). Such high velocities have been observed in water masers. For instance, the detailed study of W51M by Genzel et al. (1981) shows water masers with velocities as high as 157 km/sec.

Even if masers are not taking part in the outflow from a young stellar object, the shock created by an outflow as it impinges on the ambient medium (or on knots of material in the immediate vicinity of an outflowing star) also seems to be perfect locations for masers (water masers, in particular). The high temperatures in shocks trigger chemical reactions that produce large quantities of molecules like water (Elitzur 1992b). Shock fronts are sheet-like, so in the shock plane one would expect coherent velocities suitable for masing. The arrangement of masers in this scenario could be linear, but in general could be quite varied.

Circumstellar Disks

An exciting hypothesis for the location of masers is in circumstellar disks. In this scenario, velocity coherence of the maser molecules comes from the rotation of the material in the disk, and of course the material is sufficiently dense. Masers would be preferentially observed in disks that are edge-on for two reasons. First there is a larger column density through the plane of the disk than normal to it. This added column density creates large maser gains producing easily detectable masers. Second, above and below the plane of the disk there are most likely HII regions, created by the escaping UV photons from the poles. These regions are optically thick to the maser emission, and hence no maser radiation can get out in these directions.

There are several observations where masers seem to be located in circumstellar disks. For instance, Brebner et al. (1987) observe a linear arrangement of OH masers that lie in, and are at the same position angle as, a rotating molecular disk seen in ammonia (NH_3). Circumstellar disks have also been used to explain water maser observations in several other sources (e.g. Torrelles et al. 1996; Slysh et al. 1999).

Methanol masers also seem to display signs of existing in disks. Radio results by Norris et al. (1993, 1998) of more than a dozen 12.2 GHz (λ = 2.5 cm) and 6.7 GHz (λ = 4.5 cm) methanol maser groups (each group of maser spots being associated with a single star) indicate a very strong preference for individual methanol maser spots to be located along *lines or arcs* (size ~1000 - 4000 AU). Furthermore, in some instances the velocities of these features (determined from the Doppler shift of the maser line) show a gradient along the distribution, indicative of rotation. Norris et al. (1993) concludes that the most likely explanation is that the methanol maser spots are located in a circumstellar disks that are viewed nearly edge-on.

Embedded Sources

The idea that masers are excited by embedded protostellar objects was originally suggested by Mezger and Robinson (1968) for OH masers. Specifically, these masers would exist in the accreting envelopes of massive protostars and be excited by the energy from accretion shocks. This scenario became a legitimate explanation of the H_2O maser phenomenon when Turner and Welch (1984) discovered a massive molecular core in HCN emission at the position of an isolated H_2O maser group that exists 7″ away from the UCHII region W3(OH). While this scenario certainly has promise, observations

searching for hot molecular cores associated with embedded stellar sources have only been done for a few H_2O maser sites (Turner and Welch 1984; Cesaroni et al. 1994), but with encouraging results.

Pumping Considerations

All of the above cases for maser location satisfy the criteria for velocity coherence and large column density, but nothing was mentioned about how the masers are pumped in each scenario. This is because observations are ahead of theory, and definite pump mechanisms for each molecule in each situation simply have not been worked out. Below is a qualitative discussion of some of the possible pump mechanisms in each scenario.

The shock front scenario would most likely involve collisional pumping. This scenario has been perhaps the most theoretically worked out scenario (at least in the case of water maser emission). The energy to pump the masers can be provided by the collisional dissipation of the relative kinetic energies of the shocked and unshocked gas. Quantitative discussion for the case of water masers can be found in Elitzur (1992b) and references therein. At least for water masers, it appears that pumping by collisional excitation of rotational levels behind dissociative shocks can provide an adequate explanation.

In the outflow scenario, masers would most likely be radiatively pumped. The masers would exist near the origin of the outflow, where material is most collimated and can be heated by the outflow source. Masers in circumstellar disks would most likely be radiatively pumped as well. The central source could heat out to large distances in the disk if the disk is flared (i.e. thickness increases with increasing radius from the center; see Hartmann 1998). For embedded sources, the pumping of the masers could be via the

collisional excitation from accretion shocks, or from the radiation from the protostar or accretion disk itself.

Mid-Infrared Astronomy

It is difficult to ascertain what stellar process maser emission is tracing when it is not known where the locations of the associated massive stars are with respect to the maser spots. One way to observe the young massive stars associated with masers is to look for and image the radio continuum from the UCHII regions produced by these stars. However, surveys have discovered that many sites of maser emission have no detectable radio continuum emission (e.g. Wood and Churchwell 1989a; Walsh et al. 1998). Imaging at another wavelength is needed to find the associated young stellar sources.

Optical imaging is not useful because massive stars evolve so quickly that they stay heavily embedded in their birth clouds, even after they reach the main sequence. In the visible, dust absorbs and scatters light giving rise to significant extinction. This effect is much less of a problem in the infrared. For instance, observations towards the Galactic Center suffer 30 magnitudes of extinction in the visible, which is the equivalent of 1 out of every 10^{12} photons reaching the observer. In contrast, in the mid-infrared the extinction is only 1.2 magnitudes at 10 μm, or 33% of the photons reaching the observer, and 0.6 magnitudes at 18 μm, or 58% of the photons reaching the observer (assuming the interstellar extinction law of Mathis 1990). Therefore, because infrared radiation is much less affected by extinction than visible radiation, infrared images can probe through the cool obscuring dust enshrouding the massive stellar environment.

As one observes at longer and longer wavelengths in the infrared, one generally observes objects with lower and lower temperatures. This can be explained in the ideal case of a blackbody, whose temperature is dependent upon the peak wavelength it emits radiation at, as given by the Wien displacement law

$$T\lambda_{peak} = 2898$$

where λ_{peak} is in μm and T in Kelvin. From this law it can be seen that a blackbody that has peak emission at 10 μm will have a temperature of 290K.

In star forming regions, thermal (heat) emission from dust (and dust conglomerates such as planetesimals and planets) is the dominant source of radiation at 10 μm. Dust, such as circumstellar dust ($a \equiv 0.1$ μm to a few μm), is very efficient at absorbing radiation at short wavelengths ($\lambda \leq a$) which in turn heats the dust to temperatures up to a few hundred of Kelvin. Consequently, dust emits significant thermal radiation at mid-infrared wavelengths. However, dust absorption can also be seen in the mid-infrared as well. This occurs when there is a cooler layer of dust between the mid-infrared source and the observer. These cool dust grains absorb the mid-infrared photons, which heat the dust to a few tens of Kelvin. These cooler dust grains reemit this heat in the far-infrared around 100 μm. Hence, in the extreme where there is enough cool dust between the observer and the mid-infrared emitting dust, the mid-infrared radiation could be undetectable.

Figure 3-1a shows the process of dust emission schematically. Whittet (1988) has produced a dust emission spectrum from observations near the galactic center where there is ongoing star formation. This spectrum, shown in Figure 3-1b, has two peaks, one corresponding to the warm dust around 10 μm, and the other to the cool dust around 100

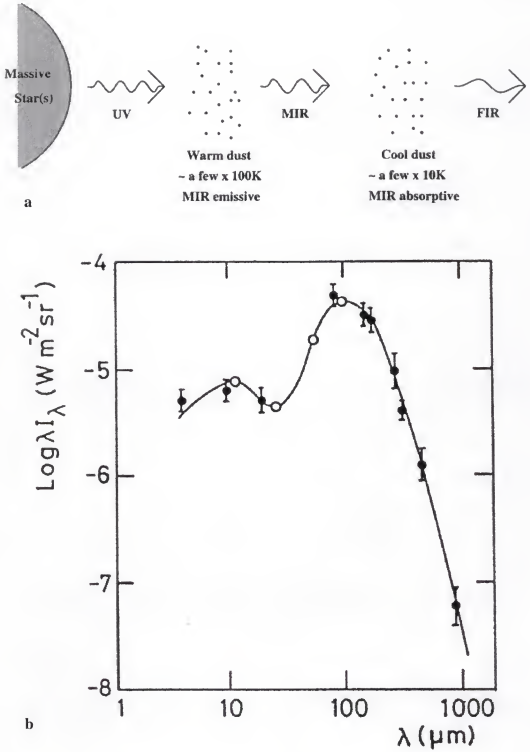

Figure 3-1: Infrared radiation and dust. (a) A schematic diagram showing the probable locations of mid-infrared emission and absorption by warm and cool dust grains, respectively in a massive star-forming region (from Fujiyoshi 1999) (b) The spectral energy distribution of dust emission from the Galactic disk between longitudes 3 and 30 degrees. It clearly indicates the presence of cool and warm dust grains (from Whittet 1988).

μm, confirming the existence of mid and far infrared emitting dust near regions of star formation.

Mid-infrared imaging presents a viable alternative to radio continuum imaging for observations of massive star forming regions. Mid-infrared radiation traces the warm dust close to the stellar sources, allowing one to observe the spatial relationship between masers and young massive stars.

A Case for the Present Work

One of the fundamental questions in astronomy is *How do stars form?* Much has been done both observationally and theoretically to understand the phenomena associated with this question. However, despite the importance of massive stars, most of these studies have focused on stars that are similar to our Sun in mass or smaller. It still remains unclear exactly how massive stars form. Studies have led to a hypothesis for the formation of low mass stars (Shu et al. 1987). This scenario is predominantly controlled by accretion, with the end product being a new star surrounded by a circumstellar disk.

Nevertheless, while the scenario of Shu et al. (1987) has worked well to explain star formation for low mass stars, it is not yet clear if it is applicable to massive star formation. It is still not known if massive stars form by accretion or by stellar mergers. Consequently, it is not known if the formation of circumstellar disks are a general characteristic of massive star formation. Furthermore, young massive stars are often associated with masers. We are only just now beginning to understand how masers of different species relate to the physical processes that occur during the formation and earliest evolutionary stages of massive stars.

The general goal of the work to be presented here is to try to determine the relationship between masers and massive stars. In the process, it is hoped that more will be learned about the properties and processes of massive star formation, and how they are different or similar to their low-mass counterparts. The approach taken in this work was to survey as many sources of maser emission as possible in the mid-infrared. No high-resolution (<1″) surveys of massive stars have ever been performed in the mid-infrared until this work. As mentioned in the last section, mid-infrared images (5-25 μm) penetrate the significant extinction in these regions and can trace the radiation from the ~200 K dust close to the stellar sources associated with the masers. Furthermore, a resolution will be achieved that is on the threshold of being able to detect and resolve circumstellar disks around these stars if they exist.

Since this work is the first survey of its kind, many questions may potentially be answered: Are massive stars surrounded by disks? Do methanol masers trace these disks? Do massive stars have a bipolar outflow phase, as is thought to be the case for low-mass stars? Are the different maser species signposts of different evolutionary stages and/or of different stellar processes? Do massive stars form in a highly clustered way? Are water masers associated with young embedded stellar sources?

The survey is divided into two sections. The first concerns the methanol maser selected survey performed in the Southern Hemisphere (Chapter 5). The second is a discussion of the water maser selected survey that was performed in the Northern Hemisphere (Chapter 6). A summary and concluding remarks concerning what has been learned from both surveys will be presented in Chapter 7.

CHAPTER 4
DATA ACQUISITION AND REDUCTION

IRTF – Water Maser Observations

All images of the water maser selected sites were obtained at the 3-meter NASA Infrared Telescope Facility (IRTF). This observatory is situated on the peak of Mauna Kea, an extinct volcano on the Big Island of Hawaii, at an elevation of 14,000 feet. Observations were made using the University of Florida mid-infrared camera and spectrometer OSCIR. This instrument employs a Rockwell 128 x 128 Si:As BIB (blocked impurity band) detector array, which is optimized for wavelength coverage between 8 and 25 μm. The field of view of the array at IRTF is 29″ x 29″, for a scale of 0.223 ″/pixel. Sky and telescope emission were subtracted out by using the standard chop-nod technique. For more on OSCIR and mid-infrared observing techniques, refer to the Appendix A.

There were two nights of observations, with the first occurring on 7 September 1997. That night, 21 maser sites were imaged centered on the H_2O maser reference feature coordinates (i.e. the brightest maser spot) given by Forster and Caswell (1989), with 30 second chopped integration times (i.e. on source plus off source) taken through a broad band N filter. This filter has a width of 5.1 μm. The physical center of the filter is at 10.8 μm, but it has an effective central wavelength of 10.46 μm. These values are used interchangeably throughout this work when the N filter is being referred to. There were

only 14 detections on this first night. The same objects were revisited on the second night of observations which occurred on 10 September 1997, this time with the exposure times were increased to 120 seconds. In addition to the N-band filter, images were also taken using 120 second exposure times with an IHW18 filter (International Halley Watch 18 μm). This filter has a width of 1.7 μm, a physical center at 18.2 μm, but an effective central wavelength of 18.06 μm (again, these last two values are used interchangeably here). Cirrus clouds terminated the second night of the survey after only the first nine sites were imaged. Even though all the observations were taken at low airmass (<1.5), cirrus clouds were unfortunately present most of the time on both nights. Cirrus presents one of the worst terrestrial hazards for mid-infrared observations, because it efficiently absorbs the mid-infrared photons from the target source, and at the same time emits copious quantities of mid-infrared radiation itself. It can therefore be assumed that the lower detection rate on the first night may have been due to low exposure times and/or poor observing conditions.

The standard star used for the calibration of the sources was Gamma Aquila. The flux densities for the star were taken to be 77.2 Jy at N and 25.6 Jy at IHW18 (from stellar atmospheric modeling of Cohen 1999).

Table 4-1 lists the targets in this water maser selected survey. The coordinates listed are the reference maser spot positions given by Forster and Caswell (1989), which were obtained with a connected element interferometer and have absolute positional accuracies of ~0.5″. Achieving accurate astrometry for infrared observations is not trivial. Most telescopes employ visual guide cameras that point exactly where the telescope is pointing. Once the telescope is moved near the position of the target it can be seen on the

Table 4-1: Positions of H_2O maser reference features and mid-infrared detections.

Target Name	H_2O R.A. (1950)	H_2O Dec. (1950)	Mid-IR Detection? 09-07-97	09-10-97
G00.38+0.04	17 43 11.23	-28 34 34.0	N	marginal
G00.55-0.85	17 47 03.83	-28 53 39.5	Y	Y
G10.62-0.38	18 07 30.56	-19 56 28.8	Y	Y
G12.68-0.18	18 10 59.17	−18 02 42.5	N	Y
G16.59-0.05	18 18 18.05	-14 33 17.7	N	Y
G19.61-0.23	18 24 50.25	-11 58 31.7	Y	Y
G28.86+0.07	18 41 08.28	-03 38 34.5	Y	Y
G32.74-0.07	18 48 47.81	-00 15 43.5	N	
G33.13-0.09	18 49 34.25	+00 04 32.2	N	
G34.26+0.15	18 50 46.36	+01 11 13.9	Y	
G35.03+0.35	18 51 29.12	+01 57 30.7	N	
G35.20-0.74	18 55 41.05	+01 36 31.1	Y	
G35.20-1.74	18 59 13.24	+01 09 13.5	Y	
G35.58-0.03	18 53 51.38	+02 16 29.4	Y	
G40.62-0.14	19 03 35.43	+06 41 57.2	Y	
G43.80-0.13	19 09 30.98	+09 30 46.8	Y	
G45.07+0.13	19 11 00.40	+10 45 43.1	Y	
G45.47+0.13	19 11 45.97	+11 07 02.9	N	
G45.47+0.05	19 12 04.42	+11 04 11.0	Y	
G48.61+0.02	19 18 12.93	+13 49 44.7	Y	
G49.49-0.39	19 21 26.32	+14 24 41.8	N	

visual camera, where it is centered in the crosshairs. Thus, the target will appear in the center of an image taken by an instrument mounted on the telescope. However, because the mid-infrared sources cannot be seen at visible wavelengths, one cannot center the targets using the visual camera. Instead, the mid-infrared absolute astrometry is obtained by offsetting the telescope to the maser reference coordinates from nearby reference stars (typically about 10 arcminutes away) whose accurate coordinates were obtained from the Hipparcos Main Catalogue. Using this technique, the error in the absolute astrometry is given by the pointing accuracy of the telescope. For the IRTF, the absolute pointing accuracy of the telescope was estimated to be about 1.0″, determined by repeatedly

offsetting between reference stars. It was therefore concluded that the relative accuracy of the astrometry between the maser reference features and the pointing is also 1.0″ at the IRTF.

Five point-spread function (PSF) stars were observed throughout the course of the second night (no PSF stars were imaged on the first night). Error in the PSF FWHM was taken to be the standard deviation of the size of the PSF stars imaged throughout the night. A target object was considered to be resolved if the measured full width at half-maximum (FWHM) was greater than three standard deviations from its closest PSF FWHM. Marginally resolved objects are between 2 and 3 standard deviations of the PSF FWHM.

CTIO – Methanol Masers Observations

Observations of the methanol maser selected survey were carried out at Cerro Tololo Inter-American Observatory (CTIO) on the Victor M. Blanco 4-meter telescope. This observatory is situated on a mountain in the Chilean Andes at an elevation of 7100 ft. Once again the University of Florida mid-infrared imager/spectrometer, OSCIR, was used. The field of view of the array at CTIO is 23″ x 23″, with a scale of 0.183″/pixel. Sky and telescope emission were removed using the standard chop-nod technique.

The methanol maser sites were observed on the evenings of 1998 July 2 and 3, under very clear skies with low relative humidity (<20%) and at low airmasses (<1.2). Images were taken using OSCIR's broad-band N and IHW18 filters with 2-minute chopped integration times, except for the G339.88-1.26 images, which were taken with 4-

Table 4-2: Positions of methanol maser reference features and mid-infrared detections.

Target Name	Methanol R.A. (J2000)	Methanol Dec. (J2000)	Mid-IR Dectection?
G305.21+0.21	13 11 13.72	-62 34 41.6	N
G305.20+0.21	13 11 10.47	-62 34 39.0	Y
G309.92+0.48	13 50 41.76	-61 35 10.1	Y
G318.95-0.20	15 00 55.40	-58 58 53.0	Y
G323.740-0.263	15 31 45.46	-56 30 50.2	Y
G323.741-0.263	15 31 45.88	-56 30 50.3	Y
G328.24-0.55	15 57 58.38	-53 59 23.1	N
G328.25-0.53	15 57 59.79	-53 58 00.9	Y
G328.81+0.63	15 55 48.61	-52 43 06.2	Y
G331.28-0.19	16 11 26.60	-51 41 56.6	Y
G336.43-0.26	16 34 20.34	-48 05 32.5	N
G339.88-1.26	16 52 04.66	-46 08 34.2	Y
G340.78-0.10	16 50 14.86	-44 42 26.4	N
G345.01+1.79	16 56 47.56	-40 14 26.2	Y
G345.01+1.80	16 56 46.80	-40 14 09.1	Y
NGC 6334F	17 20 53.50	-35 47 01.7	Y
NGC 6334F-NW	17 20 53.31	-35 46 59.7	Y
G351.44+0.66	17 20 54.67	-35 45 08.5	N
G351.77-0.54	17 26 42.55	-36 09 17.7	N
G9.621+0.196	18 06 14.78	-20 31 32.1	N
G9.619+0.193	18 06 15.04	-20 31 44.2	Y

minute chopped integration. The primary standard star for these observations was Eta Sagittarius, for which the flux densities were taken to be 188 Jy at N and 66 Jy at IHW18 (Cohen 1999). However, Eta Sgr is a known variable star, so a secondary standard (Beta Grus) was also observed, whose calibration correction agreed with that of Eta Sgr to a few percent.

Table 4-2 lists the targets in this methanol maser selected survey. The coordinates listed are the reference maser spot positions given by Norris et al. (1993), which were also obtained with a connected element interferometer and have absolute positional accuracies less than 0.5″. The mid-infrared absolute astrometry was obtained the same

way as for the water maser survey, that is, by offsetting the telescope to the maser reference coordinates from nearby reference stars (typically about 10′ away). For these reference stars, the coordinates were obtained from the Positions and Proper Motions South Catalogue (PPM/South). The absolute pointing accuracy of the Blanco 4-m telescope was estimated to be about 2.5″, determined by repeatedly offsetting between reference stars. It can therefore be concluded that the relative accuracy of the astrometry between the maser reference features and the center of the mid-infrared field of view is also 2.5″. One further note of caution is that there were also occasionally large non-reproducible offsets from 3 to 6″ when the telescope was slewed from one reference star to another. This may account for some of the larger offsets observed between the maser reference positions and mid-infrared sources.

Point-spread function (PSF) stars were imaged near the positions of most of the targets. As for the water masers, the error in the PSF FWHM was taken to be the standard deviation of the size of the PSF stars imaged throughout the night. Likewise, a target object was considered to be resolved if the measured full width at half-maximum (FWHM) was greater than three standard deviations from its closest PSF FWHM.

Data Reduction

Airmass Correction

Measured fluxes for a source decrease as one observes them closer and closer to the horizon, so one typically must make 'airmass' corrections. However, no airmass corrections were made to the flux densities observed in either survey. It was found for each night of observations that the airmass correction would be negligible, and therefore

none were applied. This is most likely due to the fact that the sources were observed over a very limited range of airmasses.

Color Corrected Fluxes

Due to the large bandwidth of the filters (especially the N filter), the observed fluxes for the sources must be 'color' corrected to account for the intrinsic source spectrum, the filter transmission, and the atmospheric transmission. For the calibration star, the spectrum was assumed to be a blackbody at its effective stellar temperature. Color corrected monochromatic flux densities, dust color temperatures, and optical depth values were obtained in a self-consistent manner by numerically integrating the product of the Planck function (B_ν), emissivity function (given by $1-e^{-\tau_\nu}$, where τ_ν is given by the Mathis 1990 extinction law), filter transmission ($T_{atmosphere}$), solid angle subtended by the source with a measured size (a), and model atmospheric transmission (T_{filter}) through the filter bandpass (ν_1 to ν_2). Because this procedure depends on source size, the method employed for color correction depends on the whether or not the sources involved were resolved or not.

Resolved sources

The general equation for flux in the manner described above is given by

$$F_\nu = \left[\pi \cdot \left(\frac{a}{2}\right)^2\right] \cdot \int_{\nu_1}^{\nu_2} \left(1 - e^{-\tau_\nu}\right) \cdot B_\nu(T) \cdot T_{filter} \cdot T_{atmosphere}\, d\nu \qquad \text{Equation 1}$$

where a is the source size. For resolved sources, the source sizes were taken to be the N-band FWHMs subtracted in quadrature from the PSF FWHM. Since there are two observed fluxes (N and IHW18), one has a situation of two equations for flux and two

unknowns, T and τ, which can be solved for. Once one has a temperature for the program source, the flux can be multiplied by the color correction, which is given by the factor

$$\frac{\int \frac{B_\nu(T^s)}{B_{\nu 0}(T^s)} \cdot T_{atm}(\nu) \cdot T_{filter}(\nu) \cdot \left(\frac{1}{h\nu}\right) d\nu}{\int \frac{\left(1 - e^{-\tau_\nu}\right) \cdot B_\nu(T^p)}{\left(1 - e^{-\tau_{\nu 0}}\right) \cdot B_{\nu 0}(T^p)} \cdot T_{atm}(\nu) \cdot T_{filter}(\nu) \cdot \left(\frac{1}{h\nu}\right) d\nu} \qquad \text{Equation 2}$$

where T^s is the effective stellar temperature of the calibration star and T^p is the temperature derived above for the program source (Appendix B). This correction factor takes into account the difference in spectral slopes between the calibration star and program source through the filter bandpasses as well. These color-corrected fluxes are then fed back into Equation 1 and solved for a new T and τ, from which the fluxes are color-corrected again, etc. This procedure is done iteratively until the values for T an τ converge to their final values, and a final color correction can be applied to the fluxes yielding the final color-corrected fluxes listed in the tables throughout this work for resolved sources.

Unresolved sources with good S/N

For unresolved sources, calculations of color-corrected fluxes were made using the resolution limiting sizes and the blackbody limiting sizes, thereby yielding upper and lower limits on the true fluxes. From the equation (Appendix B)

$$\delta_r = 2 \cdot \sigma_{psf} \left(1 + \frac{\delta_{psf}}{\sigma_{psf}}\right)^{\frac{1}{2}}$$

where, δ_{psf} is the median size (FWHM) of the PSF star measurements throughout the night of observations and σ_{psf} is the standard deviation, one can get the resolution limiting size δ_r. The N-band resolution limiting size was chosen for the calculations. For the methanol maser observations at the CTIO 4-meter $\delta_r(N) = 0.55''$, and for the water maser sources at IRTF $\delta_r(N) = 0.26''$. These values were used for the source size, and color-corrected fluxes were found using the same iterative procedure for resolved sources as defined above.

The equation for the blackbody limiting size (or optically thick lower limit size), we have the following equation for flux

$$F_{\nu_{bb}} = \left[\pi \cdot \left(\frac{a_{bb}}{2}\right)^2\right] \cdot B_\nu\left(T_{bb}\right)$$

Again, since there are two fluxes, there are two equations, so one can solve for the two unknowns, a_{bb} and T_{bb}. This is merely the limit in which τ goes to infinity in Equation 1. Using the calculated T_{bb}, we can employ the same color-correction factor as above (Equation 2) to iteratively solve for the color-corrected fluxes in the blackbody lower-limit case.

Unresolved, low S/N sources

For extremely low S/N sources, one can not be sure what the sizes of the sources are. Therefore the calculations were performed in the limits where the sources are optically thick (blackbody limit) and optically thin. The blackbody limiting size

employed is the same as that defined in the last section. The equation for the optically thin case is given by

$$F_{\nu_{thin}} = (\Omega\tau) \cdot B_\nu(T_{thin})$$

In this limit, one can only solve for the $\Omega\tau$ product and T_{thin}, where Ω is $\pi \cdot (a/2)^2$. One again can iteratively solve for color-corrected fluxes using Equation 2.

Luminosities

Mid-infrared luminosities were computed by integrating the Planck function from 1 to 600 μm at the derived dust color temperature and optical depth for each source, again using the emissivity function $1-e^{-\tau}$, assuming emission into 4π steradians, and using the estimated distance, D, to the source

$$L = 4 \cdot \pi \cdot D^2 \cdot \left[\pi \cdot \left(\frac{a}{2} \right)^2 \right] \cdot \int_{1\ \mu m}^{600\ \mu m} \left(1 - e^{-\tau_\nu} \right) \cdot B_\nu(T)\, d\nu$$

This equation is for resolved sources, and is different for the blackbody and optically thin limits, since it is a function of source size, a. For the blackbody (optically thick) limit, the extinction term drops out, and the source size used is a_{bb}. For the optically thin limit this equation becomes

$$L_{thin} = 4 \cdot \pi \cdot D^2 \cdot (\Omega\tau) \cdot \left(\int_{1\ \mu m}^{600\ \mu m} B_\nu(T_{thin})\, d\nu \right)$$

where $\Omega\tau$ is the product found above.

Sources Observed in Only One Filter

The water maser selected survey was incomplete, with only one-third of the sources being observed with the IHW18 filter. For these and all other sources that were detected at only one wavelength, one can only report the observed flux densities, and cannot estimate a color temperature, optical depth, or luminosity.

Visual Extinction, Bolometric Luminosity, and Spectral Types

Visual extinctions associated with the mid-infrared emitting dust were found for the sources in the survey. These were calculated by using the derived emission optical depth values at 9.7 μm and the Mathis (1990) extinction law, which yields the relation $A_V = 18.09 \cdot \tau_{9.7\mu m}$. For instance, it was found that half of the sources in the methanol maser selected survey have $A_V > 2.5$ in the emitting regions. Thus, >90% of the visual radiation from the star is absorbed by the surrounding dust and converted into mid-infrared radiation, assuming 4π steradian coverage. However, depending on how deeply embedded the sources are, some reabsorption of the mid-infrared photons by the dust occurs, which further reprocesses them as far-infrared photons.

Combined with the assumption of 4π steradian coverage, the mid-infrared luminosities derived from the mid-infrared fluxes can be considered reasonable lower limits to the bolometric luminosities for these sources. Those estimates of the bolometric luminosities were used to estimate zero-age main sequence spectral types for the sources using the tables Doyon (1990), which are based on stellar atmospheric models Kurucz (1979). However, because the mid-infrared luminosity measurements are lower limits, the true spectral types of the sources are likely earlier than their calculated spectral types.

For the sources in this survey that have measured radio continuum fluxes, one can derive radio spectral types to compare with the spectral types derived from the mid-infrared observations. The Lyman continuum photon rates can be derived from the standard equation for free-free emission (Appendix B)

$$S_\nu = 3.24 \cdot 10^{-14} \left[\left(\frac{a}{0.994} \right) \cdot \left(\frac{T_e}{10^4 \cdot K} \right)^{-0.35} \cdot \left(\frac{\nu}{GHz} \right) \cdot \left(\frac{N_{lyc}}{\alpha_2} \frac{1}{cm^{-3}} \right) \cdot \left(\frac{D}{cm} \right)^{-2} \right] \quad mJy$$

where S_ν is the flux density at radio wavelength ν, T_e is the electron temperature which is taken to be 10,000 K from observations of typical HII regions (Dyson and Williams 1980), D is the distance to the source. The other parameters are a, which is a slowly varying function of frequency and electron temperature that has values very close to unity, and α_2 is the recombination coefficient ignoring recombinations to the ground level (Case B recombination), which has a value of 2.6×10^{-13} $cm^3 sec^{-1}$. This equation is solved for N_{lyc}, the Lyman continuum photon rate. From there the tables of Doyon (1990) were used to find the spectral type corresponding to that Lyman photon rate. This spectral type is a much more accurate estimate of the stellar spectral type because radio emission is not as effected by dust extinction.

Adopted Distances

Finding distances to the sources in this study pose a few problems. The methods available are crude and give only a general idea of how far these regions are from the Sun. All of the distances given in this study are kinematic distances. These distances are derived from some measurement of the radial velocity of the region in question. For instance, radio recombination lines from UCHII regions may be used to determine their radial velocities. Atomic transitions like HI, molecular line transitions like formaldehyde,

and even masers themselves can yield a radial velocity estimate for a region in space. When this radial velocity information is combined with a model for the rotation of our Galaxy, distances to sources may be determined. These rotation models for the Galaxy are usually simple formulas that relate distance from the Galactic Center, $\mathbf{R}_*$, with orbital velocity, Θ_*. The model used in this work is the galactic rotation curve of Wouterloot and Brand (1989), given by $\Theta_* = \Theta_o (\mathbf{R}_* / \mathbf{R}_o)^{0.0382}$, where Θ_o is the orbital velocity of the Sun around the center of the Galaxy, which is taken to be 220 km/sec, and $\mathbf{R}_o$ is the Sun's galactocentric distance which is taken to be 8.5 kpc. This particular rotation model was chosen simply because it was oft quoted in the literature. The obvious errors associated with this distance determination method are:

1. The distance will be dependent upon the Galactic rotation curve used. Most models like the one used here are simple power laws, and do not reflect accurately the true rotation of our Galaxy. From one rotation law to another, one may expect a difference in the distance estimates to be as high as 1 kpc, in the extreme.
2. The values used for the Galactocentric distance and orbital velocity of the Sun will affect the results. The present IAU accepted values are used in this work, however, some researchers still use the older values of Θ_o = 250 km/sec and $\mathbf{R}_o$ = 10 kpc, which are quite prevalent in the literature.
3. It is not known how accurately the radial velocities derived from atomic and molecular transitions mimic the holistic velocity of the region. For instance, Forster and Caswell (1989) used the radial velocities from OH masers to calculate the distances to the associated regions. However, if the OH masers are participating in an

outflow or are tracing some other dynamic process, the radial velocity measured will most certainly not be appropriate for determining the distance to the region.

Other uncertainties include small fluctuations due to turbulence, larger variations due to peculiar velocities and the fact that rotation models do not account for velocity variations due to galactic latitude and non-circular orbital motions.

Another problem arises when the source or region in question lies within the solar circle. When this is the case, the distance to the source cannot be simply determined from its radial velocity. If simple circular orbits are assumed around the Galactic center, a line of sight will cross an orbit at two points with the same velocity but different distances from the Sun. This leads to the kinematic distance ambiguity for sources within the solar circle, as they may lie at either the near or far distance given by a radial velocity. The only exception is when the source lies at a point in its orbit where it is tangent to the line of sight. This is where the radial velocity for a source it at its maximum, and there is no distance ambiguity.

There are some methods for determining the actual distance to a source. For instance, for nearby stellar sources, one can determine a star's spectral type and UBV flux. In this way, accurate spectrophotometric distances can be obtained. However, if one only has a near and far kinematic distance, the distance ambiguity may be resolved in three ways. First, if a HII region can be seen optically, it is believed to be evidence for it being at the near distance. However, absence of optical emission does not necessarily imply the far distance because the regions such as the ones in this survey suffer heavy optical obscuration. Second, in the case of star forming regions, the galactic latitude can be a helpful clue. Star-forming regions are mostly located in or near the galactic plane. If

a region has a galactic latitude greater than ~0.5°, it is most likely at the near distance, otherwise it would be located too far out of the plane of the Galaxy. Third, absorption components of radio spectral lines at smaller velocities than that of the radial velocity determined for the region or source, means the near distance is most likely. For instance, this method is employed by Kuchar and Bania (1990, 1994) using HI absorption towards Galactic plane HII regions. They first make the reasonable assumption that the line of sight to an HII region in the plane of the Galaxy will cross several HI clouds. The HI in front of the HII region will absorb the thermal continuum from the HII region. The distance ambiguity can be resolved by measuring the maximum velocity of the HI absorption. The HI gas at higher radial velocity than the HII region will be behind the HII region and will not contribute to the absorption spectra. Therefore the absorption spectrum will only show absorption up to the velocity of the HII region (as determined from recombination lines or masers). Likewise, absorption components with velocities greater than the velocity at the tangent point is evidence for it being located at the far kinematic distance. Forth and finally, one can make an argument based upon maser luminosities, as outlined in Caswell et al. (1995a). The usual assumption is employed that the maser emission beamed in our direction is representative of the intensity in other directions, and can be considered quasi-isotropic. The peak maser luminosity is defined as Fd^2, where F is the peak maser flux density in Jy and d is the distance in kpc. Caswell et al. (1995a) argues that the maser source in their survey with the highest flux density is G9.62+0.20 at 5090 Jy. At the well-determined near distance (from absorption measurements) of 0.7 kpc, its luminosity is 2500 Jy kpc^2. The highest luminosity sources in the survey of Caswell et al (1995a) are around 80,000 Jy kpc^2. Some sources in our

survey can be excluded from the far distance because their maser luminosities would be much larger than 80,000 Jy kpc^2. For instance, G323.74-0.26 has a maser luminosity of either 37,000 or 340,000 Jy kpc^2 given the near and far distances, respectively. While there is no theoretical reason precluding a maser achieving a luminosity as high as 340,000 Jy kpc^2, it is certainly far outside the norm, and thus the source is most likely at the near distance instead.

For the maser sources where the information was available, the HI absorption observations of Kuchar and Bania (1990, 1994) or the formaldehyde absorption measurements of Downes et al. (1980) were employed to determine whether to use the near or far kinematic distance. For sources where this information is unavailable, one of the other methods was used. The only source in methanol maser survey for which the distance ambiguity could not be resolved was the source G331.28-0.19. For this source the near distance is assumed. For the water maser survey, the results presented are not strictly dependent upon the distances to the sources. For those water maser sources where there is no data available to resolve the distance ambiguity, the near distance is assumed. Since the determination of distances to these sources is fraught with error, the values quoted throughout this work should be considered estimates only.

CHAPTER 5
METHANOL MASER SELECTED SURVEY

This chapter presents a mid-infrared imaging survey of 21 methanol maser sites. This particular set of sites was chosen because they were observed in the radio methanol maser survey of Norris et al. (1993). At the time the mid-infrared survey was conducted, the sources in the Norris et al. (1993) survey were the only sites available with accurate methanol maser positions (i.e. absolute astrometry better than 1″). Furthermore, OSCIR was a facility instrument at CTIO at this time, and all of the sources are located in the Southern Hemisphere.

The main thrust of the observations was to examine the theory of Norris et al. (1993) that linearly distributed methanol masers exist in and trace circumstellar disks around massive stars. Initially, this was to be accomplished by determining if the methanol masers were situated at the exact location of the mid-infrared source peaks. This is a necessary (but insufficient) condition if the methanol masers are tracing disks around these embedded stars. It was known from radio continuum measurements that water and OH masers generally are not coincident with UCHII source peaks, however no radio continuum survey was performed for these southern sources at the time of these observations. Only recently have most of these sources been observed for UCHII regions by Phillips et al. (1998). Unfortunately, the pointing accuracy of the CTIO 4-m, and hence the absolute astrometry of the mid-infrared measurements, was only accurate to

2.5″. This disappointment was soon alleviated with the resolution of three circumstellar disk candidates, a result that will be discussed in length in this chapter.

This chapter will begin with a discussion of each source observed. The first section of this chapter will include what is known about each source from the literature, and will describe briefly the mid-infrared observations of each. The second section contains a detailed discussion of the analysis and results of the survey.

Individual Sources

This section will review the available information for each maser site and discuss briefly the mid-infrared images that were obtained. The labeling convention for the mid-infrared sources is given by the International Astronomical Union and is in the form Glll.ll±b.bb:DPT00 #, where DPT00 stands for De Buizer-Pina-Telesco-2000 and the # is the source number. For instance, the field of G309.92+0.48 has three mid-infrared sources labeled G309.92+0.48:DPT00 1, G309.92+0.48:DPT00 2, and G309.92+0.48:DPT00 3. Often in this work these labels are shorten to "1", "2", and "3".

G305.21+0.21

This site contains both OH and methanol masers (Caswell, Vaile, and Forster 1995), and is located only 22″ to the east of G305.20+0.21. One or both of these two sites lie at the center of a large-scale CO outflow (Zinchenko, Mattila, and Toriseva 1995). The outflow is elongated predominantly east-west, extending for 2′. No radio continuum emission was found from this site by Phillips et al. (1998), with an upper limit on the 8.6 GHz peak flux density of 0.5 mJy beam^{-1}. Furthermore, Walsh et al. (1999) find no near-infrared source at this site in any of their passbands (J, H, K and L).

Walsh et al. (1997) believe the site is located at either 3.9 or 5.9 kpc, due to confusion associated with deriving kinematic distances based on methanol maser velocities. This disagrees with the distances of Caswell and Haynes (1987), who derive values of 2.9 and 7.0 kpc based on OH maser velocities. Caswell and Haynes (1987) also suggest that this object lies at the near kinematic distance (because the region can be seen optically), and therefore the near distance of Walsh et al. (1997) will be adopted for this source.

Norris et al. (1993) detected a linear distribution of four methanol masers spots from this site, with a clear monotonic spatial-velocity gradient. No source was detected at this site in either the N or IHW18 filters. Table 5-1 (located at the end of this section) indicates the 95% confidence upper limits for a point source detection.

G305.20+0.21

Figure 5-1 shows a strong 10 and 18 μm detection of a single, unresolved source. This appears to be the same source observed by Walsh et al. (1999) in the near-infrared. Norris et al. (1993) describe the distribution of masers here as compact, detecting only two methanol maser spots at this site, almost coincident with each other. Like G305.21+0.21, this site contains both OH and methanol masers. Phillips et al. (1998) find no 8.6 GHz radio continuum coincident with this source with a 0.9 mJy beam^{-1} upper limit. The distance is assumed to be the same as for G305.21+0.21. This source has an unusually high emission optical depth of $\tau_{9.7\mu m}$ =1.0, giving it the highest emission optical depth for any source in this survey and also the largest optical extinction at a value of A_V=18.1.

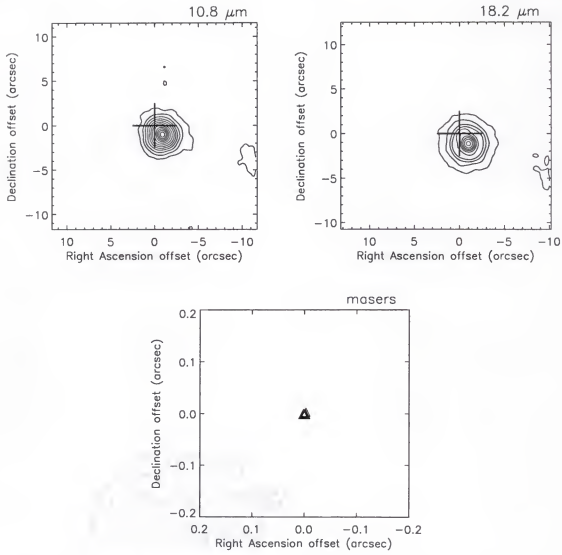

Figure 5-1: A three-panel plot for G305.20+0.21. The upper left is a contour plot of the observed N-band image, the upper right is a contour of the observed IHW18 image, and the bottom panel is the methanol maser spot distribution of Norris et al. (1993). The large crosses in the upper panels represent the location of the maser reference feature given our telescopic pointing. The thicker triangle in the lower panel denotes this maser reference feature, whose coordinates are given in Table 4-2. The size of the cross depicts the estimated error in relative astrometry between the reference feature and our telescopic pointing. In the lower panel, triangles represent 6.7 GHz methanol maser spots, and squares represent 12.2 GHz spots. The lower panel is on a larger scale for detail.

G309.92+0.48 (IRAS 13471-6120)

This site contains both OH and methanol masers, as well as radio continuum emission from a UCHII region. The OH and methanol spots are distributed along an arc that spans 1.1″ (Caswell 1997) and is concave to the southeast. The radio continuum peak is at the center of the arc. Norris et al. (1993) consider this site to have a well-defined velocity gradient in the 6.7 GHz methanol masers, and to be a disk candidate. Both methanol and OH spots show a velocity gradient, with increasingly negative velocities from north to south along the arc (Caswell 1997).

Walsh et al. (1997) find 9 methanol maser spots at 6.7 GHz (one more than Norris et al. 1993) lying at a tangent point distance of 5.4 kpc, which is slightly different than the distance of 4.7 kpc adopted by Norris et al. (1993). Walsh et al. (1997) also conclude that if the region were powered by a single star, it would have to be an O5.5 star with a luminosity of $3.1 \times 10^5 L_{sun}$ in order to explain the far-infrared (FIR) radiation observed by IRAS.

Walsh et al. (1998) report methanol maser positions that are offset 1″ from those of Norris et al. (1993). They also conclude that the methanol masers are slightly offset (0.1″) from their 8.64 GHz continuum peak. Their radio continuum observations show an azimuthally symmetric UCHII region. Phillips et al. (1998) observed the same UCHII region with an integrated flux density of 676 mJy.

The mid-infrared observations (Figure 5-2) show two resolved sources (1 and 2) at a position angle of 53°, both seen at 8.6 GHz by Phillips et al. (1998) and in the near-infrared by Walsh et al. (1999). A third source that is only seen in the mid-infrared in N-band to the west, has no associated radio continuum, but is seen in the near-infrared by

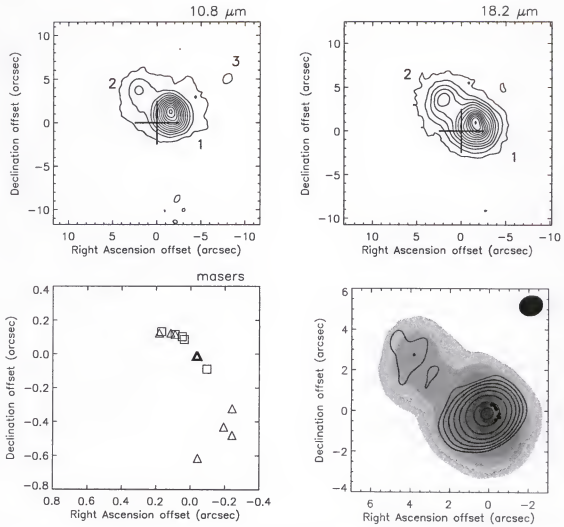

Figure 5-2: A four-panel plot of G309.92+0.48. The upper two, and lower left panels are set up the same as they are in Figure 5-1. The lower right panel shows the filled contours for our IHW18 image with the 8.6 GHz radio continuum image of Phillips et al. (1998) overlaid. The radio peak was assumed to be coincident with the mid-infrared peak. In the lower right panel, the methanol masers are shown as filled circles and the size of the radio Gaussian restoring beam is shown in the upper right of the panel. Notice that source 1 is elongated and arced in the opposite sense as the masers.

Walsh et al. (1999). At 18.2 μm, the central peak of source 1 is clearly arc-shaped and concave to the northwest in the opposite sense in comparison with the methanol masers.

Relative astrometry between the radio continuum sources and masers in Phillips et al. (1998) is stated as being better than 0.3″. Assuming radio continuum peaks are

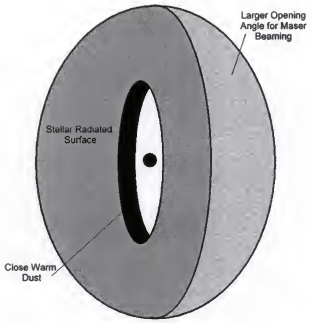

Figure 5-3: A possible model of G309.92+0.48. The black circle represents the massive star. The disk is flared, so the disk surface is irradiated by the central star (dark gray), and there is a large opening angle for the maser emission (light gray), increasing the likelihood of maser emission to be beamed towards the Earth. The bright mid-infrared emission would come from the close, warm dust near the inner edge of the disk (black) and the disk surface (dark gray).

coincident with mid-infrared peaks, the mid-infrared images were registered with those of Phillips et al. (1998) to obtain more accurate relative astrometry between the mid-infrared source 1 and maser positions (Figure 5-2, lower right panel). This technique yielded the result that the mid-infrared arc is located just southeast of the maser arc, and that they have similar extent.

There are two possible explanations for the nature of G309.92+0.48:DPT00 1. Since the masers are slightly offset from the radio continuum peak and follow the curves along the contours of constant intensity, it is plausible that they might be tracing a shock associated with the expanding UCHII region. An alternate explanation is that the arcs of methanol and thermal emission extending from the northeast to the southwest may be

tracing out a nearly edge-on flared disk (Figure 5-3). The northwest pole of the rotation axis would have to be tilted slightly away from us. In the mid-infrared, one would view the warm emission associated with the irradiated disk surface (and perhaps the inner hole). The maser photons, on the other hand, are coming through the flared edge of the disk closest to the Earth, where the line of site is unobscured at radio wavelengths. Maser photons beamed to us from the far side of the disk would not be seen, because they would have to travel through the HII gas below the disk, and would be absorbed.

G318.95-0.20 (IRAS 14567-5846)

Methanol masers were discovered at this site by Kemball, Gaylard, and Nicolson (1988) at the 12.2 GHz transition. Norris et al. (1993) show this site to have a linear distribution of seven methanol masers with a reasonable velocity gradient along them (Walsh et al. 1997 found 11 spots).

Walsh et al. (1997) find that the source may lie at kinematic distances of either 2.0 kpc or 10.9 kpc. Caswell et al. (1995) believe that the larger distance is more likely because they find no optical counterpart to this object. However, if this is the case, G318.95-0.20 would have one of the largest maser luminosities known to date (97,000 Jy kpc^2). Furthermore, given that the sources in this survey are highly embedded, one would not expect to detect anything in the optical, so the near distance given by Walsh et al. (1997) of 2.0 kpc is adopted here. Phillips et al. (1998) detect no 8.5 GHz continuum detected at this site, with an upper limit peak flux density of 0.7 mJy $beam^{-1}$.

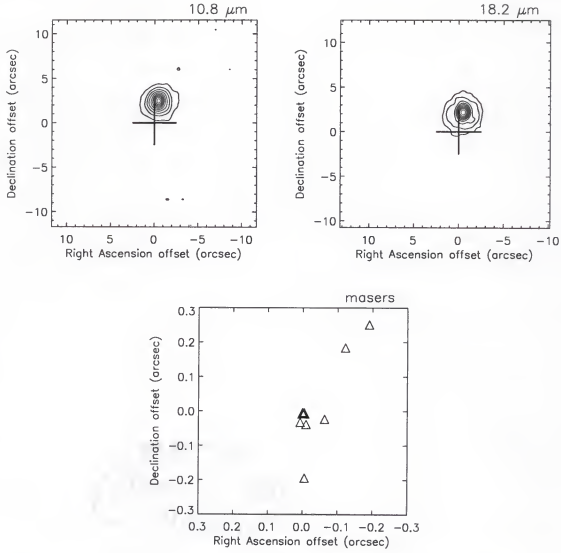

Figure 5-4: G318.95-0.20. Symbols and setup are the same as for Figure 5-1. This source appears elongated in the north-south direction, similar to the maser distribution. However, the PSF for this source is elongated in the same direction, and therefore the elongation is not believed to be real.

Ellingsen, Norris, and McCulloch (1996) estimate this to be the site of a star with a spectral type later than B2, as derived from their upper-limit non-detection of radio continuum at 8.5 GHz, and using a distance of 2.0 kpc. It was found that a single mid-infrared source is located here coincident with the near-infrared source seen by Walsh et

al. (1999), which is slightly elongated in the north-south direction, similar to the position angle of the maser spots (Figure 5-4). However, this source looks similar to the PSF star imaged near this position, and consequently the elongation in the source may not be real.

G323.740-0.263 and G323.741-0.263 (IRAS 15278-5620)

Like G318.95-0.20, Kemball, Gaylard, and Nicolson (1988) were the first to discover methanol masers at this location in the 12.2 GHz transition. This site contains two maser groups separated by 3.5″ (Phillips et al. 1998). The western grouping, G323.740-0.263, is the same observed by Norris et al. (1993), and the eastern maser grouping, G323.741-0.263, contains four maser spots distributed non-linearly. Due to the seemingly non-linear distribution of the western group of methanol masers, it is categorized as complex by Norris et al. (1993). The spots of G323.740-0.263 are not evenly distributed in a line or arc, and there is no clear velocity gradient. However, there may be two distinct lines of methanol masers crossing each other. Most points can be fit by two lines, with one at a position angle of ~300°, and the other ~20°.

Walsh et al. (1997) determined the distance to be 3.1 or 10.9 kpc. The near distance is adopted here based on the fact that at the far distance the peak maser luminosity would be abnormally large (340,000 Jy kpc^2). Using IRAS FIR fluxes, Walsh et al. (1999) determine that a single star would have a luminosity of 5.0×10^4 or 6.3×10^5 L_{sun}, with a spectral type of O8.5 or O5, respectively, for the two given distances. Phillips et al. (1998) detect no radio continuum in this area with a 4σ upper limit peak flux density of 0.2 mJy beam^{-1}.

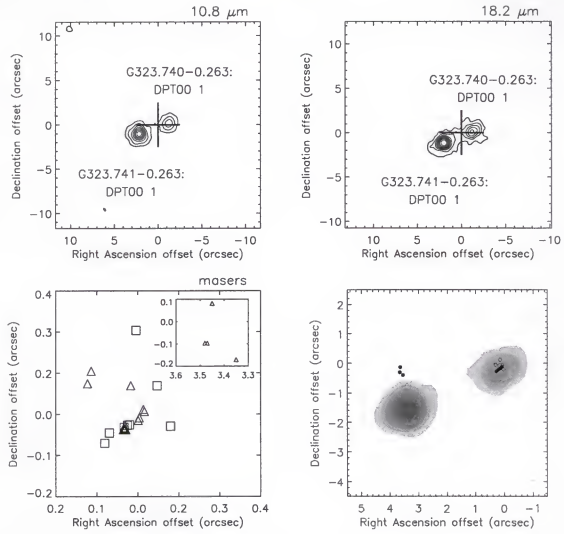

Figure 5-5: G323.74-0.26. Symbols and setup are the same as for Figure 5-2. This site contains both G323.740-0.263 and G323.741-0.263. The lower left panel shows the masers for G323.740-0.263, and the inset shows the masers of G323.741-0.263 which lie ~3.5″ to the east of G323.740-0.263. The lower right panel shows a filled contour plot of the IHW18 image with the masers overlaid as circles. The methanol masers in the western group are assumed to be coincident with the elongated western mid-infrared source, G323.740-0.263:DPT00 1. To more clearly show the line of masers associated with this source, the masers not in the linear distribution are shown as open circles. These may be tracing an outflow. The masers associated with the western mid-infrared source may also be tracing an outflow.

The mid-infrared observations of this site reveal a double source (Figure 5-5) that was also imaged by Walsh et al. (1999) in the near-infrared. The western source, which Walsh et al. (1999) detected only at L, is resolved and elongated in the mid-infrared at the

same position angle as the line of masers (300°) in G323.740-0.263. Note that a majority (12 of 17) of the 6.7 and 12.2 GHz methanol masers observed by Norris et al. (1993) at this site lie along the 300° line. The two distinct sites of methanol masers found by Phillips et al. (1998) have relative offsets similar to the offsets between the two mid-infrared sources (Figure 5-5, lower right panel). It can therefore be said with confidence that the line of masers in G323.740-0.263 is coincident with the elongated western mid-infrared source, in both location and position angle. The masers along this line may trace out a circumstellar disk, while the other remaining masers at the position angle of ~20° may be associated with an outflow (Phillips et al. 1998). The eastern mid-infrared source is unresolved. It lies 3″ away from the western source, which places the G323.741-0.263 masers seen by Phillips et al. (1998) just outside the mid-infrared contours of the eastern source. This maser group may exist in an outflow associated with the eastern source.

G328.24-0.55

This site lies approximately 82.5″ south and 13.0″ west of G328.25-0.53, and is assumed to be at the same kinematical distance. Walsh et al. (1997) determined the distance to the source to be 2.3 or 12.1 kpc, which generally agrees with Caswell et al. (1995) (2.6/11.8 kpc). Again Caswell et al. (1995) favor the larger distance because there is no optical counterpart, however the site has a galactic latitude greater than 0.5°. Therefore the near distance of 2.3 kpc is adopted here. The methanol spots are not distributed linearly, and according to Norris this source does not show a well-defined velocity gradient along the spots. Phillips et al. (1998) detect an 8.6 GHz continuum source at the location of the methanol masers with an integrated flux density of 27.7 mJy.

Phillips et al. (1998) suggest, among other scenarios, that since the masers are distributed in two clumps lying on either side of the UCHII region they may be tracing the two edges of a circumstellar disk, or two sources in a binary. No mid-infrared source was detected at this location with a 3σ upper limit on point source flux densities of 15 mJy at N and 179 mJy at IHW18.

G328.25-0.53

Walsh et al. (1997) find five masers at this site (same as Norris et al. 1993), and infer from the IRAS FIR flux that this area would contain a star with a luminosity of $4.3x10^4$ or $1.2x10^6$ L_{sun}, depending on the assumed kinematical distance (see G328.24-0.55). This corresponds to a spectral class of O9 or O4, respectively (Panagia 1973).

Phillips et al. (1998) detect no 8.6 GHz radio continuum at this site with a upper limit of 0.6 mJy $beam^{-1}$. The survey presented here, however, yielded the detection of two elongated low signal-to-noise sources at N, both of which are seen in the near-infrared by Walsh et al (1999). There is an additional source only seen at IHW18. The IHW18 detections are even lower S/N than the N-band detections (Figure 5-6). Using the mid-infrared astrometry alone, it is not clear which of the three sources the masers are associated with even though the pointing places them closest to source 2. However, the near-infrared imaging of Walsh et al. (1999) seems to confirm the association of the methanol masers with the source corresponding to the mid-infrared source 2.

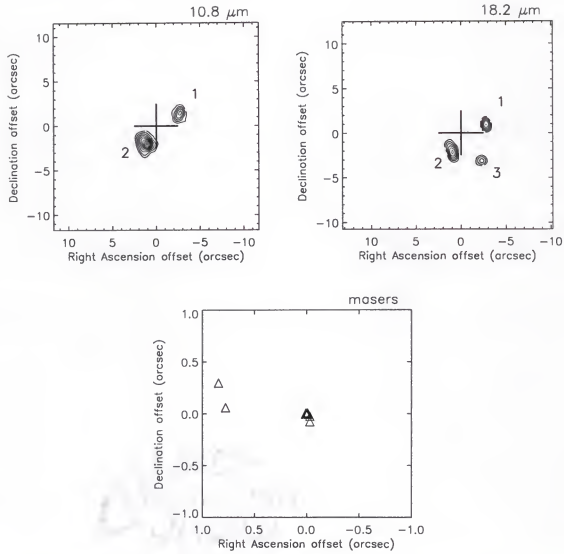

Figure 5-6: G328.25-0.53. Symbols and setup are the same as for Figure 5-1. All three mid-infrared sources have low S/N. Sources 1 and 2 are resolved and elongated. Source 2 is most likely the mid-infrared source associated with the methanol masers.

The five methanol masers are not distributed in a single line, but are in two tight groups separated by 0.8″, and are not considered linearly distributed by Norris et al (1993). Source 2 is elongated at a position angle of ~30°, and interestingly the western group of three masers are best fit with a regression line at an angle of 27°. One possibility is that the three masers are tracing a disk, and the other two masers could be excited by

an outflow or other stellar process. However, a maser grouping is not considered to be linear in this work unless there are at least four points in the linear distribution. Furthermore, it is unknown where exactly the methanol masers are with respect to source 2, and they may not be exactly coincident with the mid-infrared source.

G328.81+0.63 (IRAS 15520-5234)

This site contains OH and methanol masers, as well as prominent radio continuum emission (Caswell 1997). Caswell (1997) believes that there are perhaps two separate sites of maser emission, however they are only separated by 30 mpc, and the velocity ranges of the masers overlap. This site contains OH masers at the 1612, 1665, and 1667 MHz transitions (Caswell, Haynes, and Goss 1980), as well as the 1720 MHz (MacLeod et al. 1998) and 6.035 GHz OH maser transitions (Caswell and Vaile 1995). Methanol masers have been seen at both the 6.7 GHz transition (MacLeod, Gaylard, and Nicolson 1992; Norris et al. 1993) and 12.2 GHz transition (Norris et al. 1987). Though the methanol masers are distributed in a linear fashion, Norris et al. (1993) point out that there is no coherent velocity gradient along the spots. The OH and methanol masers at this site are intermingled spatially. Walsh et al. (1997) and Caswell et al. (1995a) detected 6 methanol masers from this region (Norris et al. 1993 found eight).

Caswell (1997) and Norris et al. (1993) both believe this source to be located at 2.6 kpc away. MacLeod et al. (1998) made formaldehyde measurements which lead to a near distance of 2.9 kpc, and a far distance of 11.7 kpc. These values are consistent with the near and far values given by Walsh et al. (1997) (3.2/13.6 kpc). Caswell et al. (1995) claim they prefer their larger kinematic distance of 11.9 kpc, because the site lacks an optical counterpart, but again, this is likely due to large extinction at optical wavelengths.

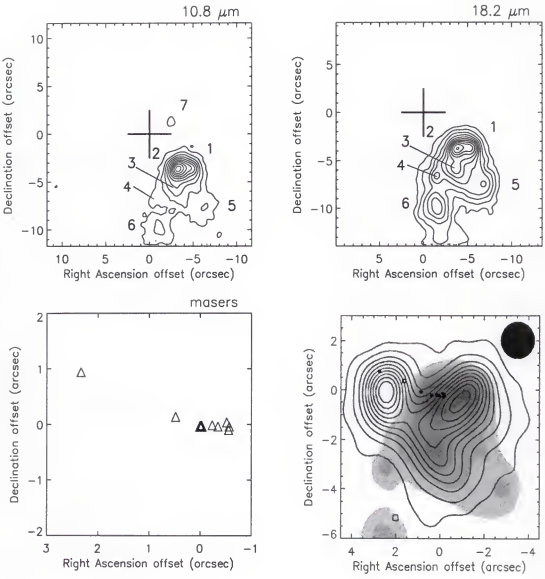

Figure 5-7: G328.81+0.63. Symbols and setup are the same as for Figure 5-2. By overlaying the 8.6 GHz radio continuum image of Walsh et al. (1998, lower right panel), we find that our astrometry as shown in the upper panels was off by almost 5″. The radio map traces our sources 1 and 3 well, however show no signs of source 2. Instead there is radio emission from an unresolved source to the east, that we do not see in the mid-infrared. Methanol masers are shown as filled circles. The methanol masers are distributed linearly over the mid-infrared peak of source 2. The open square is an OH maser from Caswell, Vaile, and Forster (1995). The size of the Gaussian restoring beam for the radio continuum is shown in the upper right of the plot.

It would seem that the near distance is probably the correct distance given the argument of Caswell (1997) who state that the far kinematic distance is unlikely in this case

because the source is greater than 0.5° from the Galactic plane. The near distance of MacLeod et al. (1998) will be adopted here, based on the fact that formaldehyde is most likely tracing the systemic motion of the molecular material in which the mid-infrared sources reside.

Caswell (1997) categorize this as one of the brightest "steep-spectrum" sources in the IRAS Point Source Catalog. This means that the spectrum of the source increases in flux rapidly towards longer infrared wavelengths, and it may indicate an early epoch in the formation of a massive star. They also observed G328.81+0.63 in 6 cm radio continuum. Using the IRAS FIR fluxes and a distance of 2.9 kpc, they estimate the spectral type of a single star in this area to be an O6.3, and using the 6 cm data they find a spectral type of O9.3. Walsh et al. (1997) concluded that the IRAS FIR flux would yield a 2.69×10^5 L_{sun} star with a spectral type of O6, if there were only one star responsible for the flux in this region. This is consistent with the findings of Caswell (1997).

Caswell (1997) finds an extended HII region with a flux density of 2 Jy, and an unresolved companion UCHII region with a flux density of 360 mJy ~3″ to the east. Walsh et al. (1998) detects both the compact and extended HII regions observed by Caswell (1997). Their astrometry places the maser group to the west coincident with the extended HII region peak, and the smaller maser group to the east coincident with the unresolved UCHII region. Osterloh, Henning, and Launhardt (1997) present a K′ (2.15 μm) image of this area. They determine it to be an embedded cluster of >4 stars sitting behind a foreground star, which precludes them from assigning the objects accurate K′ fluxes. They also find evidence for CO outflow using the deviation from the Gaussian profile in the CO(2→ 1) line.

Even contaminated with a foreground star in the K′ image, the near-infrared image of G328.81+0.63 looks similar to the mid-infrared images. However, with the observations in this survey having a factor of 3 better resolution than the K′ image and no foreground star, one can distinguish six separate objects in the IHW18 image (Figure 5-7). All six sources are not as prevalent in the N-band image (consistent with the IRAS steep-spectrum). The two brightest sources (1 and 2 in Figure 5-7) are close to each other but resolved (and perhaps a binary), and are coincident with the confused source at K′ of Osterloh, Henning, and Launhardt (1997). Once again the technique of registering the mid-infrared images with radio maps was used to achieve better relative astrometry between the mid-infrared sources and maser positions . In this case, the radio maps of Walsh et al. (1998) were used, and it was concluded that the western group of masers overlap the mid-infrared peak of source 2 (the mid-infrared pointing was poor, as seen in Figure 5-7), and are distributed at a similar position angle to that of the sources 1 and 2 (Figure 5-7, lower right panel). Sources 1 and 3 match the radio contours of the extended HII region seen by Walsh et al (1998). However, there was no detection of any mid-infrared object at the location of the compact HII region to the east, and it seems there is either a suppression or no radio continuum emission whatsoever associated with the mi-infrared source 2.

G331.28-0.19 (IRAS 16076-5134)

This site, according to Caswell et al. (1995b), is one of the few maser sites where the strength of the 12 GHz methanol masers rival that of the 6.7 GHz. Norris et al. (1993) find no coherent velocity gradient along the maser spots, though they are linearly

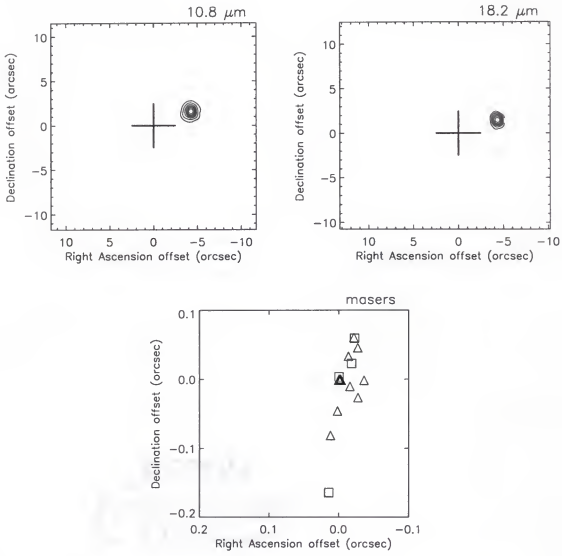

Figure 5-8: G331.28-0.19. Symbols and setup are the same as for Figure 5-1. The source appears elongated in the north-south direction, similar to the maser distribution. However, the PSF for this source is elongated in the same direction, and therefore the source elongation is assumed to not be real.

distributed. Whereas Norris et al. (1993) found nine 6.7 GHz methanol maser sources, Walsh et al. (1997) has found twelve.

Walsh et al. (1997) find that the sources lie at either 4.8 or 10.1 kpc. Norris et al. (1993) use the shorter distance, though they determined this distance to be 4.1 kpc. If this

site lies at the distance of 4.8 kpc, Walsh et al. (1997) derive a luminosity of 1.9×10^5 L_{sun} for a single star, which would be a spectral class of O6.5. At the larger distance, a single star would have a luminosity of 8.5×10^5 L_{sun} and have a spectral type of O5. The distance of 4.8 kpc is adopted here.

Henning, Chan, and Assendorp (1996) find this to be a site of an interesting 21 μm emission feature, as determined from IRAS LRS (Low Resolution Spectrometer) spectra. It is not known what the carrier of the 21 μm feature is, although the most accepted theories at present are that they are due to PAHs (polyaeromatic hydrocarbons) or PAH clusters (Hrivnak, Kwok, and Geballe 1994; Omont et al. 1995) or the inorganic substance SiS_2 (Goebel 1993). However, it should be noted that the LRS confusion limit is 6′, and these spectra may have very little to do with the source directly associated with the methanol masers.

Phillips et al. (1998) find an amorphous shaped 8.6 GHz continuum source (poorly imaged due to lack of short baselines for this observation) at the location of the masers with an integrated flux density of 4.1 mJy. The mid-infrared images (Figure 5-8) only show one source which is very slightly elongated north-south at a similar position angle as the methanol masers. However, the PSF for this object appears similarly elongated and comparable in extent. It was concluded that this mid-infrared source is unresolved. It is also not clear if the masers or the radio continuum source are directly associated with this mid-infrared source, given the fact that they are over 4″ west of the mid-infrared pointing center. Walsh et al. (1999) also fails to detect a source in the near-infrared coincident with the masers, but finds a elongated source ~2″ to the west. This

elongated near-infrared source may be associated with the source seen in the mid-infrared.

G336.43-0.26 (IRAS 16306-4758)

Norris et al. (1993) find this site to contain five 6.7 GHz methanol masers arranged in an arc and displaying an strong systematic velocity gradient. However, Caswell et al. (1995a) and Walsh et al. (1997) find eight methanol maser spots in all. Caswell et al. (1995a) also did not find any evidence for OH emission from this area. Furthermore, Phillips et al. (1998) detect no 8.6 GHz continuum here at a flux density limit of 0.3 mJy beam^{-1}.

Walsh et al. (1997) determined the distances to this site to be either 5.9 or 9.9 kpc, and so the near distance is adopted here. They give no estimate of the luminosity or spectral types for a single star at these distances because the FIR fluxes from IRAS are only given as upper limits. Walsh et al (1999) does not detect any near-infrared source coincident with the masers. Likewise, no mid-infrared sources were detected at this location, with upper limit flux densities of 14 mJy for N-band and 177 mJy for IHW18 with a confidence level of 95%.

G339.88-1.26 (IRAS 16484-4603)

Ellingsen, Norris, and McCulloch (1996) produced the first radio continuum image of this site at 8.5 GHz with an integrated flux density of 14 mJy. Their image is mostly unresolved but does show some extension in the northeast direction, which they suggest may be a UCHII region with a cometary morphology. In contrast, Walsh et al. (1998) present 8.6 GHz radio maps of the region showing a just unresolved, almost

circular source. However, there are slight elongations in the northeast and northwest directions.

Ellingsen, Norris, and McCulloch (1996) consider this to be one of the strongest sites of methanol maser emission at both 6.7 and 12.2 GHz. The maser spots of Norris et al. (1993) lie across the radio source almost perpendicular to the position angle of the continuum extension. Two OH masers are known to straddle the methanol masers in both the north-south and east-west directions (Caswell, Vaile, and Forster 1995). An H_2O maser is also known to exist ~1″ south of the methanol masers Forster and Caswell (1989).

Caswell et al. (1995a) and Walsh et al. (1997) find there to be twelve 6.7 GHz methanol masers here, whereas Norris et al. (1993) finds only 8. Norris et al. (1993) show this source to have a velocity gradient (except for their maser spot 'a') in the 6.7 GHz masers, whereas at 12.2 GHz there is no clear velocity gradient. Walsh et al. (1997) determine the distance to this site to be either 3.1 or 12.9 kpc, and since the galactic latitude is greater than 0.5°, the near distance is adopted here. If this site were to contain only one star, IRAS FIR fluxes would lead to a luminosity of 8.0×10^4 L_{sun} or 1.4×10^6 L_{sun}, with spectral types of O7.5 or earlier than O4, depending on distance.

This site was first imaged at 10 μm by the TIMMI instrument at the ESO 3.6-m telescope in March of 1998 by Stecklum and Kaufl (1998). They found a 10 μm source and assume that this is a circumstellar disk due to the elongation they observe, combined with the apparent coincidence of the position angles of the elongation and the methanol maser linear distribution. This elongation is also observed by Walsh et al. (1999) in the L-band. The mid-infrared observations show this site to contain at least two sources in

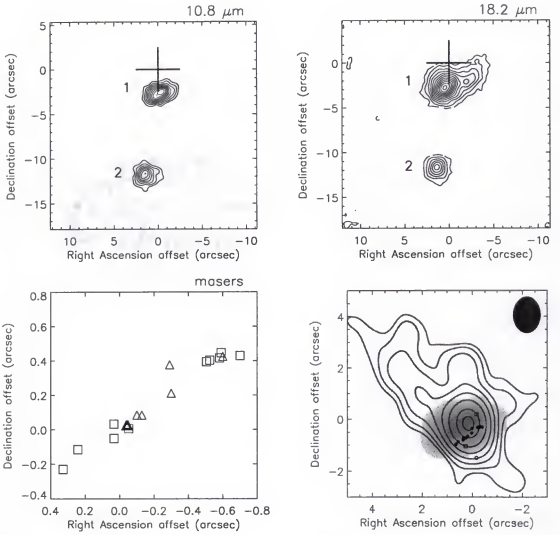

Figure 5-9: G339.88-1.26 Symbols and setup are the same as for Figure 5-2. Source 1 is clearly elongated at N, however there may be another source seen at IHW18 just to the west. The lower right panel is a filled contour plot of source 1 at N with the 8.5 GHz radio continuum image of Ellingsen et al. (1996) overlaid. Methanol masers are shown as filled circles and are distributed at the same position angle as the mid-infrared elongation of source 1. The radio continuum seems to be extended perpendicular to the mid-infrared source elongation, and may be tracing an outflow. The OH masers of Caswell, Vaile, and Forster (1995) are shown as open squares, and the water maser of Forster and Caswell (1989) is marked by the open circle. The size of the Gaussian restoring beam for the radio continuum is shown in the upper right of the plot.

the mid-infrared (Figure 5-9, sources 1 and 2). The more northerly source, 1, is the source imaged by TIMMI and by Walsh et al. (1999), but actually may be a double source,

appearing clearly elongated in the northwest direction at N, and appearing as two components at IHW18. The lower right panel of Figure 5-9 shows the radio continuum of Ellingsen, Norris, and McCulloch (1996) and the methanol masers overlaying the mid-infrared filled contour map of source 1 at N. It was assumed here that the radio peak coincides with the peak at N. It is clearly seen that the elongation in the infrared is similar to the position angle of the distribution of methanol masers. Furthermore, the ionized gas is elongated in a direction almost perpendicular to the mid-infrared elongation, perhaps tracing an outflow from the disk.

G340.78-0.10 (IRAS 16465-4437)

This is a site of OH masers, as well as methanol, and also contains a weak (9 mJy) UCHII region at 6.0 GHz detected for the first time by Caswell (1997). The OH and methanol masers found here overlap spatially and in velocity as well. Caswell (1997) observed this site over a larger velocity range than Norris et al. (1993), and observed more methanol maser spots. Caswell (1997) found this location to contain the largest velocity spread (-112 to -86 km/sec) of any known maser site. Later observations by Phillips et al. (1998) confirm this velocity range, and resolve 19 maser spots. They also detect the weak UCHII region seen by Caswell (1997). It is argued by Caswell (1997) that the kinematic distance to this site is unambiguously 9 kpc, because the systemic velocity of the region indicates a location near the tangent point, so this distance is adopted here.

The methanol maser spot morphology is very complex. It appears that the masers lie in two distinct lines: one north-south and one east-west all contained within 1 square arcsecond. Caswell (1997) suggests that this might be the site of two stars surrounded by

two toroids. Features in the north-south line within the velocity range of -92 and -86 km/sec have a velocity field more indicative of outflow, rather than rotation. Norris et al. (1993) do not find any significant velocity gradient in either of the two linear maser structures.

Like the near-infrared survey of by Walsh et al. (1999), the mid-infrared observations yielded no detection of any sources. An upper limit on the point source flux density of an N-band source is 15 mJy and 177 mJy for IHW18 with a 95% level of confidence.

G345.01+1.79

This site has methanol and OH masers, and is coincident with a UCHII region (Caswell 1997; Caswell et al. 1995a). Walsh et al. (1997) determine the distance to this site to be either 2.1 or 14.5 kpc. This is in fair agreement with Caswell (1997) who derives distances of 2.6 and 13.9 kpc. Since this site has a galactic latitude greater than 0.5°, the near value of Walsh et al. (1997) of 2.1 kpc seems reasonable. Using the distances of Walsh et al. (1997), this would yield a single star of 8.5×10^4 or 4.0×10^6 L_{sun}, and a corresponding spectral type of O7.5 or < O4, depending on which distance was chosen.

The methanol masers here are distributed in a linear fashion and show a moderately systematic velocity gradient among the spots Norris et al. (1993). They seem to be offset from the peak of the radio continuum by approximately 0.5″ to the west. The UCHII region has an integrated flux density of 260 mJy (Caswell 1997). Walsh et al. (1998) confirm the displacement of the masers with their 8.6 GHz radio map of the area,

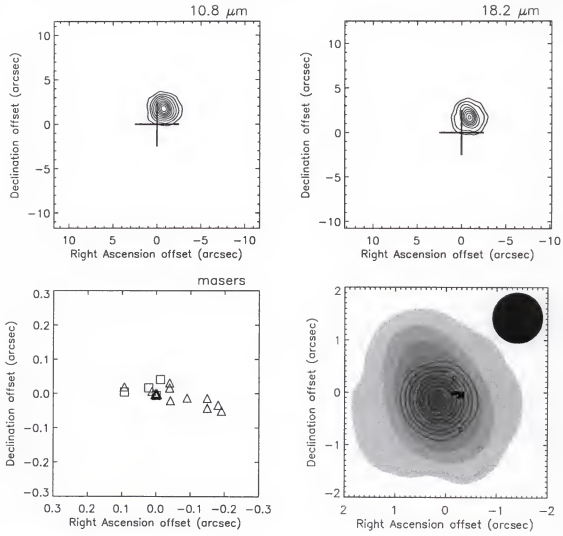

Figure 5-10: G345.01+1.79. Symbols and setup are the same as for Figure 5-2. The source appears elongated at IHW18. However, the PSF for this source is elongated in the north-south direction, and therefore the source elongation may not real. The lower right panel is a filled contour plot of the IHW18 image with the 8.6 GHz radio continuum image of Walsh et al. (1998) overlaid. Methanol masers are shown as filled circles and seem to be distributed radially to the radio continuum, and perpendicularly to the mid-infrared elongation. If the elongation is real, the methanol masers may be tracing an outflow. The OH masers of Caswell, Vaile, and Forster (1995) are shown as open squares. The size of the Gaussian restoring beam for the radio continuum is shown in the upper right of the plot.

and conclude that the masers extend radially with respect to the circular UCHII region. These masers could be indicative of outflow. The two OH masers lie above and below the methanol maser distribution.

Walsh et al. (1999) observed this site in the near-infrared and find a single source visible only at L. A single bright mid-infrared source (Figure 5-10) was found here coincident with the near-infrared source, that may be marginally resolved at IHW18. It is appears slightly elongated in the northeast direction, at a position angle that differs from the methanol maser position angle by about 50°. However, the two OH masers lie at a position angle close to that of the mid-infrared elongation. The PSF image taken at this location is elongated north-south, so it is uncertain if the source is truly elongated. If the source elongation is real, this is a large discrepancy in position angle between the methanol maser distribution and mid-infrared elongation angle. Given the fact that these methanol masers are offset from the center of the UCHII region by 0.5″ and distributed radially, they may be tracing an outflow, as suggested by Walsh et al. (1998), and the OH masers may be coming from a disk in the perpendicular direction whose elongation may be marginally resolved in the mid-infrared image.

G345.01+1.80

This site lies only 19″ away from G345.01+1.79. Caswell (1997) finds no UCHII region at 6 GHz, and neither does Phillips et al. (1998) with an upper limit on the peak 8.5 GHz continuum emission of 0.7 mJy beam^{-1}. Walsh et al. (1999) also failed to detect a source at this location in the near-infrared. Interestingly, this site has also been found to contain no OH maser emission. Caswell (1997) confirm the Norris et al. (1993) observations of the existence of a linear distribution of four methanol maser sources, spread over 0.22″ with three of the four spots showing a velocity gradient. The same kinematic distance to this region is adopted as for G345.01+1.79.

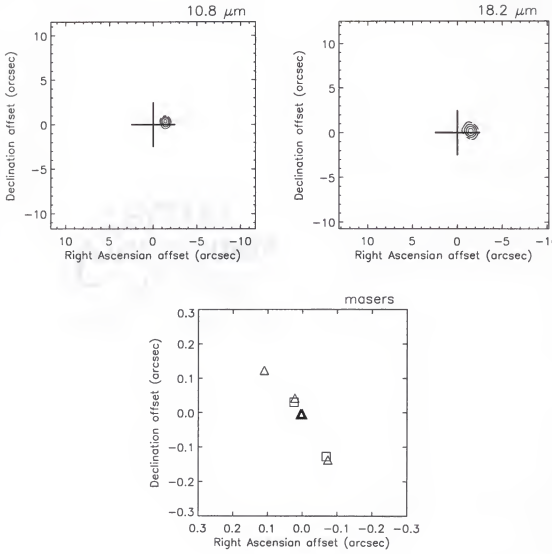

Figure 5-11: G345.01+1.80. Symbols and setup are the same as for Figure 5-1. The source has very low signal-to-noise.

The mid-infrared images reveal the discovery of a weak mid-infrared source at a low S/N at both N (S/N ~ 4) and IHW18. Because of the low S/N, nothing can be said about the morphology of the source other than it looks at this detection level to be point-like (Figure 5-11).

G351.42+0.64 (NGC6334F and NGC6334F-NW)

G351.42+0.64 is the location of a well-known cometary-shaped UCHII region named NGC6334F (Rodriguez, Canto, and Moran 1982). The methanol masers are known to exist here in two sites separated by about 6″ (Norris et al. 1998).

The southern group of methanol masers is associated with NGC6334F and are accompanied by OH masers, which run in a north-south line (Caswell 1997). Approximately 4″ north of the OH masers, water masers are known to exist in a linear pattern, pointing radially north away from the UCHII region peak (Carral et al. 1997). The distribution of methanol masers in NGC6334F does not appear to be linear, but does have a similar velocity range to that of the OH masers (-13 to -6 km/sec; Caswell 1997, Caswell et al. 1995a), and does not display a systematic velocity gradient (Norris et al. 1993).

Caswell (1997) find no 6 GHz radio continuum (same as Ellingsen, Norris, and McCulloch 1996) at the northern methanol maser site, NGC6334F-NW. Also, NGC6334F-NW does not have any associated OH or water masers. Again, there is no velocity gradient along the spots in the northern group.

Walsh et al. (1997) determined a distance to this site of either 1.9 or 12.9 kpc. This near distance is slightly different than the accepted value of 1.7 kpc, photometrically found by Neckel (1978). At the distance of 1.9 kpc, Walsh et al. (1997) determine this site would contain an O7 star with a luminosity of 1.1×10^5 L_{sun}, if it contained one star. The more accurate photometrically-derived distance of 1.7 kpc for this source will be used here.

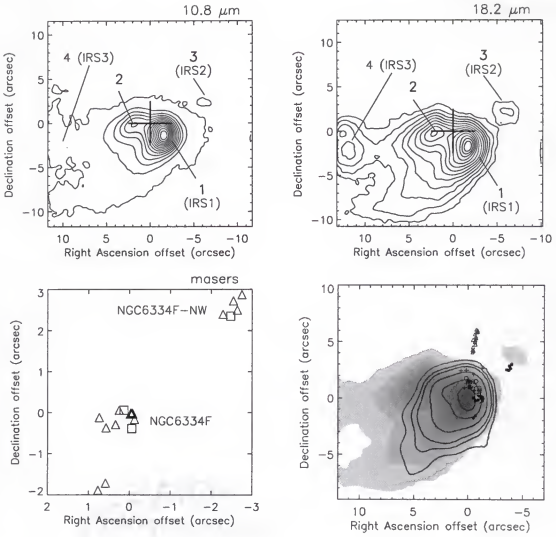

Figure 5-12: G351.42+0.64. Symbols and setup are the same as for Figure 5-2. Our source 1 is coincident with the UCHII region NGC 6334F, which is also known as IRS1 (Harvey and Gatley 1983). Source 3 is known as NGC 6334F-NW, or IRS2. Source 4 is also known as IRS3. The lower right panel is a filled contour plot of the IHW18 image with the 6.7 GHz radio continuum image of Caswell (1997) overlaid. Methanol masers are shown as filled circles. The OH masers of Gaume and Mutel (1987) are shown as open circles, whereas the OH masers of Forster and Caswell (1989) are shown as crosses. The OH masers and methanol masers seem mixed both spatially and in velocity, and most likely trace the shock associated with the sharp western boundary of the expanding UCHII region. The methanol masers near source 3, are not coincident with the mid-infrared source, and may be tracing an outflow. The water masers of Forster and Caswell (1989) are also plotted here as triangles, and may be tracing an outflow from source 1 as well.

Harvey and Gatley (1983) observed 20 μm infrared sources at the locations of both NGC6334F-NW (to within 1″, named IRS2) and NGC6334F (IRS1). The mid-infrared images reveal at least four sources in this region (Figure 5-12). The UCHII region NGC6334F is very prominent, and labelled source 1 in Figure 5-12. The infrared source associated with NGC6334F-NW (source 3) can best be seen at IHW18. Just to the east of the UCHII region is an elongated mid-infrared object (source 2).

Another source (or sources) is seen about 14″ east of the NGC6334F (source 4). This is designated IRS3 by Harvey and Gatley (1983). IRS3 appears to be a double source in the IHW18 images positioned in the north-south direction. It might also be an edge on circumstellar disk, as pointed out by Kraemer et al. (1999), who base this assumption upon morphology only.

Once more the technique of registering the mid-infrared images with radio maps to achieve better relative astrometry between the mid-infrared sources and maser positions was performed. In this case the radio maps of Caswell (1997) were used, and it can be concluded that the southern methanol masers seem to be located at the sharp western boundary of the mid-infrared contours of the UCHII region (source 1, see Figure 5-12, lower right panel). These masers may therefore be associated with a shock front, rather than a circumstellar disk. This astrometry also places the northerly group of methanol masers about 1.5″ below source 3. These masers may also be tracing an outflow or shock region rather than a disk.

This area is also the site of a large-scale CO outflow, with a lobe redshifted in the northeast direction and another blueshifted in the southwest direction. Some authors speculate that NGC6334F-NW may have a disk and be the source of the outflow,

however the thermal images show this source to be resolved and elongated in the east-west direction, and the position angle of the source elongation is not parallel to that of the methanol maser distribution nor perpendicular to the outflow axis. Other authors speculate that NGC6334F is the center of the outflow, but water masers are seen emanating to the northwest in a linear fashion and are thought to be tracing an outflow or jet (Figure 5-12, lower right panel). If this is the case, NGC6334F would most likely not be the source of the outflow to the northeast as well. The elongated source 2 is near the center of the CO outflow and is perpendicular to the outflow axis. This could mean that source 2 may be a disk, and the outflow may originate there. Source 3 (NGC6334F-NW) may be a disk, but the methanol masers may instead trace a southerly outflow since they are offset from the mid-infrared peak and distributed almost perpendicular to the mid-infrared elongation.

G351.44+0.66

Although included in their survey, Norris et al. (1993) do not present any data on this source, and there was no detection any objects at this site in the mid-infrared. There is also a dearth of information in the literature on this particular site as well. Therefore this object will not be considered any further in this work, but only to mention it here for completeness.

G351.77-0.54 (IRAS 17233-3606)

This site contains the largest peak intensity of any known OH maser, at 1000 Jy (Caswell et al. 1995). It is also found to contain a highly variable OH and methanol maser (Fix et al. 1982; Caswell et al. 1995a). Norris et al. (1993) only found four methanol

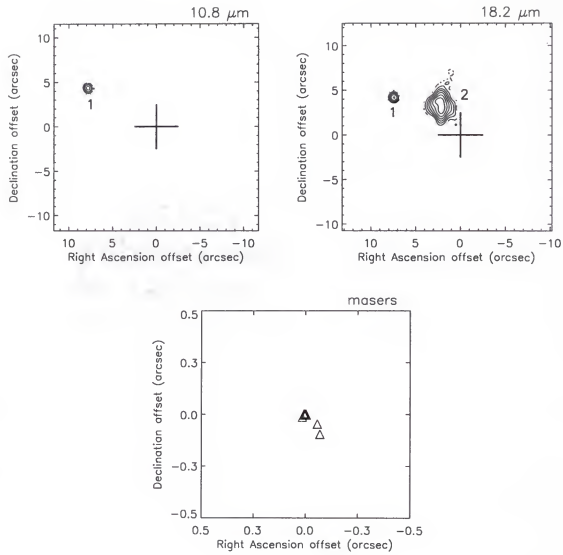

Figure 5-13: G351.77-0.54. Symbols and setup are the same as for Figure 5-1. It is not known if source 2 is real. Both sources are low signal-to-noise detections.

masers here coincident with the location of these OH masers, and they display a well-defined velocity gradient along the spots. Forster and Caswell (1989) detected a water maser about 3″ west of the OH and methanol maser location.

Walsh et al. (1997) found four methanol sources here, like Norris et al. (1993), but could not determine a useful distance to the site because of large errors associated with the observations of this location. However, Caswell (1997) determined the distance

to be either 1.9 or 15.0 kpc and reason that the far distance is unlikely because the source is greater than 0.5° from the Galactic plane. Therefore the near value of 1.9 kpc from Caswell (1997) is adopted.

This is another site considered by Caswell (1997) to be a "steep-spectrum" IRAS point source. They derive the spectral type (using their distances above) for a single star based upon the FIR IRAS data to be B0.0, and from their radio work B0.3 for 6 cm or B0.4 for 20 cm emission.

Fix et al. (1982) observed this site at 5 and 1.4 GHz and find a large, amorphous continuum source (310 mJy at 5 GHz) lying almost 12″ directly east of the OH maser location. Haynes, Caswell, and Simons (1979) observed a very weak continuum source at the location of the OH masers at 5 GHz, which Fix et al. (1982) also sees weakly (3 mJy) in the same location at 5 GHz but not at 1.4 GHz. Walsh et al. (1998) also detected the extended continuum associated with the UCHII region lying 12″ to the east of the OH masers at 8.6 GHz. However, they find nothing at the maser location. Hughes and MacLeod (1993) believe that they have discovered a binary source associated with the location of the OH and methanol masers at a resolution of 0.3″ at 6 cm. They also see the diffuse continuum source 12″ to the east. They believe that this diffuse source contains about 12 B0.5 stars.

Fix et al. (1982) and Walsh et al. (1999) also observed K-band sources at both sites. Fix et al. (1982) claim the near infrared object at the location of the masers is extended (15-20″ in diameter) and has uniform surface brightness (K=10.7). However, images by Walsh et al (1999) show that these may be several field stars, but they do find a single source coincident with the methanol masers at L and a source coincident with the

extended radio emission to the east. Fix et al. (1982) looked for, but did not detect any 10 μm sources, but they did find evidence for extended CO emission in the area.

Caswell (1997) points out that the velocity spreads in all the maser types are large. The water masers at this site observed by Forster (1990) covered a velocity range of -38 to +22 km/sec. They are also arranged in a circular fashion over an area on 4″. Some are found to be blueshifted and others redshifted, and the overall geometry is similar to that of an expanding ring. They conclude that the compact size, wide velocity spread in the masers, and a lack of strong continuum emission points to this being a star in some kind of expansion phase (Forster and Caswell 1989). They also point out that the geometry may be due to outflow of some kind.

This survey yielded the detection of a compact, low S/N object at a location about 10″ east of the position of the methanol masers (Figure 5-13, source 1). Also detected was a very diffuse and large extended object (source 2) about 3″ northeast of the maser location. At such a low detection level it is difficult to comment much on the morphologies or coincidences of these sources.

G9.621+0.196 and G9.619+0.193 (IRAS 18032-2032)

This region contains two methanol maser sites separated by ~12″ in declination. The northern site, G9.621+0.196, contains a 6.7 methanol maser with the highest flux known. Norris et al. (1993) observed methanol masers at both sites and consider them to be compact or complex, with no linearly distributed methanol masers. Forster and Caswell (1989) also found OH masers coincident with the two groups of methanol masers.

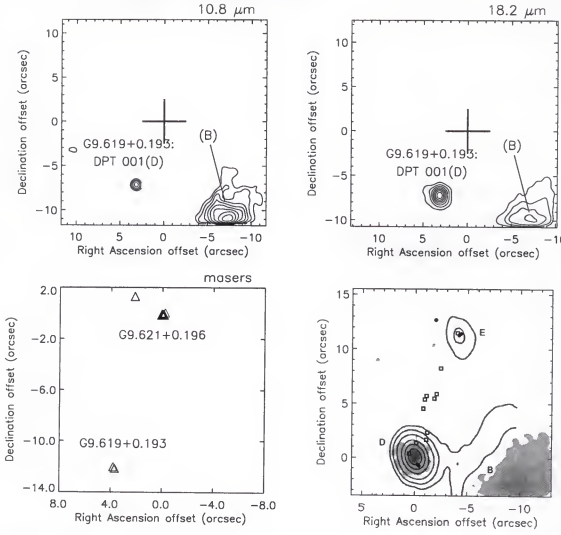

Figure 5-14: G9.62+0.19. This site contains both maser sources G9.621+0.196 and G9.619+0.193. We detected a mid-infrared source associated with G9.619+0.193 only. Labels in parentheses are sources from Garay et al. (1993). Symbols and setup are the same as for Figure 5-2. The lower right panel is a filled contour plot of the IHW18 image with the 23 GHz radio continuum image of Cesaroni et al. (1994) overlaid. The radio continuum sources B, D, and E (using the nomenclature of Garay et al. 1993) are indicated. Methanol masers are shown as filled circles. The water masers of Hofner and Churchwell (1996) are shown as open squares, and form a line stretching from radio components D to E.

Norris et al. (1993) observed 5 masers at the location of G9.621+0.196. It was also found to contain a 19 mJy source at 15 GHz by Garay et al. (1993), which they call source E. Nothing was detected in the 8.6 GHz maps (3.5 cm) of Walsh et al. (1998), or

the 3.6 cm continuum map from the VLA by Kurtz, Churchwell, and Wood (1994). However, Cesaroni et al. (1994) and Hofner and Churchwell (1996) did observe a source at the location of G9.621+0.196 at 1.3 cm. Not only is this source coincident with a thermal ammonia core, but among the methanol masers is located the first ever discovered $NH_3(5,5)$ maser (Cesaroni et al. 1994).

The southern site, G9.619+0.193, was found to contain two 6.7 GHz methanol masers by Norris et al. (1993). It also contains a 110 mJy source observed at 15 GHz by Garay et al. (1993), which was named source D. Walsh et al. (1998) find a single unresolved 8.6 GHz (3.5 cm) continuum source in this location coincident with two methanol masers, whereas Kurtz, Churchwell, and Wood (1994) did not. Hofner and Churchwell (1996) and Cesaroni et al. (1994) find 1.3 cm radio emission at this location, as well. Walsh et al. (1998) point out that the G9.619+0.193 methanol masers associated with the D source are offset about 1″ to the south of the peak in the radio continuum emission.

This site also contains a large (~15″), diffuse and amorphous HII region located west and south of G9.619+0.193 by about 14″ (Walsh et al. 1998; Hofner and Churchwell 1996; Kurtz, Churchwell, and Wood 1994). Cesaroni et al. (1994) detect the 1.3 cm continuum of this large HII region. Garay et al. (1993) detect this site at 15 GHz and call it source B. Continuum maps at 2 and 3.6 cm at the VLA by Kurtz, Churchwell, and Wood (1994) show the source as well.

Interestingly, there is a string of water masers found by Hofner and Churchwell (1996) extending from the location of the methanol masers at G9.621+0.196 to the methanol masers at G9.619+0.193. Also, found lying stretched between the two locations

is thermal ammonia emission (Hofner et al. 1994). This may be another case where the water masers are coincident with embedded sources that are being traced by the ammonia emission.

Cesaroni et al. (1994) detect an additional continuum source further north of G9.621+0.196. To use the nomenclature of Garay et al. (1993), the source furthest to the north is the C source. Continuum maps at 2.0 and 3.6 cm at the VLA by Kurtz, Churchwell, and Wood (1994) show C. Another source, source A of Garay et al. (1993), is further west of the HII region B, and is another large (30″) and diffuse HII region.

There is considerable disagreement in the distance to this site. Wink, Altenhoff, and Mezger (1982) derived distances of 0.6 and 19.1 kpc, and consider the near distance most likely based on the absence of H_2CO absorption. Garay et al. (1993) feel that the source lies at a far distance of 16.1 kpc, based on the observed UV-to-radio luminosity ratio. Kurtz, Churchwell, and Wood (1994) obtained near and far distances of 0.7 and 16.1 kpc, consistent with the distance of Wink, Altenhoff, and Mezger (1982). Walsh et al (1997) could not determine a distance to this site due to large errors. A distance of 0.7 kpc seems to be the best distance because it is based on absorption line measurements.

This seems to be a very complex site which appears to be a ridge of molecular material, as evidenced by the string of water masers and elongated distribution of thermal ammonia, where star forming activity is present in several locations. The mid-infrared observations reveal the large diffuse HII region (source B of Garay et al. 1993, see Figure 5-14), as well as an unresolved mid-infrared source at the location of the southern maser location G9.619+0.193. Interestingly, Walsh et al. (1999) found no evidence of a near-infrared source at this location. Like Walsh et al. (1999), there are no signs of a thermal

infrared source at the site of the northern masers of G9.621+0.196, nor the most northern radio source C (source A was not in the field).

Results and Discussion

A summary of the derived and adopted quantities and properties of the sources in the methanol maser selected survey, as discussed in the last section, are given in Table 5-1. Sources marked with an 'm' are those most likely associated with the maser emission.

Summary of Mid-Infrared Sources Associated with Linearly Distributed Methanol Masers and the Circumstellar Disk Candidates

In this mid-infrared survey of 21 sites, 10 have methanol masers distributed linearly. Of those 10, mid-infrared sources were detected in 8. Three of those eight sites have sources which are resolved at mid-infrared wavelengths by this survey. All three resolved sources are elongated at the same position angle as their associated methanol masers. These sources are G309.92+0.48:DPT00 1, G323.740-0.263:DPT00 1, and G339.88-1.26:DPT00 1, all of which appear the most elongated at 18 μm. Interestingly, the three resolved sources are in close proximity to other sources which lie at similar position angles to the maser distribution angles.

Of the remaining five mid-infrared source detections where the methanol masers are linearly distributed, there appears to be an elongated source associated with G328.81+0.63:DPT00 2, which is in a close pair of sources. By subtracting out a Gaussian model for source 1, it was effectively removed from the image, leaving an elongated source 2. This may be another case where one source in a double is elongated

Table 5-1: Physical parameters derived from the mid-infrared observations

Target Name	D (kpc)	Source	$F_{10.46\ \mu m}$ (Jy)	$F_{18.06\ \mu m}$ (Jy)	T_{dust} (K)	$\tau_{9.7\ \mu m}$	A_V	L_{MIR} (L_{sun})
Resolved Sources								
G309.92+0.48	5.4	1(m)	52.36±0.05	178.53±0.32	168	0.42	7.6	23100
		2	2.53±0.03	36.66±0.33	117	0.15	2.7	5190
G323.740-0.263	3.1	1(m)	0.37±0.02	3.44±0.09	128	0.03	0.5	147
G328.25-0.53	2.3	1	0.77±0.02	1.80±0.10	184	0.0025	0.05	44
		2(m)	0.30±0.01	1.32±0.09	153	0.0021	0.04	30
G339.88-1.26	3.1	1(m)	0.49±0.01	12.50±0.20	105	0.13	2.4	690
		2	0.49±0.01	3.00±0.10	141	0.0026	0.05	123
G351.42+0.64	1.7[2]	1(m)	64.46±0.16	263.59±0.73	159	0.41	7.4	3310
		2	11.01±0.12	76.23±0.41	137	0.17	3.1	950
Unresolved Sources								
G305.20+0.21	3.9	1(m)	28.61/34.69 ±0.08	117.53/120.80 ±0.29	191/171	∞/1.0	∞/18.1	12700/8320
G318.95-0.20	2.0	1(m)	4.04/5.19 ±0.06	18.78/19.41 ±0.26	183/161	∞/0.19	∞/2.9	541/337
G323.741-0.263	3.1	1(m)	0.58/0.78 ±0.02	5.44/5.62 ±0.10	150/136	∞/0.14	∞/2.5	448/234
G328.81+0.63	2.9[1]	1	3.00/3.83 ±0.01	10.00/10.36 ±0.12	205/176	∞/0.06	∞/1.1	594/396
		2(m)	0.73/0.94 ±0.01	12.98/13.35 ±0.13	128/120	∞/0.79	∞/14.3	1230/552
G331.28-0.19	4.8	1(m)	0.91/1.17 ±0.04	3.27/3.39 ±0.18	200/172	∞/0.02	∞/0.4	532/349
G345.01+1.79	2.1	1(m)	4.46/5.±0.05	27.43/28.31 ±0.31	168/151	∞/0.40	∞/7.2	918/537
G9.619+0.193	0.7[3]	1(m)	0.18/0.23 ±0.03	3.56/3.66 ±0.18	125/117	∞/0.56	∞/10.1	170/73
Unresolved, Low S/N Sources								
G328.81+0.63	2.9[1]	3	0.26/0.36 ±0.01	8.74/9.03 ±0.11	112/105	--	--	1180/430
		4	0.07/0.10 ±0.01	3.66/3.78 ±0.09	102/97	--	--	678/211
		5	0.50/0.70 ±0.01	11.05/11.42 ±0.19	122/113	--	--	1170/478
		6	0.25/0.37 ±0.01	12.10/12.50 ±0.20	105/99	--	--	2050/662
G345.01+1.80	2.1	1(m)	0.18/0.23 ±0.02	0.90/0.39 ±0.25	178/156	--	--	29/18
G351.42+0.64	1.7[2]	3	0.05/0.08 ±0.01	6.43/6.64 ±0.24	90/86	--	--	764/187
G351.77-0.54	1.9[1]	1	0.16/0.21 ±0.03	1.11/1.10 ±0.09	164/146	--	--	8/4
Non-Detections and Sources Detected in Only One Filter								
G305.21+0.21	3.9	--	<0.015	<0.197	--	--	--	--
G309.92+0.48	5.4	3	0.19±0.01[A]	<0.178	--	--	--	--
G328.24-0.55	2.3	--	<0.015	<0.179	--	--	--	--
G328.25+0.53	2.3	3	<0.015	0.92±0.07[A]	--	--	--	--
G328.81+0.63	2.9[1]	7	0.06±0.01[A]	<0.181	--	--	--	--
G336.43-0.26	5.9	--	<0.014	<0.177	--	--	--	--
G340.78-0.10	9.0[4]	--	<0.015	<0.174	--	--	--	--
G351.44+0.66	1.7[5]	--	<0.015	DNO	--	--	--	--
G351.77-0.54	1.9[4]	2	<0.016	3.21±0.15[A]	--	--	--	--
G9.621+0.196	0.7[3]	--	<0.015	<0.178	--	--	--	--

Note. -- All distances are from Walsh et al. (1997) unless otherwise noted: 1) MacLeod et al. (1998), 2) Neckel (1978), 3) Wink, Altenhoff, and Mezger (1982), 4) Caswell (1997), 5) Norris et al. (1993). An (m) denotes the source closest to the methanol masers. The monochromatic flux densities are quoted with their statistical errors. The absolute photometric accuracy for the night is estimated to be ±7% for N and ±10% for IHW18. Optical depth given here is emission optical depth at 9.7 μm, from which A_V is derived. Unresolved sources have values listed in the form BB/UL, where BB is the lower (blackbody) limit size of the source, and UL is the upper limit given by the resolution. Unresolved, low S/N sources have values listed in the form BB/OT, where OT is the optically thin upper limit on the source size. DNO means did not observe with this filter. A triangle means observed (i.e. non color-corrected) flux.

at the same position angle as the methanol maser distribution. However, higher resolution images are needed to resolve both sources and see if source 2 is truly elongated.

The two sources, G318.95-0.20:DPT00 1 and G331.28-0.19:DPT00 1 appear slightly elongated at the position angle of the methanol masers. The FWHM major-to-minor axis ratio for both of these is 1.3. However, the PSF stars for these objects are elongated in the same direction and with the same axis ratio. Therefore, these sources are considered to be unresolved.

The two remaining mid-infrared detections showing linearly distributed methanol masers are G345.01+1.79 and G345.01+1.80. In the case of G345.01+1.80:DPT00 1, a source at 10 and 18 μm was barely detected. With such low S/N, no comments can be made on its morphology. G345.01+1.79 is an elongated source whose mid-infrared position angle is different from the methanol maser position angle. However, it must again be pointed out that this object is marginally resolved at best, and the PSF observations nearby are elongated in the north-south direction. If the elongation is real, these masers may be associated with a different process such as outflow.

Also resolved were the sources associated with the methanol masers of NGC 6334F, NGC 6334F-NW, and G328.25-0.53. Both NGC 6334F and NGC 6334F-NW are considered to have linear distributions of methanol masers by Norris et al. (1993). However, the masers of NGC 6334F are spread out over a relatively large area of 1 square arcsecond. These masers are not considered here to be linearly distributed, and when viewed with the other masers in the area (Figure 5-12, lower right panel), the methanol masers seem to follow the OH masers in tracing the contours of the sharp edge of the UCHII region. Most likely these methanol masers exist in the shock front of the

UCHII region of NGC 6334F. As for the resolved source associated with NGC 6334F-NW, the mid-infrared source is offset from the methanol masers by ~1.5″. These masers may exist in an outflow, rather than tracing a disk, or may be associated with a deeply embedded source just south of NGC 6334F-NW. For G328.25-0.53, it is unknown where exactly the masers are located with respect to the mid-infrared sources, however it seems likely that they are most closely associated with the mid-infrared source 2. This source is elongated at a similar position angle to the western group of three methanol masers. However there are other masers nearby (Norris et al. 1993 describes this maser site as complex), and given the astrometry of the mid-infrared survey, it cannot ascertained which masers are coincident with source 2.

Further evidence that the circumstellar disk candidates are indeed disks comes from theory and observation of binary star formation. As mentioned earlier, the resolved sources G309.92+0.48:DPT00 1, G323.740-0.263:DPT00 1, and G339.88-1.26:DPT00 1 exist near other sources which lie at similar position angles to the maser distribution angles. However, at separations of 24000, 12000, and 9000 AU, respectively, it seems unlikely that these are gravitationally bound binaries. Nevertheless, wide binaries could initially form via the growth of an instability in the outer parts of a massive circumstellar disk (Bonnell 1994). In this formation scenario, the spin axes of the binary components will always be aligned, and their circumstellar disks would be coplanar to the binary position angle. Observational evidence seems to support the hypothesis that wide binaries form in such a way to produce coplanarity. Polarimetry work by Monin, Menard, and Duchene (1998) of binaries with separations between 1200 and 5200 AU show that the binary components have preferentially the same orientations. Even at smaller separations

(200-1000 AU), polarimetry of disks around binary components have been observed to be preferentially aligned with each other (Jensen et al. 2000).

Norris et al. (1993) argues that the simplest explanation for the observed properties of the linearly distributed methanol masers is that they lie in circumstellar disks. While it seems not all linearly distributed masers trace disks, there does seem to be much circumstantial evidence that points to this being the case for these circumstellar disk candidates. Three of the eight thermal sources observed are coincident with, and elongated at the same position angle as the methanol masers. In all three cases the methanol masers overlap the radio continuum and mid-infrared peaks to within an arcsecond. This means that the masers are most likely coincident with the stellar/proto-stellar source, which is a requirement if they trace disks. In the case of G309.92+0.48:DPT00 1, the methanol masers have a well-defined velocity gradient indicative of some sort of rotation. Furthermore, all three disk candidates have sources nearby that lie at similar position angles as the methanol maser distributions, and observational evidence points to binary formation mechanisms which favor binary components with disks aligned to the same position angle as the binary system. It seems the simplest explanation for the thermal elongations of G309.92+0.48:DPT00 1, G323.740-0.263:DPT00 1, and G339.88-1.26:DPT00 1 is that they are indeed circumstellar disks.

The Nature of Massive Stars Exhibiting Methanol Maser Emission

Of the 21 sites of methanol maser emission in this mid-infrared survey, Phillips et al. (1998) find only 11 have detectable radio continuum. The absence of UCHII regions has also been observed by Walsh et al. (1998) to be a general characteristic of methanol

maser sites. Likewise, Caswell (1996a) finds that only 3 out of 57 sites contain UCHII regions in a methanol maser survey. There are several reasons suggested as to why many methanol maser sites lack detectable UCHII regions (outlined by Phillips et al. 1998), but three seem to be most viable: (1) The stars associated with the maser emission may be at the earliest stages of stellar formation, and are deeply embedded. Therefore, they would have little or no detectable radio continuum emission because infall from the surrounding envelope would confine the UCHII region to the immediate vicinity of a star, making the surroundings optically thick in the radio and keeping the ionized region geometrically small in projected area. Tofani et al. (1995) observe a low frequency of association of H_2O masers with UCHII regions, and use this hypothesis to explain their data. (2) The stars associated with the maser emission may be less massive stars that are non-ionizing or weakly-ionizing. According to Churchwell (1991), stars with spectral types later than B3 do not produce enough Lyman continuum photons to effectively produce a detectable UCHII region at the kiloparsec distances of the massive stars such as those in this survey. (3) The methanol masers are not associated with a process directly coincident with a forming star. For instance, a star with an outflow impinging on knots of interstellar material in the vicinity of the star could produce a shockfront which would collisionally excite maser emission.

Walsh et al. (1998) favor explanation (1). They propose that methanol maser emission begins at the earliest stages of star formation before the stars are hot enough or evolved enough to ionize their surrounding gas, and continues for 40% the lifetime of the UCHII region and then shuts off. However, given the near-infrared data of Walsh et al. (1999), this seems to be an unlikely scenario. Of the 9 sites of methanol maser emission

Table 5-2: The nature of the sources associated with methanol masers

Name	Linear Masers?	IR Detections	Mid-IR Morphology	Radio Continuum Flux	Radio Spectral Type	Mid-IR Spectral Type
Mid-Infrared Sources Without Radio Continuum						
G305.20+0.21:DPT00 1	no	H,K,L,N,IHW18	C,S	<0.9	<B2.7	B1.6
G318.95-0.20:DPT00 1	yes	H,K,L,N,IHW18	C,S*	<0.7	<B3.6	B6.9
G323.740-0.263:DPT00 1	yes	L,N,IHW18	C,E	<0.2	<B3.8	B8.3
G323.741-0.263:DPT00 1	no	H,K,L,N,IHW18	C,S	<0.2	<B3.8	B7.5
G328.25-0.53:DPT00 2	no	K,L,N,IHW18	E(L)	<0.6	<B3.5	A1.5
G345.01+1.80:DPT00 1	yes	L,N,IHW18	C(L)	<0.7	<B3.5	A3.7
G351.42+0.64:DPT00 3	no	N,IHW18	E(L)	<6.3	<B2.7	B7.9
Mid-Infrared Sources With Radio Continuum						
G309.92+0.48:DPT00 1	yes	H,K,L,N,IHW18	C,E	351	B0.3	B0.7
G328.81+0.63:DPT00 2	yes	NEAR,N,IHW18	?	1640[a,*]	?	B5.8
G331.28-0.19:DPT00 1	yes	N,IHW18	C,S*	4.1	B2.1	B6.8
G339.88-1.26:DPT00 1	yes	H,K,L,N,IHW18	E	14[b]	B1.9	B5.4
G345.01+1.79:DPT00 1	yes	L,N,IHW18	C*	260[a]	B0.9	B5.9
G351.42+0.64:DPT00 1	no	H,K,L,N,IHW18	E	2780	B0.4	B2.5
G9.619+0.193:DPT00 1	no	N,IHW18	C,S	92	B1.5	A0.2
Radio Continuum Sources Without Mid-Infrared Continuum						
G328.24-0.55	no	DNO	--	27	B1.9	--
G340.78-0.10	no	--	--	9[a]	B1.1	--
G351.77-0.54	no	K,L	--	3[c]	B2.7	--
G9.621+0.196	no	--	--	6	B2.6	--
Sources Without Radio Continuum and Without Mid-Infrared Continuum						
G305.21+0.21	yes	--	--	<0.5	<B3.0	--
G336.43-0.26	yes	--	--	<0.3	<B2.9	--

Note. – A ? denotes when a value or property can not be ascertained due to confusion. Unless otherwise noted, all sources were observed at H, K, L, N, and IHW18. Listed in column 3 are those filters where there were detections. NEAR denotes a detection in the near-infrared, but there is confusion caused by multiple sources and a foreground star which do not permit accurate near-infrared flux density estimates. DNO means the source was not observed in the near-infrared. Column 4 is the mid-infrared morphology of the closest mid-infrared source to the methanol masers given the errors in astrometry: C=compact, S=symmetric, E=elongated, (L)=low S/N. A * means that the PSF star for this observation appeared elongated at the same position angle. All values are integrated 8.5 GHz flux densities from Phillips et al. (1998), unless otherwise noted: a) Caswell (1997), 6.7 GHz; b) Ellingsen et al. (1996), 8.6 GHz; c) Fix et al. (1982), 5 GHz. A diamond indicates the radio flux may not be coming from the source associated with the maser emission.

without UCHII regions in this survey, 4 are seen in the survey of Walsh et al. (1999) at K. If these four sources are at such an early stage of formation that they are not producing significant UCHII regions, they would be so highly embedded that there should be no detectable emission at near-infrared wavelengths. Instead, because these sources can be seen in the near-infrared and do not have any detectable radio continuum emission, it seems most likely that they are young, but less massive stars of weakly-ionizing spectral types. Consistent with this idea, the lower-limits to the bolometric luminosity from the mid-infrared fluxes given in Table 5-2 yield a range in spectral types between B6.9 and A3.7 (excluding G305.20+0.21:DPT00 1) for sources without UCHII regions, and a range of B0.7-B6.8 (excluding G9.619+0.193:DPT00 1) for sources with UCHII regions[1]. Furthermore, of the 7 mid-infrared sources that do not have radio continuum emission (Table 5-2), six are either compact and unresolved, or have low S/N (or both). One would expect that lower mass stars would not heat dust as far out as the massive, ionizing stars, and it would therefore be harder to detect any extension in emission in the mid-infrared at the distances of these sources. This seems to imply that scenario (2) is

[1] We have excluded G305.20+0.21:DPT00 1 and G9.619+0.193:DPT00 1 from this discussion for the following reasons. G305.20+0.21:DPT00 1 is unique in that it has a flux at 11 μm which is twice as high as the IRAS flux for the region. It also has the highest flux at 18 μm compared to its IRAS value (Table 6-2). Our lower limit estimate of the bolometric luminosity is greater than 12000 L_{sun} for this source. However, even though it is visible at all near and mid-infrared wavelengths and therefore cannot be heavily embedded, it has no radio continuum. Similarly peculiar is G9.619+0.193:DPT00 1, which has the largest differential in radio continuum derived spectral type compared to mid-infrared derived spectral type. The source was not detected at L by Walsh et al. 1999, and is brighter in our 18 μm image, compared to the 10 μm image. It may be that the mid-infrared flux is substantially reduced by foreground extinction, possibly associated with the nearby large HII region. If this is the case, it would result in a large underestimate of the true source luminosity.

most likely correct, and that the stars without UCHII regions are less massive and therefore do not produce detectable amounts of radio emission.

Table 5-2 also lists the four sources that display weak radio continuum, but do not have mid-infrared emission. These sources may be massive stars in an early stage of formation when they are too embedded to have detectable emission at near- and mid-infrared wavelengths, and have not developed a sufficiently extended circumstellar ionized envelope. This would be analogous to the Class 0 phase of stellar evolution (Andre, Ward-Thompson, and Barsony 1993; Lada 1987), when the source is visible only at far-infrared wavelengths or longer.

The forth section of Table 5-2 lists the two sites which have no near-infrared, mid-infrared, or radio continuum emission. There are two possible explanations for these two sites which only display methanol maser emission. First, these may be extremely young stellar sources which are so highly embedded that they are self absorbed at near- and mid-infrared wavelengths as well as being optically thick at radio wavelengths, as in scenario (1) above. The other possibility is that these sources of methanol maser emission are offset from a non-ionizing star and are collisionally excited in an outflow. In this scenario, a young stellar source (of any mass) which is in outflow may have methanol maser emission associated with the shock of the outflow on the surrounding ambient gas or upon some nearby knot of material. Bachiller et al. (1998) observed spectacular enhancements of methanol abundance toward the shocked molecular gas in the bipolar outflow of the low- mass young stellar source NGC 1333:IRAS 2. These areas of enhanced methanol abundance lie approximately 25,000 AU away from the stellar source. It is therefore plausible that methanol masers may form in these outflow shock

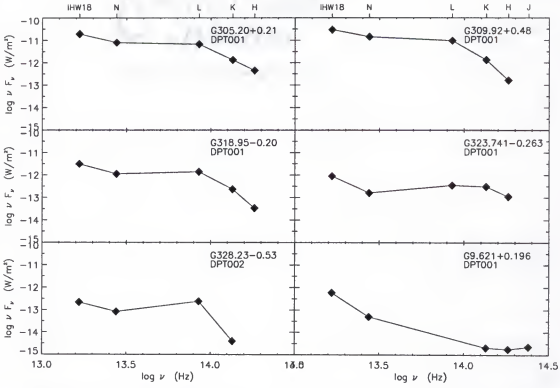

Figure 5-15: Spectral energy distributions for six sources. All sources overlap the near-infrared survey of Walsh et al. (1999), and all six are Class I sources.

zones, and could very well be a scenario by which a significant portion of the methanol masers are generated.

Further information on the nature of the stars associated with methanol masers can come from spectral energy distributions (SEDs). SEDs were created for the sources in the near-infrared survey of Walsh et al. (1999) that overlapped the sources in this mid-infrared survey. There are six sources that were detected in both surveys, and their SEDs are shown in Figure 5-15. The N-band point is slightly suppressed in all six SEDs. This is most likely due to silicate absorption at 9.7 μm, showing that these sources are indeed embedded. Furthermore, using the classification scheme of Greene et al. (1994) all of these sources are Class I sources, having positive spectral indices ($\alpha = d log(\lambda F_\lambda)/d log\lambda$)

of $0.51<\alpha<2.67$. Class I sources are considered to be in the early stage of stellar evolution when the star and disk are embedded in an infalling envelope.

The Relationships between Mid-Infrared, IRAS and Radio Observations

The closest IRAS sources associated with the methanol maser sites were determined from the IRAS Point Source Catalog (PSC). Table 5-3 shows the associated 12 and 25 μm IRAS fluxes and the fluxes obtained at 10.46 and 18.06 μm by OSCIR for the whole area in the field of view. It should be pointed out that the offsets of the presumed center of the IRAS beam are anywhere from 4″ to 2.5′ from the actual location of the methanol maser location. Also found were IRAS LRS (Low Resolution Spectrometer) spectra (7 to 25 μm wavelength range) for six of the sources in the survey (IRAS Science Team 1986; Volk et al. 1991; Chan et al. 1996). The monochromatic flux densities obtained from the LRS spectra at 11 and 18 μm are also listed in Table 5-3, however it must be noted that objects less than 6′ apart are considered to be confused.

Comparing the different flux densities observed for the sources in Table 5-3 shows that the IRAS PSC fluxes from the region associated with the methanol emission are, in many cases, much larger than the fluxes determined with OSCIR. Because of its ~75″ x 1.5′ spatial resolution at 12 and 25 μm, IRAS presumably measured flux from sources that lie outside field of view of this survey, as well as extended emission associated with these sources. In many cases the mid-infrared observations from this survey reveal multiple sources which would be confused in the IRAS beam. It is therefore entirely reasonable that IRAS with its larger beam will likely detect more flux than what was detected with OSCIR. Consequently, the single source associated with the

Table 5-3: Total integrated flux density observed in the OSCIR field of view and corresponding IRAS flux density measurements

Target Field	OSCIR N/IHW18 (Jy)	IRAS PSC Name	IRAS 12/25 μm (Jy)	IRAS 11/18 μm (Jy)	LRS 11/18 μm (Jy)
G305.2+0.2[a]	36.13/117.72	13079-6218	28.32/249.72	18.44/155.03	72/600[x]
G309.92+0.48	50.25/208.60	13471-6120	76.31/667.88	49.76/415.67	--
G318.95-0.20	5.07/18.81	14567-5846	33.80/300.79	21.96/186.14	9/128[y]
G323.74-0.26[b]	1.17/8.81	15278-5620	23.57/166.66	16.41/110.38	33/80[yz]
G328.2-0.5[c]	1.12/3.94	15541-5349	12.04/110.69	7.52/68.18	--
G328.81+0.63	6.70/58.89	15520-5234	15.49/537.93	5.23/206.50	--
G331.28-0.19	1.02/3.27	16076-5134	35.96/237.28	24.42/160.86	35/217[x]
G336.43-0.26	<0.01/<0.18	16306-4758	15.60/68.03	12.37/51.78	--
G339.88-1.26	0.99/15.15	16484-4603	9.93/192.04	4.76/92.08	--
G340.78-0.10	<0.02/<0.17	16465-4437	4.12/4.45	4.07/4.75	--
G345.0+1.8[d]	6.01/28.39	16533-4009	26.40/471.28	12.88/232.26	25/405[x]
G351.4+0.6[e]	75.59/336.43	17175-3544	103.51/1400.36	56.77/758.54	--
G351.77-0.54	0.21/4.26	17233-3606	4.50/228.80	1.30/76.05	--
G9.62+0.19[f]	0.25/3.59	18032-2032	38.63/292.41	26.00/191.14	38/133[y]

Note. – Column 1 has fields containing multiple sources: a) G305.20+0.21 and G305.21+0.21; b) G323.740-0.263 and G323.741-0.263; c) G328.24-0.55 and G328.25-0.53; d) G345.01+1.79 and G345.01+1.80; e)G351.42+0.64 (NGC 6334F and NGC 6334F-NW) and G351.44+0.66; f) G9.621+0.196 and G9.619+0.193. For column 5, the color-corrected IRAS flux densities at 12 and 25 μm were fit with a blackbody curve from which an extrapolated value was found at 11 μm and an interpolated value was found at 18 μm. Column 6 is monochromatic flux densities from IRAS Low Resolution Specta. These values were found from several different papers: x) Volk et al. (1991); y) IRAS Science Team (1986); z) Chan, Henning, and Schreyer (1996).

methanol masers cannot be modeled correctly with the fluxes that were obtained by IRAS for the whole region surrounding the source. For instance, in the discussion of the individual sources luminosities and spectral types were presented for several sites from Walsh et al. (1997) and Caswell (1997), who both used IRAS far-infrared fluxes to derive their results. These should be considered in most cases to be extreme upper limits. In fact, spectral type estimates given by these authors are mostly O types. Interestingly, spectral types estimated from radio continuum and fluxes (Table 5-1) show that none of the stellar sources associated with methanol masers in this survey are as massive as an O star.

The LRS monochromatic flux densities that were tabulated are also larger than those determined with OSCIR. Given the 6′ resolution, and the fact that O and B stars are often found in associations and complexes, flux values for these maser sources are most likely not well determined by the LRS spectra either. Furthermore, a simple interpretation of the LRS silicate features for the sources associated with the methanol masers is not possible. Comparisons of the mid-infrared data to the LRS monochromatic fluxes support these assumptions, by virtue of the LRS flux density values being 2 to 58 times larger than the OSCIR values. Likewise, as was described in the discussion of the individual sources, a few sources are considered "steep spectrum" or contain a "21 μm feature", as determined from the LRS spectra. Once again, it is hard to determine the significance of these spectral features as they relate only to the stellar sources associated with the maser emission.

It has been suggested that methanol masers may be pumped by far-infrared radiation. Interestingly, van der Walt, Gaylard, and MacLeod (1995) and Walsh et al. (1997) show that there is little to no correlation between the methanol maser flux densities observed and IRAS flux densities, which seemingly contradicts this hypothesis. Furthermore, since the methanol masers are directly coincident with young stellar sources, far-infrared pumping seems unlikely because the far-infrared emission from cool material might exist too far from the maser sources to be the dominant pump mechanism. Walsh et al. (1997) point out that some methanol masers exist where there is no apparent far-infrared radiation, and state that methanol masers seem more dependent on the abundance of methanol instead.

In addition to the lack of correlation with far-infrared radiation, Walsh et al. (1998) could not establish any correlation between radio continuum emission and methanol maser emission. Indeed, many sites of methanol maser emission have no detectable radio continuum emission. This therefore seems to shows that maser emission cannot be significantly influenced by radio continuum photons.

Data from this survey was compared to several methanol maser parameters as well, to see if there were any trends or correlations. There seems to be no correlation between mid-infrared flux and methanol maser flux (i.e. peak spot flux, average spot flux, or summed flux for all spots), nor between mid-infrared flux and number of maser spots.

Extensive modeling has been performed for the 6 and 12 GHz maser transitions by Sobolev and Deguchi (1994) and Sobolev, Cragg, and Godfrey (1997). They conclude that the methanol masers lie in projection against the background of radio continuum photons from a UCHII region, which provides the source photons for amplification. Pumping is achieved not by far-infrared photons, but through mid-infrared photons emitted by the warm >150K dust which surrounds the methanol-rich matter near the YSO. These mid-infrared photons provide an infrared continuum source close enough to the location of the maser to pump the methanol to the first and second torsionally excited states required for the maser transition.

Consistent with this modeling, there is a possible relationship between mid-infrared source size and methanol maser distribution in this survey. Figure 5-16 shows 18 μm infrared source sizes versus extent of the maser spot distribution. Plotted here are only the mid-infrared sources which could be identified to be coincident with the

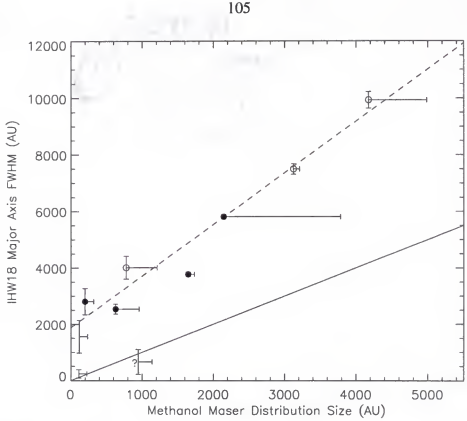

Figure 5-16: Methanol maser distribution size versus physical IHW18 extent for all sources where masers are coincident with the mid-infrared sources. Open circles represent the FWHM of the disk candidates along the axis parallel to the methanol maser distribution. Left to right these are G323.740-0.263, G339.88-1.26, and G309.92+0.48. The filled circles (left to right) represent resolved sources G328.25-0.53, G345.01+1.79 (which may be marginally resolved), NGC 6334F (which has methanol masers that may instead be located in shock regions), and G328.81+0.63. The IHW18 PSF was subtracted in quadrature from each FWHM. The sources plotted without symbols are unresolved, and the error bars in the y-direction show the range between the resolution limiting upper-limit and blackbody lower-limit size. Top to bottom these are G305.20+0.21, G318.95-0.20, and G9.621+0.196. Errors in the x-direction for all points are taken to be the average separation between maser spots. The solid line is the line indicating when the IHW18 size is equal to the methanol maser distribution extent. Notice all points plotted lie above this line, indicating that the masers preferentially lie within the mid-infrared emitting region (except for G318.95-0.20, marked with an '?', whose masers are offset by 2.5″, and may not be associated with the mid-infrared source). The dashed line is a least squares fit to the points. There seems to be a rough correlation between mid-infrared size and methanol masers distribution size.

methanol masers, and hence may be radiatively rather than collisionally pumped. The plotted infrared source sizes are from the longest axis of the mid-infrared source, and have had the PSF FWHM subtracted in quadrature. Also plotted is the 1:1 line. Figure 5-

16 suggests a trend in which larger methanol maser distributions correspond to larger mid-infrared emitting regions. But more importantly, all of the points in the plot lie above the 1:1 line, indicating that conditions for methanol maser emission lie within the mid-infrared emitting regions, assuming that the methanol masers are coincident with the mid-infrared peaks. This is the first direct observational evidence which suggests that the mid-infrared flux associated with the warm, dense, molecular gas and dust is the main contributor to the pumping of methanol masers.

Figure 5-17 shows the extent of the maser spot distribution for the population of sources in the mid-infrared survey with UCHII regions and for the population without UCHII regions. The sources with UCHII regions tend to have methanol masers distributed over a larger physical extent, than those without UCHII regions. A majority of sources without UCHII regions have methanol maser distributions spanning less than 1000AU. This supports the hypotheses advanced here that methanol masers are contained within the mid-infrared emitting region. If the hypothesis that methanol masers are pumped by mid-infrared photons is correct, one would expect to see methanol masers come from larger extents for the sources with UCHII regions. This is because our analysis has shown that stars without radio continuum are most likely less massive stars. The higher mass ionizing stars would produce a flux capable of heating out to larger distances than lower mass non-ionizing stars. Therefore, not only would the methanol maser distribution extents be larger for stars with UCHII regions, but so would the mid-infrared sources. In Table 5-2 it can be seen that all of the sources without UCHII regions (except for G323.740-0.263), are unresolved or have low signal-to-noise (or both).

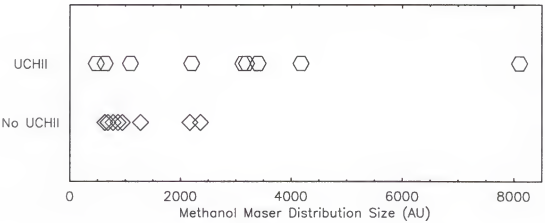

Figure 5-17: Methanol maser distribution sizes for sources with and without UCHII regions. The sources with UCHII regions (hexagons) have methanol masers spread over a larger region, than those without UCHII regions without (diamonds). Furthermore, this plot shows most sources lacking UCHII regions have their methanol maser distributed over less than 1000 AU.

The modeling described above and these subsequent mid-infrared observations may explain methanol maser excitation and pumping in the presence of a UCHII region, but it does not easily explain the presence of methanol masers where there are no UCHII regions and no apparent mid-infrared flux. If these objects are less massive stars, one would expect there would be little radio continuum to amplify. However, it is pointed out by Sobolev, Cragg, and Godfrey (1997) that for sources with no UCHII regions, one could get high enough maser brightness temperatures at 6.7 GHz from the amplification of 2.7 K microwave background photons alone. Pumping would still need to be achieved via a warm, methanol rich dust clump, or perhaps several clumps in a disk.

Alternatives to the Disk Hypothesis

Recent papers have suggested that linearly distributed methanol masers can best be described by a shock model. Sobolev and Deguchi (1994) and Walsh et al. (1998) both advance a shock hypothesis, but each with a variation on that central theme.

Sobolev and Deguchi (1994) and Sobolev, Cragg, and Godfrey (1997) describe a "clump" hypothesis in which the maser sources are separate elongated clumps of material. They suggest that a shock front, preceding the ionization front delimiting the UCHII region of a forming star, impinging on the surrounding interstellar cloud could create the clumps, or the clumps could be pre-existing, interstellar knots of material. Conditions for the existence of methanol masers in these clumps, such as methanol abundance, density enhancement, and radially elongated structures, are argued to be produced by the shock wave itself. The portion of the shock wave moving towards the observer would create the necessary geometry and conditions for the masers because the radially elongated masing clumps would be projected in front of a background of radio continuum emission. They further point out that the shock could also align the clumps, and in the process possibly distribute them in some organized fashion. A problem with this scenario is that the gas temperature behind shocks are high (Frail and Mitchell 1998), and the methanol maser models require low gas temperatures so that the masers are not quenched by the de-exciting collisions of the gas with the methanol molecules.

Walsh et al. (1998) agree with Norris et al. (1993) that there are more linear arrangements of methanol masers than can be explained by a chance probability in their survey. However, because most of the sites observed do not have a systematic velocity gradient, they feel that the circumstellar hypothesis could not explain all of the data. They suggest that an "expanding shock" model explains their data better. They contend that

dense knots of material have been compressed and accelerated by the passage of a shock. These knots would not necessarily lie along the line of site to the UCHII region. If these knots of material lay far from the point of origin of the shock, it would explain why methanol maser emission is often seen without a UCHII region present. They contest that since one observes the component of the shock velocity only along our line of sight, a shock wave impinging on several separated spots on the plane of the sky would show a smooth velocity gradient. In general however, one would expect the shock wave to expand non-uniformly as it propagates through an inhomogeneous medium. Again, there is the problem of the post-shock gas being high enough in temperature to quench the masers, unless some sort of efficient cooling mechanism is present.

Sobolev, Cragg, and Godfrey (1997) find fault in the circumstellar disk hypothesis because the gas in the disk may be too hot. However, models show that disks are stratified, with a warm atmosphere above and below the disk, and a cooler dense central region. The warm material sandwiching the cooler disk could provide it with a large supply of mid-infrared photons for pumping. This seems consistent with the findings as shown in Figure 5-15, which indicate that conditions for methanol maser emission lie within the mid-infrared emitting regions. The mid-plane of the disk would be cool enough to satisfy the low kinetic gas temperatures needed to avoid maser quenching. Also, the disk would have a density gradient, where densities lessen as one approaches the disk/disk-atmosphere interface. With the disk arranged so that the observer sees it nearly edge-on, the maser's path would come through the disk at a angle which would contain the appropriate density needed for the existence of the maser. Furthermore, maser spot properties such as radial velocities, brightness, and location would be subject to

many local variables in a disk where the turbulent velocities are comparable to the disk's slow rotation. Therefore, one would not expect to always get velocity gradients along the spots, and a velocity gradient may not be a general property of methanol masers in disks. Thus, attempts to prove or disprove the circumstellar hypothesis on these grounds (i.e. deriving masses of central stars, and plotting position-velocity diagrams) may be futile.

Elitzur (1992b) has suggested that OH masers can lie in-between the shock and ionization front of expanding UCHII regions. Interestingly, methanol masers are often spatially coincident with OH masers. This may indicate, contrary to the temperature argument about quenching, that the conditions in shock fronts may in fact be viable for the existence of methanol masers. Indeed, at least one source in this survey, G351.42+0.64:DPT00 1 (NGC 6334F), seems to have masers associated with the sharp western boundary of the extended UCHII region. Here the methanol masers exist spatially coincident with OH masers and seem to most likely to exist in the shock region of the UCHII region. There are also other sources in the survey which may be displaying methanol masers in an outflow. As discussed in Chapter 3, water masers are known to exist in linear distributions that point radially away from UCHII regions, and so are thought to exist in outflow (Felli, Palagi, and Tofani 1992). In the same manner, sources are seen in this survey where methanol masers are distributed radially with respect to the closest mid-infrared source, G323.741-0.263:DPT00 1 and G351.42+0.64:DPT00 3 (NGC 6334F-NW), for example. It therefore seems reasonable to assume that linearly distributed methanol masers, and methanol masers in general, can be associated with shocks, outflows, and disks.

CHAPTER 6
WATER MASER SELECTED SURVEY

This chapter presents a mid-infrared imaging survey of 21 water maser sites observed in the radio survey by Forster and Caswell (1989). This water maser survey is the largest survey to date with such high-accuracy absolute astrometry (<0.5"). Of the 74 water maser sites listed by Forster and Caswell (1989), 21 sites were chosen that would be at the best airmass for the night of observing. This chapter will begin with a discussion of each source observed. The observations of the sources in this survey are incomplete. Only 7 of the 21 sites could be imaged at both N and IHW18 due to poor weather. The remaining sites are short-exposure N-band images only. This chapter therefore presents the data that was acquired as a comparative study to the methanol maser selected survey, and discusses the limited results that were obtained.

The objective in this survey was to find supportive evidence to the hypotheses that water masers are associated with outflows and embedded sources, as described in the introductory chapters. The first section of this chapter will include what is known from the literature about each source that was detected, and will describe briefly the mid-infrared observations of each. The second section contains a detailed discussion the analysis and results of the survey.

Individual Sources

The physical parameters derived for these sources are given in Table 6-1 at the end of this section, and may be referred to in the discussion that follows. Many of the sites in the water maser selected survey contain methanol maser emission, as found by Caswell et al. (1995a, 1995b). However, the absolute astrometry for the methanol maser observations is only accurate to 10", so it is not certain if they are coincident with any of the mid-infrared sources or the water maser spots.

G00.38+0.04 (IRAS 17432-2835)

This site contains water, OH, and methanol masers, but no UCHII region. Forster and Caswell (1989) failed to detect 1.36 cm continuum here with an upper limit of 70 mJy, and Forster and Caswell (2000) also did not detect a UCHII region here with a upper limit of 0.2 mJy at 3 cm. The site also lacks the molecular core signatures of CS and NH_3 (Anglada et al. 1996). Walsh et al. (1997) and Fosrter and Caswell (1989) both agree on the distance of 10.0 kpc to this site.

This object was not detected in the mid-infrared on the first night of observations with 15 second exposure times. The observations on the second night with a one minute exposure time gave only the hint of a signal seen in Figure 6-1. The S/N is very low at 10.8 μm and non-existent at 18.2 μm, and therefore the no flux is given in Table 6-1. It can not be ruled out that the source seen is in fact not a real source at all but only background sky noise. The only reason it is believed that this is a marginal detection is that the source is located close to the water maser location.

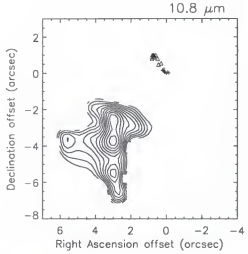

Figure 6-1: G00.38+0.04. A contour plot of the observed N-band image. The crosses represent the water maser positions and the triangles represent the OH maser positions from Forster and Caswell (1989).

G00.55-0.85 (IRAS 17470-2853)

This site is also known as RCW 142 and contains water, OH, and methanol masers, as well as radio continuum. While Forster and Caswell (1989) failed to detect 22 GHz continuum here with an upper limit of 240 mJy, Walsh et al. (1998) did detect continuum at 8.6 and 6.7 GHz. Plume, Jaffe, and Evans (1992) detected CS and CO toward this site. Anglada et al. (1996) confirm the detection of CS and find NH_3 as well. Forster (1990) found that the water masers here are linearly distributed, and advances a disk or ring hypothesis to explain their distribution. Caswell (1998) suggests that since the various masers are spread over a large area, this may be a case where the masers are tracing an extended source rather than the masers tracing a cluster of individual sites.

There is some confusion as to what the distance to this site is. Walsh et al. (1997) adopt a distance of 9.1 kpc to this site from the radial velocities of the methanol masers, whereas Forster and Caswell (1999) believe it is either 2.0 or 18.0 kpc, depending on near

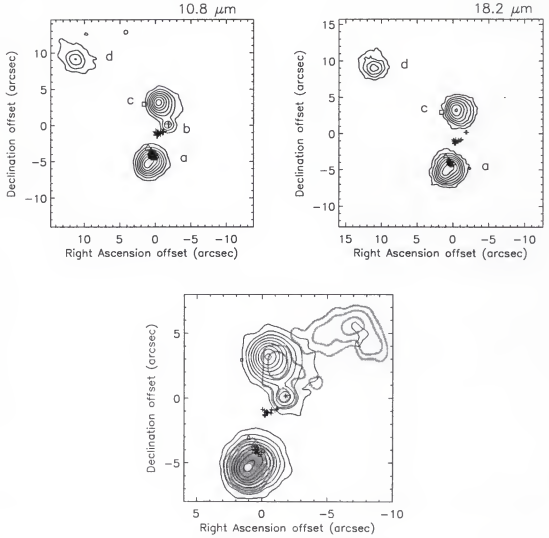

Figure 6-2: G00.55-0.85. This three-panel display shows the N-band contours in the upper left and the IHW18 contours in the upper right. The symbols are the same as in Figure 6-1. The box in these plots represents the near-infrared source from Testi et al. (1994). The lower plot shows the N-band contours once again, overlaid with 3.5 cm contours (thick gray) from Walsh et al. (1998).

or far kinematic distance, from the OH maser velocities. This disagreement in distance is somewhat confusing since the OH and methanol masers at this location are not only coincident spatially, but overlap in velocity as well. Both molecules have radial velocities that span from +8 to +20 km/sec. Kinematic distances were independently derived here using these velocities and the galactic rotation curve of Wouterloot and Brand (1989), as

discussed in Chapter 4. It was found that radial velocities in this range should yield a tangent distance close to 9 kpc, so in this paper the distance of Walsh et al. (1997) of 9.1 kpc is adopted.

Given this distance, Walsh et al. (1997) conclude that if a single star were responsible for the IRAS far infrared radiation it would be an O4. Testi et al. (1994) find a single near infrared source here, closest to the water maser group. However, at least four mid-infrared sources were detected by this survey at this site.

In order to achieve better astrometry between the mid-infrared sources and the masers, the 8.6 GHz continuum map of Walsh et al. (1998) were overlaid on the mid-infrared image. The relative astrometry between the radio continuum and maser spots is estimated as being accurate to better than one arcsec. There is a good match between the radio sources and the mid-infrared *a* and *b* sources. The water masers seem to be associated with the mid-infrared source *b*. The string of water masers appear to emanate from source *b* and point radially away from it. Two isolated water masers appear to be coincident with the peak of source *b* as well. The southern mid-infrared source *a* is elongated and contains both the methanol and OH masers within its contours. The OH and methanol masers appear coincident to within the errors in astrometry. The near infrared source given by Testi et al. (1994) is probably associated with source *c*. Source *d* is very amorphous and may be part of an extended HII region.

The closest mid-infrared source to the water maser reference feature is source *b*, which is only seen at N. The fact that this sources does not show up at IHW18 implies that this object is very hot. This is puzzling since this is the only source in this survey that is associated with maser emission and does not appear in an 18 μm image. OSCIR is,

however, less sensitive at IHW18 than at N, due to the smaller filter bandwidth. The complex morphologies at this site may be explained by source *b* exhibiting an outflow. The string of water masers to the southeast are tracing the outflow in that direction. The lower contour levels (5 and 10%) of the radio continuum are slightly concave, perhaps owing to the outflow impinging on this source. Furthermore, the methanol and OH masers could be explained as being collisionally excited by the shock of the outflow on source *a*. The northwestern lobe of the outflow may be traced by the radio continuum seen in that direction, which is bow shock or cometary shaped in the proper sense. Source *c* would then be a source not effected by the outflow, perhaps lying slightly in the foreground or background.

G10.62-0.38 (IRAS 18075-1956)

This is the site of a UCHII region that is part of the W31 complex. It also contains water and OH masers. The UCHII region has been imaged at 1.36 cm (Forster and Caswell 1989), 2 cm (Hofner and Churchwell 1996; Wood and Churchwell 1989a), 3.5 and 4.5 cm (Walsh et al. 1998), and 6 cm (Wood and Churchwell 1989a). Several molecular species have also been detected here, such as CS, CO, HC_3N, and CH_3CN (Olmi and Cesaroni 1999; Wyrowski, Schilke, and Walmsley 1999; Hauschildt et al. 1993; Plume, Jaffe, and Evans 1992; Churchwell, Walmsley, and Wood 1992), indicating that this is the site of a molecular core.

This site has a complex maser morphology. Most of the water masers here are strung out in a linear fashion. The OH masers are spread out over ~5 square arcseconds.

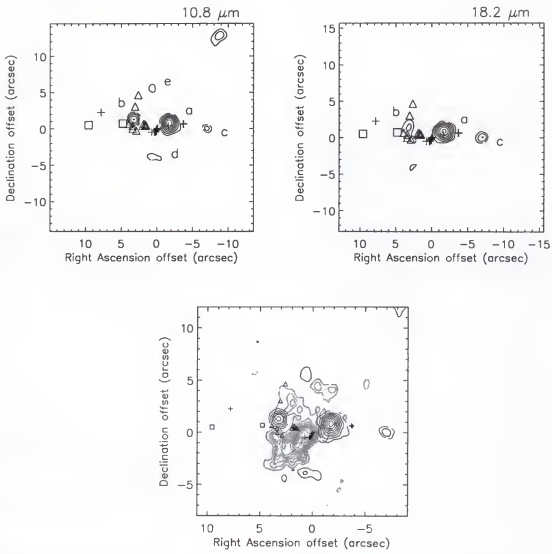

Figure 6-3: G10.62-0.38. The symbolics and layout are the same as for Figure 6-2. The lower panel shows the N-band contours with the 6 cm contours (thick gray) from Wood and Churchwell (1989).

This field does contain methanol masers, but they are located over 11″ away from the UCHII region and the concentration of water and OH masers.

A series of papers by Keto, Ho and Haschick (1987, 1988) observed the velocity field of the UCHII region using the NH_3 inversion lines. They conclude the motions indicate that remnant infalling material is still accreting onto the central massive star.

They claim the gas is even seen to spin up as it gets closer to the UCHII region. The rotation axis of the material is oriented perpendicular to the string of water masers. Once again the water masers may be participating in an outflow.

The distance to this site given by Walsh et al. (1997) is 6.5 kpc (tangent point). This is in relatively good agreement with the measurements of Forster and Caswell (1989) who adopt a distance of 6.0 kpc.

The 30 second exposure at N of this maser site on the first night showed the *a* and *b* sources quite well, with a hint of the remaining 5 mid-infrared sources. Seen in more detail on the second night of observations, the 2 minute exposure time revealed a complex arrangement of sources (Figure 6-3). The water masers are pointing radially away from the mid-infrared source *a*. The OH maser seems to be associated with the *b* source, but their arrangement is complex.

Testi et al. (1994) detected two near IR sources in this field, one of which seems to be associated with source *b*. The second source does not seem to be associated with any mid–infrared source. Sources *c* and *e* are lower S/N point-like sources, whereas *d* and *f* seem to be low S/N and amorphous. Source *f* does not appear in the IHW18 image.

Once again the continuum image was overlaid on the mid-infrared image to check the astrometry with respect to the maser locations. It was found that the UCHII region is not associated with any of the mid-infrared sources. The UCHII region peak is most probably located in right ascension almost midway between and the *a* and *b* sources, and is offset slightly (~2″) south in declination. In this configuration no 6 cm continuum is associated with the *a* or *b* sources, however the radio continuum wraps around these sources. In other words, in this case the areas that lack radio continuum seem to be the

locations of the mid-infrared sources. Also in this configuration almost all of the water and OH masers are contained within either the radio or mid-infrared contours.

Interpretation of this region is difficult. Perhaps there is an outflow which, in the plane of the sky, is oriented to the southeast, but is also more or less oriented towards us, and emenating from an embedded source *a*. This would explain the strange radio morphology, and would also explain why the masers are distributed in such a complex manner.

G12.68-0.18

There is no IRAS source associated with this site. It contains OH, water, and methanol masers, however and there does not seem to be any UCHII regions here. This region does contain a rather large and diffuse radio continuum source covering ~20 square arcseconds (Codella et al. 1997; Forster and Caswell 2000) known as W33B. The OH and water masers do not appear to be contained within this large radio source. Molecular tracers are found toward this site, such as CS, CO, and NH_3 (Plume, Jaffe, and Evans 1992; Anglada et al. 1996; Codella et al. 1997).

There is considerable discrepancy between the values for the distance to this site given by observations in the past. Codella et al. (1997) give a distance of 11.5 kpc based upon the radial velocity of NH_3 lines. Braz and Epchtein (1983) give a distance of 4.5 kpc, based upon the velocity of the brightest water maser line. Forster and Caswell (1989) adopt a distance of 6.4 kpc based on the OH maser velocities. When the kinematic distances were recalculated based on the NH_3 velocity given by Codella et al. (1997), it was found that the near and far distances were 4.9 and 11.6 kpc, respectively. Codella et al. (1997) may have chosen the far distance based upon the fact that this was the only site

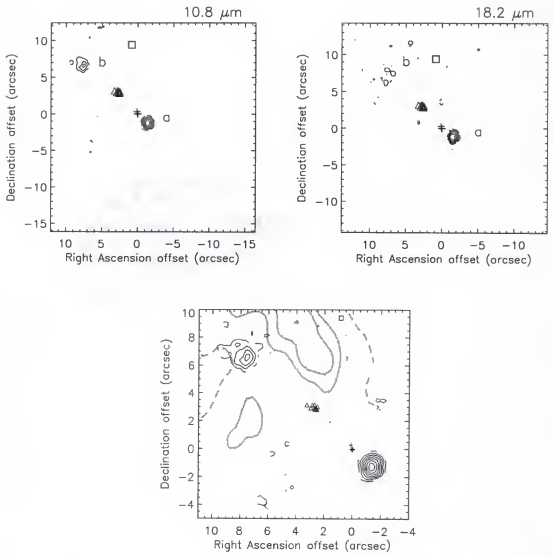

Figure 6-4: G12.68-0.18. The symbols and layout are the same as for Figure 6-2. The lower panel shows the N-band contours overlaid with the 1.3 cm radio map (thick gray) of Codella et al. (1997).

in their survey in which they did not detect an NH_3 molecular core. Since the value of 4.9 kpc is close to the value of Braz and Epchtein (1983) and to that of Forster and Caswell (1989, when corrected for the now accepted values for the solar distance and velocity), this value is adopted here.

There was no mid-infared detection of this object at an integration time of 30 seconds. The second night of observations did however reveal two mid-infrared sources. Source *a* is located very close to the water maser reference position. Source *b* is semi-amorphous, and is low S/N at N and extremely low at IHW18 (Figure 6-4). No accurate flux density is therefore given for this source at IHW18 in Table 6-1. The near-infrared source given by Testi et al. (1994) does not seem to be associated with any of the mid-infrared sources seen at this site.

By overlaying the 1.3 cm radio continuum map of Codella et al. (1997), it was found that there were no sources with which to register the mid-infrared image, so no corrections could be made to the mid-infrared astrometry. By registering the masers from the radio continuum plot with those plotted on the mid-infrared plot, it can be seen that source *b* is probably associated with a knot of material in the amorphous radio continuum source of W33B. The mid-infrared source *a* can be considered associated with the water masers to within the astrometric error. The OH masers do not seem to be associated with any object seen in the radio or mid-infrared. They may be associated with a knot of material in W33B, or may be excited by an outflow from source a impinging on the material of this large HII region.

G16.59-0.05 (IRAS 18182-1433)

This source is the site of water, OH, and methanol masers, and there is very weak radio continuum source present. Forster and Caswell (2000) detect an extremely weak (0.3 mJy at 3 cm) UCHII region that is just above the 3σ detection level, and is coincident with the OH and water masers. This is also the site of molecular emission from NH_3 and CS (Codella et al. 1997; Bronfman et al. 1996).

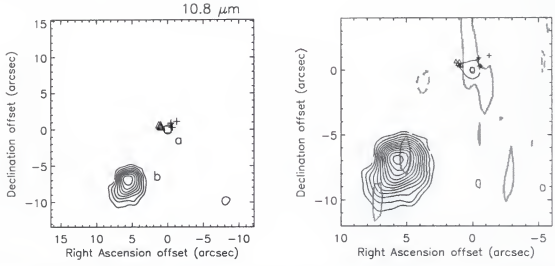

Figure 6-5: G16.59-0.05. A two panel display showing the N-band contours in both panels. The right panel shows an overlay of the 3 cm contours (thick gray) from Forster and Caswell (2000).

The distance to this site as given by Codella et al. (1997) is 4.7 kpc. This is close to the distance given by Forster and Caswell (1989) when corrected for a solar distance of 8.5 kpc from the galactic center. The distance of 4.7 kpc will therefore be adopted for the purposes of this paper.

A faint mid-infrared source (*a*) was detected at the location of the water masers, coincident with the weak UCHII region seen by Forster and Caswell (2000). A larger amorphous mid-infrared source (*b*) was also detected, and is located to the southeast. Testi et al. (1994) also claim to have detected a faint near-IR source at the location of the masers as well. This may be an embedded molecular core which is just beginning to show signs of weak radio emission from the central stellar source.

G19.61-0.23 (IRAS 18248-1158)

This is an extremely interesting and complex site. It contains OH, water, and methanol masers, and a grouping of UCHII regions and extended radio continuum. The radio

continuum emission from this region comes from five main sources, all of which are discussed in detail in a paper by Garay et al. (1998). There are molecular tracers here in the form of CS, NH_3, and CO (Larionov et al. 1999; Plume, Jaffe, and Evans 1992; Garay et al. 1998). There seems to be good agreement in the literature on the distance to this site, and so the distance of 4.0 kpc is adopted here.

Figure 6-6 shows the region has quite a complex distribution of mid-infrared sources. It appears very similar to the radio continuum images of Garay et al. (1998). For conciseness, this discussion will concentrate only on the sources associated with the maser emission or sources seen only in the mid-infrared. By registering the mid-infrared image with the 1.6 GHz image of Garay et al. (1998), comment can be made on individual sources as they appear in both wavelengths.

The brightest mid-infrared source is source *b* (labeled A by Garay et al. 1998), which is also the brightest radio source. Source *b* is bright and cometary shaped, it's tail sweeping to the west. It seems to be diamond shaped, and therefore might contain several stellar objects embedded it the same material. The near-infrared source of Testi et al. (1994) seems to be coincident with source *b*, but not very close to the mid-infrared peak. Perhaps it is coincident with a source in a different part of the extended object seen in the mid-infrared. The water and OH masers seen here by Forster and Caswell (1989) lie close to this source, and most of the masers are located in the in the outer traces of source *b*. The water masers seem to be lined in a string pointing radially away from source *b*. Garay et al. (1998) find extended ammonia emission here that has peaks located at approximately 5″ to the northwest, and ~8″ west of source *b*. The water masers in the string may be associated with the northwest ammonia peak. No mid-infrared emission

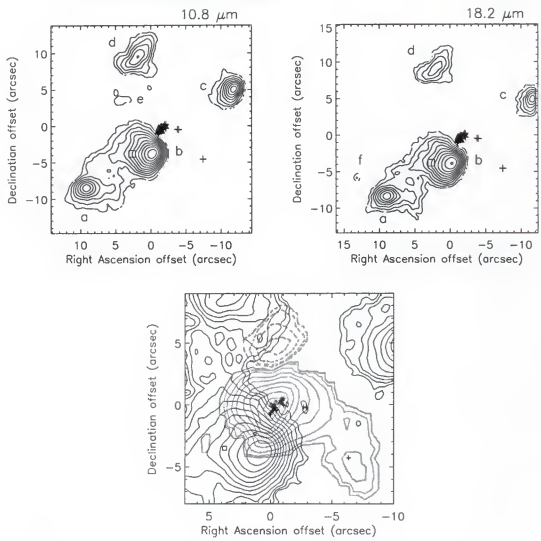

Figure 6-6: G19.61-0.23. The symbols and layout are the same as for Figure 6-2. The lower panel shows the IHW18 contours with the ammonia contours (thick gray) from Garay et al. (1998).

was detected at this location. There is a solitary water maser located coincident with the western ammonia peak, as well, and may be an embedded molecular core. Again, there was no detection of any mid-infrared emission from this location. Another isolated clump of three water masers is located 2″ to the west of the string of water masers. A very faint mid-infrared source was found at this location (source h). The northwest ammonia peak

and emission are elongated towards this location. There might be another embedded molecular clump here as well, that is unresolved from the clump responsible for the northwestern peak in the VLA observations. If these molecular clumps are embedded massive protostars, they would be in an extremely early stage of formation, before they have had a chance to ionize their surroundings.

There are two sources here that are not associated with masers but also do not have a radio continuum component. These are the sources farthest east (*f*) and west (*g*, not shown in Figure 6-6). These are also most likely young protostars as well.

G28.86+0.07 (IRAS 18411-0338)

This site contains all three maser types, but does not have any detectable UCHII region. Codella et al. (1997) find no 1.3 cm continuum emission here with an upper limit of 0.34 mJy. However, this site does contain molecular emission from NH_3, CS, and CO (Codella et al. 1997; Anglada et al. 1996; Plume, Jaffe, and Evans 1992). Anglada et al. (1996) and Forster and Caswell (1989) both agree that the distance to this site is 8.5 kpc, so this distance is adopted here.

At exposure times of 30 and 120 seconds, the N-band image of this object reveals a very bright source *a*, but source *b* is barely present, and *c* is non-existent. IWH18 at an integration of 120 seconds reveals an amorphous *b* source and a *c* source to the south, both with low S/N (Figure 6-7). Source *a* is extended to the east. In this case, the water masers are coincident with the mid-infrared peak of source *a* to within a half of an arcsecond. The OH masers are in a somewhat linear pattern lying east-west, and can be found in the eastern extension of source *a*. The near-infrared source from Testi et al. (1994) could be associated with either source *a* or *b*, but lies 3-4″ from both objects. If

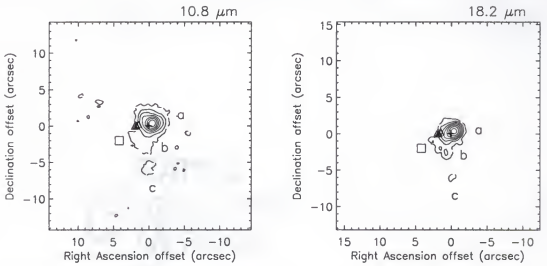

Figure 6-7: G28.86+0.07. This two panel display shows the N-band contours to the left and the IHW18 contours to the right. The symbols are the same as for Figure 6-2.

the K-band source is associated with the mid-infrared source, then source is most likely a young intermediate mass stellar source. If the near infrared source is a field star not associated with the mid-infrared source, then this may be another molecular core candidate.

G34.26+0.15 (IRAS 18507+0110)

This is another well-studied site of complex emission. This region has four radio continuum components, lying at a distance of 4.2 kpc (Forster and Caswell 1989). Following the nomenclature of Reid and Ho (1985) and Gaume et al. (1994), there is a cometary UCHII region here labeled source C. In front of the head of source C are two compact UCHII regions, B to the north and A to the south. Another large (D > 90″) HII region lies to the southeast of A, B, and C. A molecular core is seen in front of the head of source C in NH_3 (Heaton, Little, and Bishop 1989; Keto et al. 1992) and CH_3CN (Watt and Mundy 1999) between components A and B. In a paper that tests the two most

popular scenarios that might be the cause of the cometary morphology of source C, Gaume, Fey and Claussen (1994) rule out both the bow-shock and champagne flow models.

Their hypothesis for the morphology of the C source is that the compact UCHII regions A and B have stellar winds or outflows which impact the site of source C. They say that the cometary UCHII region lies at the edge of the molecular core, and the material being photoevaporated from the core is being swept past the stellar source C creating a tail. In a recent study, Campbell et al. (2000) claim that there is no contact between the molecular core and the cometary UCHII region, and though they look coincident, they are separated in distance to the Sun. They claim that the sources A and B are still the cause of the tail in source C, however it is the remnant material left over from the formation of the stellar source in component C that is being swept into a tail.

The water and OH masers in this area are curiously distributed. Most of the OH masers (Gaume and Mutel 1987) trace the bright limb of the cometary head, with the exception of the group which are coincident with the northern UCHII region B. This was thought by Van Buren et al. (1990) as being evidence of the bow-shock model because OH masers can exist in, and be pumped by, shocks. However the water masers in this region (Gaume, Fey, and Clauseen 1994) exist mostly east of the UCHII region head, though some are located in projection against source C. The water maser run linearly north-south extending from just south of B to a point 2″ south of A. These masers lie in the region occupied by the NH_3 (3,3) emission seen by Heaton, Little, and Bishop (1989). Therefore, these masers may be tracing this density enhancement (in which Keto et al. 1992 suggest is where several intermediate-mass stars may be forming). There may also

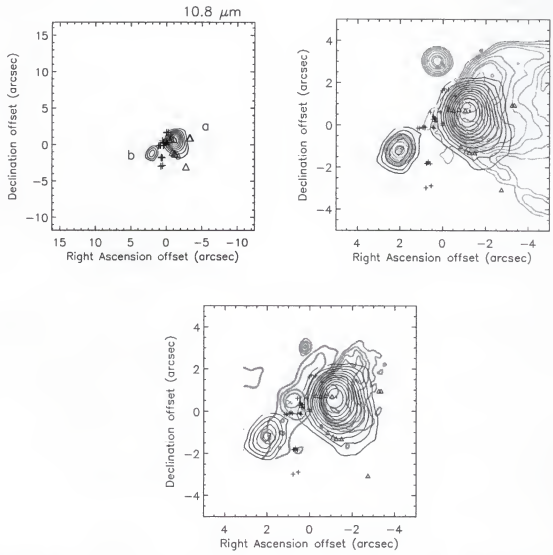

Figure 6-8: G34.26+0.15. This three panel display shows the N-band contours in each panel. The upper right panel shows an overlay of the 2 cm radio continuum contours (thick gray) from Gaume, Fey, and Claussen (1994). The lower panel shows an overlay of the ammonia contours (thick gray) from Keto et al. (1992).

be an interaction between in molecular core and the outflow from A and B which is stimulating maser emission.

The mid-infrared observations yield two bright mid-infrared sources at this maser site that were detected on both nights of observations. In the mid-infrared, the source morphology for C (which is labeled *a*) does not appear to contain such a drastic diffuse

tail. In fact, there is very little, if any, diffuse mid-infrared emission associated with source C in these images. The source is elongated in the north-south direction. Also detected was a mid-infrared source associated with UCHII region A, which is labeled *b*. Gaume, Fey, and Claussen (1994) see a double peak in the 2 cm emission of source C. These peaks are at the correct angle to explain the elongation of the mid-infrared source.

Interestingly, Keto et al. (1992) present a 12.5 μm image of this site which shows source A and C, just as in this survey. In addition, however, they see a third faint source east of source C. This 12.5 μm source is only 70 mJy, and is not coincident with any water masers, nor the molecular peak. No S/N is given, so the validity of this source can not be assessed.

A final point to be made for this source is that the most intense masers are located just east of the center of the head of source C. Interestingly, the lowest contour of Gaume, Fey, and Claussen (1994) pulls out toward this location. Careful inspection of the mid-infrared contours show this as well. This may be low level emission from the NH_3 clump, or part of a bridge of emission between A and C.

G35.20-0.74 (IRAS 18556+0136)

This site has been observed at multiple wavelengths and is found to be a region of complex activity. This location has been referred to as G35.2-0.74N, G35.2-0.7N, or simply G35.2N, and is thought to be one of the clearest examples of a bipolar molecular outflow surrounded by a molecular disc (Brebner et al. 1987). Indeed, this site lies at the center of a well-collimated outflow, which has been imaged in CO and +HCO by Little et al. (1983) and Matthews et al. (1984). The outflow lies at a position angle of ~45 degrees and is thought to exist nearly in the plane of the sky, with a hint of blueshift in the

northeast component in +HCO (Brebner et al. 1987) and ^{18}CO (Little, Kelly, and Murphy 1998). Bisecting this outflow emission is an elongated molecular source that is believed to be in rotation, as seen from a velocity gradient in NH_3 emission (Dent et al. 1985). However, the situation is not as simple as a central stellar source within a rotating molecular disk that is collimating the stellar winds into an outflow. Indeed, when infrared and radio observations are folded into this picture, things become messy.

The OH masers were observed here by Forster and Caswell (1989), who determine this site to lie at 2.3 kpc (a distance agreed upon in the literature and adopted in this paper). The OH masers were also studied by Brebner et al. (1987) and they find that they lie in a line at the same position angle as the NH_3 elongation. They also exhibit a rotation, however the sense is opposite that of the molecular disk. In fact, most of the masers are blueshifted, indicating an expansion. Maps made at 6 and 2 cm by Heaton and Little (1988) show four UCHII components. The three brightest UCHII regions lie in a line with a position angle of 0 degrees, inconsistent with the position angle of either the disk or outflow. Furthermore, there are bridges of radio continuum connecting all three sources.

Near infrared images at K by Dent et al. (1985) show an elongated source at a similar position angle to that of the UCHII regions. The peak of the K band emission is in between the northern and central UCHII regions and is offset slightly to the east. Neutral carbon maps of the area made by Little, Kelly, and Murphy (1998), also show an extended 'tongue' of emission to the north extending for over 20″. Higher resolution near infrared observations of this region reveal two lobes of emission separated by a dark lane, which Walther, Aspin, and McLean (1990) believe to be the location of the OH masers.

They say that the OH masers may be coincident with the exciting source for this region, but do not believe the central UCHII region seen at 6 and 2 cm is that source. This does not make sense, since the central UCHII region and the OH masers coincide in position. Both Walther, Aspin, and McLean (1990) and Dent et al. (1985) believe that the near-infrared radiation may be reflection off the northwestern cavity of the outflow from the central source.

It seems there may be three axes of interest at this site. One is at ~45 degrees and is traced by CO and +HCO. The second is orthogonal to this in the plane of the sky and is traced by an elongation seen in NH_3 and continuum emission at 1100 μm (Dent et al. 1989). The third axis of interest is at the position angle of 0 degrees and is traced by neutral carbon, radio continuum, near-infrared, and the mid-infrared observations. This mid-infrared source is highly elongated in the north-south direction with the peak offset to the south. The peak is coincident with the overlapping water and OH masers, and therefore coincident with the central UCHII region seen at 6 and 2 cm (Figure 6-9). In fact, the mid-infrared emission follows the radio emission bridge between the central and northern radio sources. The mid-infrared emission overlaps some of the northern near-infrared emission seen by Walther, Aspin, and McLean (1990). If the near and mid-infrared are tracing the same source, it could not be reflected light from the inner cavity of an outflow, because this could not produce the thermal emission seen in the mid-infrared images. Heaton and Little (1988) also point out that they believe the central UCHII region is the outflow source and that the northern and southern UCHII regions are ionized by the outflow and/or UV radiation from this central source.

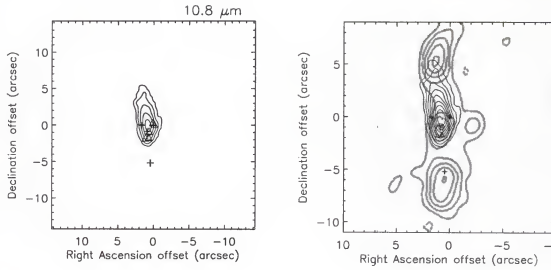

Figure 6-9: G35.20-0.74. The N-band contours are shown in both panels. Symbols are the same as for Figure 6-2. The right panel shows an overlay of the 2 cm radio contours from Heaton and Little (1988).

A different hypothesis can be argued for this site. It can be argued that each UCHII region is the site of a forming star. In fact the double peaked nature of the northern and southern UCHII regions may indicate that they house two stellar sources each. These 'strings' of forming stars are seen elsewhere in this survey (G00.55-0.85, G10.62-0.38, and G19.61-0.23), suggesting this scenario is plausible, contrary to the argument of Heaton and Little (1988). Furthermore, the NH_3 emission seen here may not be from a disk at all. The NH_3 (3,3) map shows emission coming from many large knots of material, and not one homogeneous elonagated disk-like source. It is plausible that the molecular emission here is from a group of dense molecular cores. The UCHII regions would simply be stars in various stages of formation within the molecular cores. In this way the near and mid-infrared sources are tracing UCHII regions which are centrally heated by a stellar source or sources. The elongated diffuse tail seen in the mid-infrared would be due to the density gradient in this area from the molecular cores. The motion

observed in the NH_3 may have triggered (or may still be triggering) the star formation in the southernmost density enhanced regions, leading to the UCHII regions and infrared sources seen today.

There is also a group of water masers from Forster and Caswell (1989), that are not coincident with the OH masers and lie just south of the mid-infrared source. Given the mid-infrared astrometry, they are coincident with the northern peak of southern UCHII region (Figure 6-9). This may be another case where the isolated water maser groups are coincident with an embedded source.

Finally, what of the CO outflow seen in this region? If the CO here is tracing outflow, and not a molecular density enhancement, then the outflow could come from any of the radio or infrared sources. In fact, it is likely that if these are all young stars, more than one star is in an outflow stage. This coupled with the fact that the center of the CO outflow map is anything but well determined, it would be difficult at best to understand the CO morphology given this scenario.

G35.20-1.74 (IRAS 19592+0108)

This site contains water, OH, and methanol masers, and contains a large cometary UCHII region. The UCHII region is known as W48A and lies about 20″ away from the location of the water and OH masers. This region has been well-studied. There is CO in the area with a peak to the west of W48A (Zeilik and Lada 1978; Valle and MacLeod 1990) and the whole region is within extended (~1′) amorphous submillimeter emission. W48A is a very interesting and complex source, however there are no masers associated

with it, and it seems unlikely that there is any relationship between it and the masers located 20″ away.

The distance quoted in the literature for this site range between 2.9 and 3.2 kpc (Forster and Caswell 1989; Churchwell et al. 1990; Hofner and Churchwell 1996; Downes et al. 1980), showing fairly good agreement. In this work, the distance of Hofner and Churwell (1996) of 3.1 kpc will be adopted.

The mid-infrared images in this survey reveal a bright point source at the location of the water masers, as well as the UCHII region to the south-east. A paper by Persi et al. (1997), presents observations of G35.20-1.74 at 11.2 μm and at K. They claim to see six mid-infrared sources in the area, and detect the same source seen in this survey coincident with the masers at both 11.2 μm and K. The mid-infrared observations also reveal the same six mid-infrared sources at N. The source Persi et al. (1997) labeled MIR3 corresponds to the UCHII region W48A, and can be see quite predominantly in the mid-infrared images (Figure 6-10). The source labeled MIR1 corresponds to the source in this survey that is seen coincident with the maser features. K images of this source by Persi et al. (1997) show the source to have an elongation or tail pointing to the southwest. This elongation is not seen in either of the N or IHW18 images, nor in the 11.2 μm image of Persi et al. (1997). Though the group of water masers given by Forster and Caswell (1989) are found to the northeast of the mid-infrared source, the water maser of Hofner and Churchwell (1996) is coincident with it. The OH masers appear to be pointing radially away from this mid-infrared source towards the northeast, in the opposite sense as the near infrared tail of emission. Perhaps in this case the OH and water masers are tracing an outflow in the northeastern lobe, and the near infrared emission is reflected

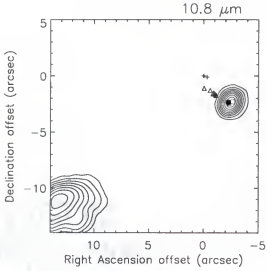

Figure 6-10: G35.20-1.74. The N-band contours, with symbols shown as they are in Figure 6-2. The black dot marks the location of the water maser of Hofner and Churchwell (1996).

light coming from the inner wall of the cavity produced by the southwestern outflow lobe. Unfortunately, the only available CO maps are those of Zeilik and Lada (1978) which have a 3′ resolution and it is difficult to tell if there is any semblance of outflow on such a crude scale.

G35.58-0.03 (IRAS 18538+0216)

This site contains radio continuum emission, water and OH masers, but no methanol masers. Caswell et al. (1995a) failed to detect any methanol maser emission here with an upper limit of 250 mJy. Kurtz, Churchwell, and Wood (1994) find the radio continuum here to be coming from two extremely close UCHII regions, which appear just resolved in their 3.6 and 2 cm maps. Kurtz et al. (1999) have 21 and 3.6 cm maps showing the UCHII regions to be lying in large scale extended continuum emission. They consider the two UCHII regions separate sources: G35.578-0.030 to the west, and

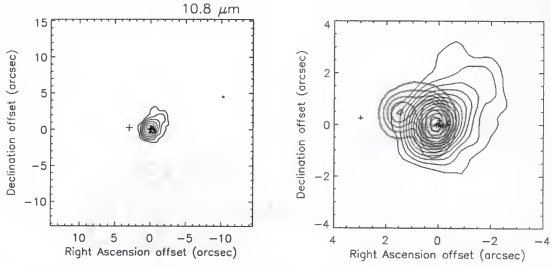

Figure 6-11: G35.58-0.03. This two-panel display shows the N-band contours in both panels. The right panel in overlaid with the 3.6 cm contours (thick gray) from Kurtz, Churchwell, and Wood (1994). Symbolics are the same as in Figure 6-2.

G35.578-0.031 to the east. Plume, Jaffe, and Evans (1992) detect CO and CS toward this site. However, Anglada et al. (1996) did not detect NH_3 emission here.

There is pretty good agreement in the literature concerning the distance to this site. Kurtz et al. (1999), Forster and Caswell (1989), and Downes et al. (1980) all agree on a distance of about 3.5 kpc. This distance is adopted here.

There is good agreement in position between the western UCHII region of Kurtz, Churhwell, and Wood (1994) and the water and OH masers located here. It was also found that the mid-infrared source is situated close to the masers. This source is relatively bright at N (1.6 Jy) and elongated to the northwest. The mid-infrared astrometry shows the water maser reference feature is offset by a little more than an arcsecond to the north of the peak of the mid-infrared source. By comparing the mid-infrared image with the 3.6 cm radio image of Kurtz et al. (1999), it can be seen that there is a little extension in the western UCHII region at approximately the same position angle as the mid-infrared

source elongation. It can therefore be concluded with some confidence that the mid-infrared source is in fact the same source as the western UCHII region G35.578-0.030. There are, however, no signs of mid-infrared emission from the eastern UCHII region, G35.578-0.031.

G40.62-0.14 (IRAS 19035+0641)

This site contains all three maser types and a UCHII region. The OH and water masers here are coincident and well mixed spatially. The UCHII region detected here at 6 cm by Hughes and MacLeod (1993), is unresolved with their 3″ resolution. It is also a weak radio source, having an integrated flux density of 3.8 mJy. The molecular species that have been detected toward this site are CS and CO, but not NH_3 (Larionov et al. 1999; Anglada et al. 1996; Plume et al. 1992). There are several distances quoted in the literature, all which hover around the value given by Forster and Caswell (1989) of 2.3 kpc, so this value will be adopted here.

A fairly bright and unresolved source was detected in the mid-infrared at this site. Even though most of the masers are within the contours of the mid-infrared source, the water maser reference feature is offset from the mid-infrared source peak. The mid-infrared source peak is 1.7″ west and 1.0″ south of the water maser reference feature. The astrometry may be off, but most likely it is accurate. The UCHII region peak of Hughes and MacLeod (1993) is also off by 1.9″ west and 1.1″ south of the water maser feature coordinates. This offset is therefore most likely real and that the UCHII region is the radio continuum component of the source seen in the mid-infrared. Osterloh et al. (1997) found a K′ source situated 3″ to the northeast of the mid-infrared source. It is elongated in

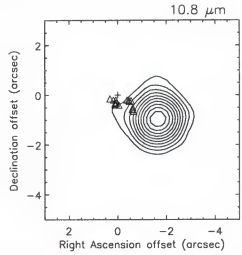

Figure 6-12: G40.62-0.14. N-band contour plot with symbols as described in caption of Figure 6-2.

the northeastern direction as well. They state that it may appear elongated because the near infrared light is being reflected off of an outflow cavity from the star within the UCHII region which is too heavily embedded to have a near-infrared component of its own. If this is true, the OH and water masers, which are distributed somewhat linearly and at the correct position angle, may be tracing the outflow into this cavity.

G43.80-0.13 (IRAS 19095+0930)

This site contains water, OH, and methanol masers, as well as radio continuum emission. Kurtz, Churchwell, and Wood (1994) say that the radio source here is unresolved, however there are in fact two sources that can be seen in their maps at 3.6 and 2.0 cm. There are also molecular lines of CO and CS detected here (Osterloh et al. 1997; Larionov et al. 1999, Plume, Jaffe, and Evans 1992), but no NH_3 was found (Anglada et al. 1996).

There is considerable agreement in the near kinematic distance to this site of 3.1 kpc (MacLeod et al. 1998; Osterloh et al. 1997; Forster and Caswell 1999). However, Forster and Caswell (1999) suggest that the far kinematic distance is more likely, but do not suggest why. The closer kinematic distance is adopted here, in the absence of a compelling argument otherwise.

Two distinct sources were detected in the mid-infrared. The eastern source is very low S/N and has no associated UCHII region or masers. The western mid-infrared source is kidney bean shaped and is coincident with the OH and water masers. By overlaying the radio continuum maps of Kurtz, Churchwell, and Wood (1994) it was found that the double peaked UCHII region matches the kidney bean shape seen in the mid-infrared. Given the absolute astrometry of the radio continuum map of Kurtz, Churchwell, and Wood (1994), it was found that the water maser positions given by Forster and Caswell (1989) are offset from the UCHII region by 2.5″. This is nearly the same offset seen in the mid-infrared image given the pointing accuracy alone between the masers and the mid-infrared source. However, Forster and Caswell (1989) claim to see a UCHII region coincident with the water maser reference feature. It can be concluded that the UCHII region seen by Forster and Caswell (1989) and the UCHII region seen by Kurtz, Churchwell, and Wood (1994) are most likely the same source. This would indicate that the absolute astrometry given by Forster and Caswell (1989) for this particular set of masers is in error. Similar errors have been pointed out by Forster and Caswell (1999) for other sources in the Forster and Caswell (1989) survey. Figure 6-13 is shown with this correction to the maser positions.

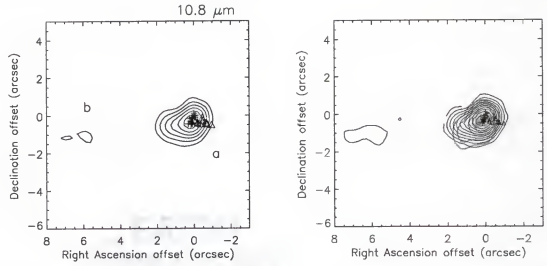

Figure 6-13: G43.80-0.13. This two panel display shows N-band contours. The right panel has an overlay of the 3.6 cm radio contours (thick gray) from Kurtz, Churchwell, and Wood (1994). The symbols are the same as for Figure 6-2.

The mid-infrared source is elongated east-west, and also to the northwest. Interestingly, the OH masers lie predominantly in an east-west fashion, whereas the water masers lie in an elongated distribution pointing to the northwest. It is not certain what sort of processes are being traced by the masers here. It is also not known what the relationship is, if any, between the faint eastern source and the activity surrounding the western source.

G45.07+0.13

This is a well-studied site which contains all three masers types and a UCHII region. The water and OH masers are intermixed and exist in two groups separated by about 1.7″. Hofner and Churchwell (1996) present a 2 cm map of this site, which shows a solitary unresolved UCHII region. The southern group of water masers lie across the continuum in a linear fashion at a position angle of approximately -45 degrees. A multi-

wavelength study (CO, CS, millimeter, submillimeter) of G45.07+0.13 was performed by Hunter, Phillips, and Menten (1997). They find this site to be the center of a molecular outflow. Their CS maps show the outflow is centered close to the UCHII region, and that the bipolar outflow axis is roughly the same as that of the water masers. Hofner and Churchwell (1996) suggest that the water masers here trace the outflow.

There is pretty much unanimous agreement in the literature that this site lies at the far kinematical distance of 9.7 kpc (Faison et al. 1998; Forster and Caswell 1989; Braz and Epchtein 1983; Downes et al. 1980), but no reason is given as to why the far distance is favored. The value of 9.7 kpc is adopted here.

Hunter, Phillips, and Menten (1997) believe that G45.07+0.13 is a single star early in its evolutionary phases. To the contrary, their are three mid-infrared sources within 8″ of the water maser reference feature (Figure 6-14). Two of the sources seem to be associated with the masers in the area. Sources *a* and *b* are close mid-infrared sources, with the water and OH maser reference features closest to source *a*. In fact the mid-infrared astrometry puts the water maser reference feature within 0.25″ of the peak of source *a*. The offset between the northern maser group and southern maser group is exactly the angular separation between the mid-infrared sources *a* and *b*. The southern water masers lie in a line that goes through the peak of source *a*. The southern OH masers lie in a line at a position angle of 45 degrees, perpendicular to the outflow axis and the water masers. The OH masers in the northern group are linearly distributed at the same position angle as the southern OH maser group. The 2 cm map of Hofner and Churchwell (1996) were registered with the mid-infrared image. It was found that the UCHII region peak is offset from the peak of the mid-infrared source by 1″ to the east. It is difficult to

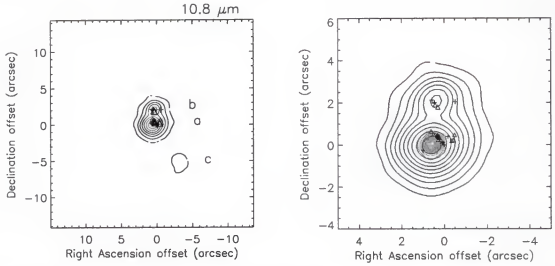

Figure 6-14: G45.07+0.13. A two panel N-band contour plot. The right panel has an overlay of the 2 cm radio continuum emission (gray) from Hofner and Churchwell (1996).

determine whether or not this offset is real. However, it is not unreasonable to assume that for unresolved sources at both mid-infrared and radio wavelengths, that the peaks should coincide. Therefore, the mid-infrared source was shifted to coincide with the UCHII region peak (Figure 6-14).

G45.47+0.05

This source contains water and OH masers, as well as methanol masers and a UCHII region. Interestingly, there is no IRAS point source within 2′ of the water maser reference feature. Molecular tracers such as CS, HCO, SiO, and NH_3 have been detected towards this site (Olmi and Cesaroni 1999; Cesaroni et al. 1992). There is also a submillimeter and millimeter source coincident with the UCHII region here. The UCHII region, as seen by Wood and Churchwell (1989a), has a kidney bean shape and is coincident with the water and OH masers.

There is a fair amount of variation on the distance to this site in the literature, from 6.0 kpc (Hatchell et al 1998) to 9.7 kpc (Downes et al. 1980). However, the recent distance estimate of 8.3 kpc made by Kuchar and Bania (1994) is adopted here, which is based upon the method of using HI absorption measurements.

An interesting argument has arose concerning this object. Cesaroni et al. (1992) found emission and red-shifted absorption towards this site in NH_3. They claimed this is due to a cloud surrounding the UCHII region collapsing onto the UCHII region. Further observations were performed at higher resolution by Wilner et al. (1996) in HCO and SiO. They claim that the cloud core as seen in HCO emission appears clumpy and fragmented. They say that it is likely that this site is in an early stage of forming an OB star cluster. They claim that their HCO images provide no evidence for a spherical collapse localized to the UCHII region as suggested by the observations of Cesaroni et al. (1992). However, the most recent observations of NH_3 by Hofner et al. (1999) suggests that this source is indeed undergoing infall of the remnant molecular core onto a UCHII region where a massive star has recently formed.

The mid-infrared data may not be able to help solve this controversy, however it is interesting to note that the NH_3 in this area, as seen by Hofner et al. (1999), is elongated at a position angle of about -40 degrees. The mid-infrared observations of this site show a single elongated source lying at a position angle of -40 degrees. If the material is indeed falling into the UCHII region, which is thought to exist in the center of the NH_3 emission, then this may be an accretion disk around the central stellar source.

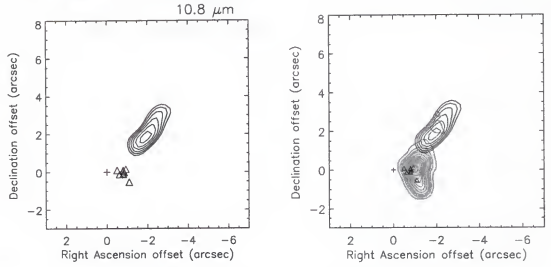

Figure 6-15: G45.47+0.05. A two panel plot of N-band contours. The right panel shows the overlay of the 6 cm radio continuum contours (thick gray) from Wood and Churchwell (1989). Symbols are the same as in Figure 6-2.

The relative astrometry between the UCHII region seen by Wood and Churchwell (1989a), the masers seen by Forster and Caswell (1989), and the mid-infrared source is uncertain. Whereas the UCHII region seems to be located coincident with the OH masers and only slightly offset from the water maser reference feature (~1″), the astrometry places the mid-infrared source peak ~2.5″ northwest from the UCHII region peak. It seems unlikely that the mid-infrared astrometry could be that far off, but an error in astrometry can not be ruled out. If the mid-infrared astrometry is assumed to be accurate, the positional offset between the UCHII region, masers, and the infrared source is given in Figure 6-15. There may be two different stellar sources, one associated with the mid-infrared source and one with the radio source. There is a hint of radio emission from the location of the peak of the mid-infrared source as seen in Figure 6-15

G48.61+0.02 (IRAS 19181+1349)

This site contains water and OH masers but no methanol masers. Caswell et al. (1995a) put an upper limit on the detection of methanol masers here at 200 mJy. This site also contains a complex arrangement of radio continuum that was imaged at 3.6 and 2 cm by Kurtz, Churchwell, and Wood (1994), who identified three ultracompact components in a field of extended continuum. G48.606+0.023 lies to the southeast, G48.606+0.024 lies in the middle, and the diffuse and extended G48.609+0.027 lies to the north. This area was also found to have CO and CS, but no NH_3 (Anglada et al. 1996; Plume, Jaffe, and Evans 1992).

The far kinematical distance is adopted to this site, following the precedent started by Solomon et al. (1987) based upon his results from studying HI absorption towards this location. The general agreement for the far distance is 11.8 kpc, as given by Forster and Caswell (1989).

There are three low S/N mid-infrared sources located at this site, and a bright double source located to the north. The water and OH masers seem to be located between sources *b* and *c*, which are separated by about 5″ (Figure 6-16). By overlaying the radio continuum maps of Kurtz et al. (1999) on the mid-infrared image, there was no single registration between the two that would yield a coincidence for all of the mid-infrared sources. However, if one assumes the observed astrometry between the mid-infared image and the water masers is good, and the radio map of Kurtz et al. (1999) is registered with the water maser position, a good match is found for the bright infrared sources in the northwest (not seen in Figure 5-16) and the UCHII region designated G48.609+0.027. A consequence of this is that the radio emission from G48.606+0.024 is just to the

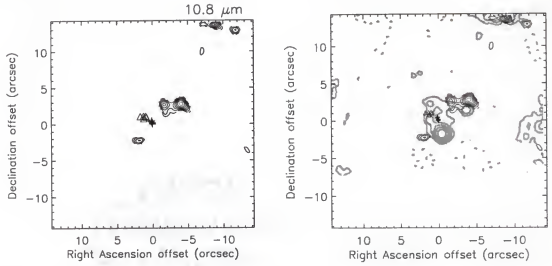

Figure 6-16: G48.61+0.02. A two panel N-band contour plot. The right panel shows a radio continuum overlay from the contours of Kurtz et al. (1999). Symbols are the same as for Figure 6-2.

northwest of source *a*, and G48.606+0.023 is just to the southeast of source *c*. This means that G48.606+0.023 is most closely associated with the water masers here, and its extended emission towards the northwest contains the OH masers. What relationship the mid-infrared sources *a* and *c* have with G48.606+0.024 and G48.606+0.023 respectively, is unclear. The mid-infrared astrometry may be off, such that the mid-infrared source *a* is coincident with G48.606+0.024. In this case, there would still be a coincidence between the bright mid-infrared binary and G48.609+0.027, however, source *c* would not be coincident with any radio source.

G49.49-0.39

This site lies in an extensive (D ~ 12′) star forming region named W51. The closest IRAS point source is 19213+1424, however this is coincident with W51-North, which is about 1′ away from where the water maser location. Martin (1972) observed this

region in centimeter continuum emission and named the eight components here as W51 a-h. The strongest radio continuum emission is from W51e and d. Scott (1978) found the two small UCHII regions, in addition to the larger HII regions e and d. Because of their proximity to W51e, they were named e1 and e2. More recently, Gaume and Johnston (1993) discovered two more compact continuum components near the large e HII region at 3.6 cm, which were named e3 and e4. Most recently Zhang and Ho (1997) discovered a source named e8 at 1.3 cm that lies between e4 and e1. The water and OH masers are spread over a 10″ region, within which these small HII regions (e1-e4, and e8) are located.

The distance to this site is quoted as 7.3 kpc in the literature. This is the far kinematic distance, which was chosen because of the results of Kuchar and Bania (1994). They find the HI absorption spectra towards the HII regions W51 e and d clearly show absorption beyond the recombination line velocity, indicating the far distance. They say that if all of the sources are at the same distance then the far distance of 7.3 kpc is preferred. This distance will be adopted here.

The observations in the mid-infrared for this region show a single unresolved point source lying ~15″ south from some extended emission (Figure 6-17). This nebulosity is the southern portion of W51e. Given the astrometry of this survey, it was found that none of the masers in this area correspond to the point source seen it the mid-infrared. However, by overlaying the radio continuum maps of several authors, it was found that the mid-infrared source lies only 2″ west of e1. It is uncertain if the source seen in the mid-infrared is e1 or another embedded source. However, even if the mid-infrared source is coincident with e1, nothing new is learned about the excitation of the

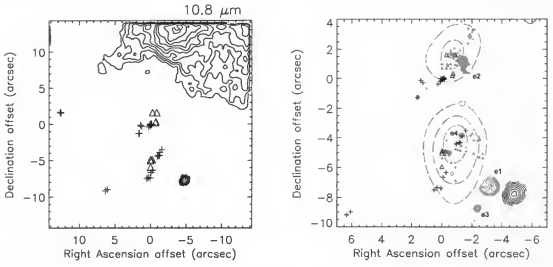

Figure 6-17: G49.49-0.39. A two panel N-band contour plot. The right panel shows the 3.6 cm radio continuum (continuous gray) contours of Gaume, Johnston, and Wilson (1993), and the ammonia contours (broken gray) from Ho et al. (1983). Symbols are the same as for Figure 6-2. The same gray symbols are other water and OH masers as observed by of Gaume, Johnston, and Wilson (1993).

masers in this area because e1 is not coincident with any known masers. All of the masers in this area lie close to, or are coincident with, the UCHII regions e2, e4, and e8 (Figure 6-17). Furthermore, there are two ammonia clumps in this area, one coincident with e2, and the other with e4 and e8 (Ho et al. 1983). These molecular clumps can also be seen at 2 mm, CS, and CH_3CN. It is therefore likely that the maser are excited by stars embedded in these molecular clumps and with the sources already seen because of their radio continuum emission.

Results and Discussion

A summary of the observed and derived quantities for the sources in the water maser selected survey, as discussed in the last section, are given in Table 6-1. Sources

Table 6-1: Observed and derived parameters for the mid-infrared sources

Target Name	D (kpc)	Source	$F_{10.4\mu m}$ (Jy)	$F_{18.0\mu m}$ (Jy)	T_{dust} (K)	$\tau_{9.7\mu m}$	Av	L_{MIR} ($L_{\odot m}$)
G00.38+0.04	10.0[1]	--	0.59±0.01	<0.10	--	--	--	--
G00.55-0.85	9.1[1]	a (o)	2.54±0.02	20.03±0.15	133	0.044	0.8	7220
		b (w)	0.27±0.01	<0.10	--	--	--	--
		c	1.88±0.02	13.66±0.13	136	0.064	1.6	4880
		d	0.37±0.01	5.54±0.12	115	0.037	0.7	2240
G10.62-0.38	6.5[1]	a (w)	0.26±0.01	2.04±0.02	133	0.026	0.5	374
		b (o)	0.15±0.01	0.51±0.01	165	0.003	0.05	95
		c[▼]	0.03/0.05 ±0.01	0.38/0.39 ±0.01	143/130	∞/0.006	∞/0.11	148/73
		d	0.07±0.01	<0.10	--	--	--	--
		e[▽]	0.07/0.09 ±0.01	0.28/0.29 ±0.01	193/167	--	--	84/54
G12.68-0.18	4.9[2]	a (w)	0.19±0.01	0.81±0.08	155	0.005	0.09	83
		b	0.11±0.01	<0.10	--	--	--	--
G16.59-0.05	4.7[3]	a (w,o)	0.03±0.01	<0.10	--	--	--	--
		b	0.29±0.01	<0.10	--	--	--	--
G19.61-0.23	4.0[4]	a	4.24±0.03	21.88±0.16	147	0.037	0.7	1490
		b (w,o)	9.86±0.04	54.57±0.21	144	0.059	1.1	3710
		c	3.00±0.03	9.52±0.25	167	0.011	0.20	671
		d	3.70±0.04	15.50±0.18	155	0.006	0.11	1060
		e[▽]	0.22/0.33 ±0.03	27.95/28.85 ±0.09	89/85	--	--	18000/4370
		f	<0.01	10.83±0.05	--	--	--	--
		g	<0.01	13.92±0.08	--	--	--	--
		h (w)	<0.01	0.23±0.03	--	--	--	--
G28.86+0.07	8.5[5]	a (w,o)	2.24±.0.01	6.61±0.13	171	0.058	1.0	2130
		b[▽]	0.06/0.08 ±0.01	0.71/0.74±0.05	141/129	--	--	482/235
		c[▽]	0.03/0.04 ±0.01	0.35/0.36±0.05	141/115	--	--	236/115
G32.74-0.07	2.5[5]	--	<0.01	--	--	--	--	--
G33.13-0.09	7.1[6]	--	<0.01	--	--	--	--	--
G34.26+0.15	4.2[5]	a	4.52±0.04	--	--	--	--	--
		b	0.74±0.02	--	--	--	--	--
G35.03+0.35	3.0[5]	--	<0.01	--	--	--	--	--
G35.20-0.74	2.3[5]	-- (w,o)	2.81±0.09	--	--	--	--	--
G35.20-1.74	3.1[6]	-- (w,o)	2.33±0.03	--	--	--	--	--
G35.58-0.03	3.5[5]	-- (w,o)	1.55±0.04	--	--	--	--	--
G40.62-0.14	2.3[5]	-- (w,o)	0.93±0.03	--	--	--	--	--
G43.80-0.13	3.1[5]	a (w,o)	1.00±0.04	--	--	--	--	--
		b	0.48±0.03	--	--	--	--	--
G45.07+0.13	9.7[7]	a (w,o)	20.41±0.04	--	--	--	--	--
		b (w,o)	4.26±0.02	--	--	--	--	--
		c	0.89±0.02	--	--	--	--	--
G45.47+0.05	8.3[8]	--	0.29±0.03	--	--	--	--	--
G45.47+0.13	9.3[5]	--	<0.01	--	--	--	--	--
G48.61+0.02	11.8[5]	a	0.07±0.01	--	--	--	--	--
		b	0.12±0.02					
		c	0.06±0.02	--	--	--	--	--
G49.49-0.39	7.3[8]	a	1.77±0.04	--	--	--	--	--
		b	0.24±0.04	12.74±0.05	96	1.685	30.5	5310

Note. – Distances in column 2 are from: 1) Walsh et al. (1997); 2) This work; 3) Codella et al (1997); 4)Genzel and Downes (1977); 5) Forster and Caswell (1989); 6) Hofner and Churchwell (1996); 7) Wood and Churchwell (1989a); and Kuchar and Bania (1994). A 'w' denotes the mid-infrared source closest to the water masers, and an 'o' the closest to the OH masers. A diamond means that the source was unresolved, and values are given in the form BB/UL (as described in Table 5-1). A upside-down triangle designates unresolved, low S/N sources, whose values are given by BB/OT (as described in Table 5-1). The flux densities are quoted with their statistical errors. The estimated absolute photometric accuracy is ±8% at N and ±10% at IHW18.

marked with a 'w' are those closest to the water maser emission, and those marked with an 'o' are closest to the OH masers.

The Search for Embedded Sources and Outflows

Since there are a significant number of water masers that are not coincident with radio continuum sources, there have been two main hypotheses suggested to resolve this puzzle. The first hypothesis is that the water masers are excited by embedded massive stellar sources, and exist in their accreting envelopes (Mezger and Robinson 1968). These stars are too young and too obscured to show signs of significant radio emission. However, it was only recently that data has been obtained that supports this hypothesis. The paper by Cesaroni et al. (1994) remains the most comprehensive work on the subject, even though their work involved molecular ammonia observations towards four UCHII regions only. In all four cases they found ammonia clumps near the UCHII regions, and in all four cases the water masers were directly coincident with the ammonia emission rather than the radio continuum emission in the area.

Before furthering the discussion on embedded sources, a potentially confusing issue of nomenclature must first be cleared up. Very often in the literature one sees the words 'molecular clump' and 'molecular core', and often these terms are used by the same authors to describe the same object. However, there are two physically distinct types of molecular emission in massive star forming regions. The first is the wide-spread molecular material that the star-forming region is made out of. This will be referred to here as a molecular 'core'. It is a sub-condensate inside of, and made from, a giant molecular cloud. These cores, in turn, can have sub-condensates of their own, which will

be referred to as 'clumps'. These clumps are most likely are the precursors to stars and their UCHII regions. Cores can be observed by molecular transitions which trace cool, less-dense material (CS 2-1, for instance). Clumps are observed through molecular transitions that trace hot, dense molecular material. For example, Cesaroni et al. (1994) used observations in the (4,4) line of ammonia, which traces gas with kinetic temperatures of 50-200 K and densities approximating $n_{H2} \sim 10^7$ cm^{-3} ($n_{NH3}/n_{H2} > 10^{-6}$).

Cesaroni et al. (1994) argue that gas and dust would be well mixed in the ammonia clumps and that there would be a high rate of collisions between the dust and gas. Krugel and Walmsley (1984) estimate that temperature equilibrium between gas and dust should exist when $n_{H2} > 10^5$ cm^{-3}. Given the high densities of these clumps, it can be concluded that the gas kinetic temperature is a fair approximation to the dust temperature. The gas temperatures were observed by Cesaroni et al. (1994) to be between 50 and 165 K. They argue that at these temperatures, the mid-infrared would be a perfect wavelength regime for the discovery of more of these hot molecular clumps.

Five embedded source candidates were found in this mid-infrared water maser selected survey. These candidates are G12.68-0.18a, G16.59-0.05a, G19.61-0.23h, G28.86+0.07a, and G45.07+0.13b. The compact, low-luminosity source (L_{MIR}=83 L_{sun}) G12.68-0.18a is close, but does not seem coincident with, the water masers given the mid-infrared astrometry. However, it is not unlikely, within the errors of the mid-infrared and the radio maser astrometry, that G12.68-0.18a is indeed coincident with the water maser group. G12.68-0.18 also has no radio component, signifying it's youth. Furthermore, the area is rich in molecular material as found from observations of CS, CO, and NH_3. In the case of G16.59-0.05, there is a weak source detection at N and a 2σ

detection at IHW18. This source is coincident with both the water masers and the OH masers in this area. It is also the location of an extremely weak radio continuum source (0.3 mJy at 3 cm) as seen by Forster and Caswell (2000). Molecular tracers such as NH_3 and CS have also been observed towards this site. A point that does not favor the embedded source hypothesis is that Testi et al. (1994) claim there is a source here, which they observed at J, H, and K. It is entirely possible, however, that the source they are seeing is a field star, and not the same source observed here in the mid-infrared. For G19.61-0.23, a very weak (230 mJy) source was detected at IHW18 only, coincident with an isolated group of water masers. The ammonia emission maps of Garay et al. (1998) show that the main string of water and OH maser here are directly coincident with the elongated ammonia peak. A small clump of four masers just to the west of the main maser group, still lie within the extended ammonia clump. The location where G19.61-0.23h is located is one of the few areas in this field where there is no radio continuum emission. Source G28.86+0.07a is a mid-infrared source that is directly coincident with a small group of water masers. This site contains molecular tracers such as NH_3, CS and CO, but has no detectable radio continuum. Testi et al. (1994) find a near-infrared source in this region, but it is located almost 5″ from either the water masers or the peak of source *a*. This may mean that the near-infrared source is not likely associated with the mid-infrared source or the water masers, and may be a field star. Finally, G45.07+0.13b is a mid-infrared source located just 2″ north of a UCHII region. It is rather bright (~ 4 Jy at N), and is directly coincident with the isolated northern group of water and OH masers in this region. Molecular emission is found here from CS and CO studies.

There are three reasons why it is believed that these five mid-infrared sources are sources embedded in molecular clumps. First, this survey has relatively good astrometry and these sources are directly coincident with clusters of water masers. Second, all of the mid-infrared sources have no (or barely detectable) radio continuum emission, implying that they are indeed young and embedded. And finally, there are observations providing evidence of molecular emission coming from each of these regions, a necessary condition if these are molecular clumps. These three pieces of evidence combined lead to the belief that these are indeed young stellar sources embedded in molecular clumps.

The second hypothesis for the excitation of water masers away from radio continuum sources is the outflow hypothesis. There are two ways in which one can get maser emission from an outflow. The first is when masers trace the high-collimated outflow near the stellar source, and the second is when the outflow impinges upon the ambient medium or on a pre-existing knot of molecular material.

The water masers that trace outflow are most likely associated with a jet. A jet is well-collimated flow, with an opening angle no more than a few degrees, and can exist concurrently with the wider angled bipolar molecular outflow. Gwinn et al. 1992 speculate that the masers may be gas condensations or 'bullets' that move out from a common center. A later paper by Mac Low et al. (1994) propose that the masers come from the shell of swept-up gas that is driven out by a jet. These cocoons are very elongated and expand quickly along the ends in the direction of the jet, but slow along the transverse sides. Specifically, the water masers are formed in the outer shock of the expanding jet cocoon. One source in the water maser selected survey has been viewed as an example of this phenomena in the literature. G45.07+0.13 has a known CO outflow

(Hunter, Phillips, and Menten 1997) and has water masers (as observed by Hofner and Churchwell 1996) distributed in a linear fashion parallel to this outflow angle, and running through the UCHII region peak. Hunter, Phillips, and Menten (1997) claim that this strongly supports the theoretical ideas that a protostellar jet from a massive star can power H_2O masers. Hofner and Churchwell (1996) also claim that these water masers are located along the flow axis and show good correspondence with the outflow velocities. They too claim this is strong evidence that the water masers are taking part in the bipolar outflow. The OH masers are also linearly distributed here, with a position angle near perpendicular to the water masers and outflow axis. These may delineate a circumstellar disk, however the masers are offset from the UCHII and mid-infrared peak by 0.5", and there is no hint of elongation in the thermal dust distribution.

Other possible sources where water masers may be tracing outflow in this manner are G00.55-0.85b and G10.62-0.38a. For G00.55-0.85, there is a string of water masers pointing radially away from source *b* towards source *a*. Though CO has been detected toward this site (Plume, Jaffe, and Evans 1992), there is no other information available concerning CO outflow. One notices when looking at source *a* that the OH masers are situated at a position angle perpendicular to the water masers, but near the edge of the UCHII region. These OH masers may be shock-excited by the outflow (as traced by the water masers) impinging upon source *a*. As for source G10.62-0.38a, the situation is a little more complicated. The string of masers in this case appear to lie in a line that goes through the peak of mid-infrared source *a*. The radio emission is coincident with the water and OH masers here, and not the mid-infrared sources. Since outflows can contain partially ionized gas (~10%, Masson and Chernin 1993), they are easily observed at radio

wavelengths longer than 1 cm (Rodriguez, 1994). An alternative scenario could be that the water masers are, indeed, tracing an outflow from source *a*. This outflow is to the southeast, but also angled toward the Earth. The 6 cm radio emission in Figure 6-3 is from the ionized material in this outflow. Inspection of this radio emission reveals that it exists everywhere east of source *a*, but does not overlap source *b*. Source *b* could be situated in this star forming region a little closer to the Earth than source *a*, and the outflow impinging upon it could create the OH maser emission. This scenario not only describes the linear arrangement of water masers, but also the strange distribution of radio emission and OH masers.

The second way an outflow can stimulate water maser emission is, as was explained above, by the shock of the outflowing gas on surrounding material. Elitzur (1992b) describes a model where water masers are locally created and pumped by the interaction of the outflow from a young star with clumps or inhomogeneities in the surrounding cloud. Unfortunately, this is a difficult hypothesis to try to prove with the mid-infrared survey alone. One would have to look for water masers offset from a mid-infrared source, but could not be sure if they are associated with an outflow or simply associated with, say, an embedded source too cool to detect in the mid-infrared. One would need auxillary information, such as CO outflow data, in order to be confident that the water masers are in fact associated with shocks from outflows.

The Nature of Sources with Water Maser Emission

Because the mid-infrared survey was incomplete and only a third of the target list was observed at two wavelengths (only 7 fields), no assessment of the survey as a whole

can be made based on physical properties (such as spectral type or temperature). Results are therefore limited to a discussion of the source morphologies and their spatial relationship with respect to the water (and OH) maser distributions. Fortunately, the astrometry of the water maser selected survey is accurate enough to allow such an analysis.

The mid-infrared survey contains 21 targets, however G19.61-0.23 has three centers of water maser emission, and G45.07+0.13 has two centers of water maser emission. It is difficult to assess if the masers spread throughout G34.26+0.15 and G49.49-0.39 are from separated centers of emission or perhaps just maser sources spread out in an extended source. Assuming the masers from G34.26+0.15 and G49.49-0.39 are each a large but single group of masers, there is a total of 24 water maser groups. Mid-infrared sources were detected within 4 arcsec of 18 of the 24 centers of water maser emission (75%). This is similar to the ratio for compact radio continuum emission, which is found near 17 of 24 centers in this survey (71%). This is also consistent with the results of Churchwell et al. (1990) who searched for water maser emission from a large number of UCHII regions. They used the Effelsburg 100 m radio telescope, which has a FWHM of 40 arcsec, and detected water maser emission in 67% of the cases.

There are only two targets in this survey that do not have either radio or mid-infrared sources associated with the water masers, G32.74-0.07, and G45.47+0.13 (which also has no IRAS component). Water masers only associated with a mid-infrared source, means that the sources may be very young, but not necessarily massive. Water maser emission has been found in association with outflows from young lower mass star, such as T-Tauri stars (Garay et al. 1998). On the other hand, the sources with both mid-

infrared and radio emission are most likely young massive stars that have the ability to ionize their surroundings. From this result it can be concluded that water masers are indeed associated with young and/or massive stars and their stellar processes.

Hofner and Churchwell (1996) found that the median separation from UCHII region peaks to water maser centers is 2.9″ or 0.091 pc (19,000 AU). In a near-infrared survey of water maser emission by Testi et al. (1998), they identify a K-band source within 5″ of the water maser components in 73% of the cases (they claim their astrometry is good to 1″). They caution, however, that their survey may have some contamination from field sources. It was found in the mid-infrared survey that the median angular separation between the water masers and the mid-infrared source peak is 1.22″, and the median physical separation is 0.042 pc (8690 AU). A similar result was found for the coincidence of OH masers with the mid-infrared sources (1.33″, 8590 AU). The mid-infrared results exclude the masers associated with G34.26+0.15 because there was confusion in identifying which source the masers were associated with (though most were within ~3″ from *a* or *b*). Also excluded were G00.38+0.04 and G49.49-0.39, which are most likely not associated with any of the water masers in their field. It can be concluded that for the sources in this survey, water (and OH) maser emission is more closely associated with mid-infrared emission than radio continuum emission. Furthermore, there also seems to be a better association of water masers with mid-infrared sources than near-infrared sources.

Figures 6-18a and 6-18b present histograms showing the number of water and OH masers given the separation from the mid-infrared source center. These results can be compared with those from Hofner and Churchwell (1996), for the distribution of water

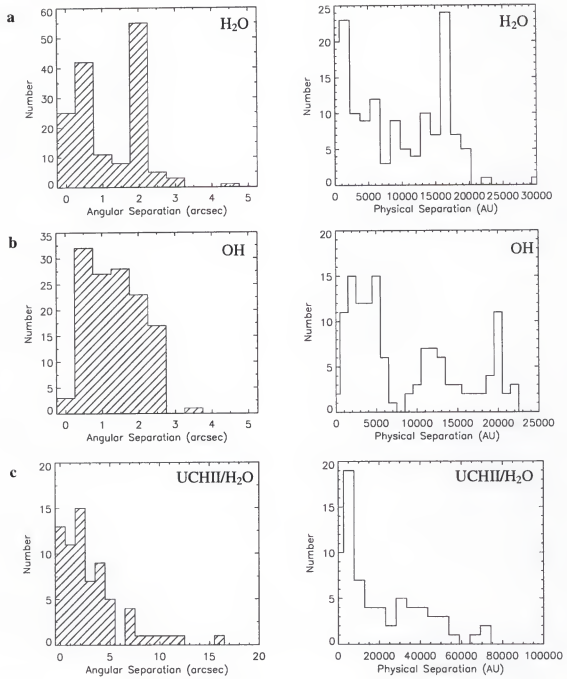

Figure 6-18: Separations between masers and mid-infrared and UCHII region source peaks. (a) Histograms showing the water maser number as it is related to distance from the nearest mid-infrared source. (b) These histograms show the OH maser number as it is related to distance from the nearest mid-infrared source. (c) Another set of histograms showing water maser numbers with respect to distance from UCHII regions (from Hofner and Churchwell 1996).

masers with UCHII region centers (Fig 6-18c). The statement made above about the water masers being concentrated closer to the mid-infrared centers than the UCHII region peaks can be seen graphically. Furthermore, there are a significant number of masers located >5 arcsec from the UCHII peaks, in contrast to the mid-infrared sources.

There are also some differences in the distributions seen in the histograms in Figures 6-18a and 6-18c. First there are two peaks in the water maser distributions as seen in the angular separation and physical separation histograms. In terms of physical separations, there seems to be a peak near 0 and one near 17,000 AU. This second peak is due to the enormous concentration of water maser offset from G00.55-0.85b. This source has 25 water masers strung in a line from 16,500-19,000 AU way from the source center. This physical separation corresponds to an angular separation of 1.8 to 2.0″, and is therefore responsible for the peak in angular separation histogram as well.

Inspection of the OH maser distributions reveals a three-peaked distribution in physical separation. This again is due to weighting of the distribution from individual sources with large amounts of OH masers concentrated at a certain distance from a source center.

The Relationship Between Mid-Infrared , IRAS and Radio Observations

The closest IRAS sources to the water maser sites are tabulated in Table 6-2, and were compiled from the IRAS Point Source Catalog (PSC). The actual separations between the IRAS source centers and the mid-infrared sources in this survey are between a few arcseconds and two arcminutes. Fields with IRAS sources more than 2 arcminutes away are considered to not have an IRAS counterpart. It is interesting to point out that two of the 4 sites with no mid-infrared sources also have no IRAS counterpart.

Table 6-2: Total integrated flux density observed in the OSCIR field of view and corresponding IRAS flux density measurements

Target Field	OSCIR N/IHW18 (Jy)	IRAS PSC Name	IRAS 12/25 μm (Jy)	IRAS 11/18 μm (Jy)
G00.38+0.04	0.6/<0.10	17432-2835	25.02/246.37	13.20/134.79
G00.55-0.85	5.2/38.0	17470-2853	42.38/5475.57	12.86/1240.85
G10.62-0.38	0.6/3.1	18075-1956	23.48/148.44	13.64/94.34
G12.68-0.18	0.3/0.8	NO IRAS	--	--
G16.59-0.05	0.3/ 5.7	18182-1433	2.49/35.35	1.21/17.08
G19.61-0.23	20.1/103.4	18248-1158	47.84/406.90	26.05/233.95
G28.86+0.07	2.1/7.4	18411-0338	8.59/105.18	4.32/53.44
G32.74-0.07	<0.08/<0.10	18487-0015	3.47/7.87	2.53/7.04
G33.13-0.09	<0.02/--	18496+0004	3.25/24.11	1.82/14.52
G34.26+0.15	5.3/--	18507+0110	140.18/1106.12	77.57/652.31
G35.03+0.35	<0.02/--	NO IRAS	--	--
G35.20-0.74	2.8/--	18556+0136	4.26/217.26	1.58/67.77
G35.20-1.74	2.3/--	18592+0108	114.48/1022.63	61.67/578.28
G35.58-0.03	1.6/--	18538+0216	6.01/77.07	2.99/38.55
G40.62-0.14	0.9/--	19035+0641	2.27/66.71	0.95/25.14
G43.80-0.13	1.5/--	10095+0930	5.30/129.12	2.30/51.88
G45.07+0.13	25.6/--	19110+1045	57.62/494.34	31.31/283.39
G45.47+0.13	<0.02/--	NO IRAS	--	--
G45.47+0.05	0.3/--	19120+1103	78.78/640.53	43.31/373.93
G48.61+0.02	0.4/--	19181+1349	24.93/175.30	14.15/107.49
G49.49-0.39	1.8/--	19213+1424	424.24/4344.36	221.85/2345.47

Note. – For column 5, the color-corrected IRAS flux densities at 12 and 25 μm were fit with a blackbody curve from which an extrapolated value was found at 11 μm and an interpolated value was found at 18 μm.

Table 6-2 has a column that lists the extrapolated value for the IRAS flux at 11 microns, and an interpolated value of the IRAS flux at 18 microns. Therefore, in the same manner as for the methanol maser selected survey, one can compare the IRAS and OSCIR fluxes. Inspection of Table 6-2 shows that, in most cases, the IRAS fluxes are much larger than the fluxes seen in the entire 29″×29″ field of view. Once it can be concluded that the IRAS measurements do not accurately approximate the true mid-infrared fluxes for the sources directly coincident with the maser emission. Therefore spectral energy distributions, like those compiled by Testi et al. (1994) using their observed near-infrared fluxes and the IRAS 12, 25, 60 and 100 μm fluxes, inaccurately

Table 6-3: Radio continuum flux and derived spectral types

Name	$\nu_{radio}(\lambda_{radio})$ (GHz, cm)	Radio Reference	Source	Radio F_ν (mJy)	Radio Spectral Type	Mid-Infrared Spectral Type
G00.38+0.04	8.5 (3.5)	FC2000	--	<0.2	<B2.6	--
G00.55-0.85	8.5 (3.5)	FC2000	a	167.4	B0.2	B1.8
			b	NFG	--	--
			c	35.6	B0.7	B2.1
			d	<0.2	<B2.7	B2.8
G10.62-0.38	5.0 (6.0)	WC1989	a	<1.0	<B2.2	B6.6
			b	<1.0	<B2.2	B9.0
			c	<1.0	<B2.2	B8.3/B9.5
			d	<1.0	<B2.2	--
			e	<1.0	<B2.2	B9.2/A0
G12.68-0.18	8.5 (3.5)	FC2000	a	<0.2	<B3.1	B9.2
			b	<0.2	<B3.1	--
G16.59-0.05	8.5 (3.5)	FC2000	a	0.3	B3.3	--
			b	<0.2	<B3.1	--
G19.61-0.23	5.0 (6.0)	G1998	a	890	B0.1	B3.5
			b	1370	O9.9	B2.4
			c	530	B0.2	B5.4
			d	2650	O9.7	B5.2
			e	CNS	--	B0.9/B2.2
			f	CNS	--	--
	1.7 (18.0)	G1998	g	<0.31	<B2.6	--
			h	CNS	--	--
G28.86+0.07	23.0 (1.3)	C1997	a	<0.34	<B3.0	B2.9
			b	<0.34	<B3.0	B6.0/B7.5
			c	<0.34	<B3.0	B7.5/B8.7
G34.26+0.15	5.0 (6.0)	WC1989	a	1526.6	O9.9	--
			b	33.5	B1.0	--
G35.03+0.35	8.5 (3.5)	KCW1994	--	14.0	B1.9	--
G35.20-0.74	15.0 (2.0)	HL1988	--	0.8	B3.7	--
G35.20-1.74	5.0 (6.0)	WC1989	--	<1.8	<B2.5	--
G35.58-0.03	8.5 (3.5)	KCW1994	--	197.0	B0.8	--
G40.62-0.14	5.0 (6.0)	HM1993	--	3.8	B2.4	--
G43.80-0.13	8.5 (3.5)	KCW1994	a	62.6	B1.3	--
			b	<0.6	<B3.2	--
G45.07+0.13	5.0 (6.0)	WC1989	a	141.9	B0.1	--
			b	<0.1	<B1.8	--
			c	<0.1	<B1.8	--
G45.47+0.05	5.0 (6.0)	WC1989	--	<1.0	<B1.8	--
G48.61+0.02	8.5 (3.5)	KCW1994	a	4.2	B1.3	--
			b	<0.6	<B2.1	--
			c	<0.6	<B2.1	--
G49.49-0.39	5.0 (6.0)	ZH1997	a	<12.0	B1.0	--
			b	CNS	--	B2.1

Note. – References are: FC2000-Forster and Caswell (2000); WC1989-Wood and Churchwell (1989a); G1998-Garay et al. (1998); C1997-Codella et al. (1997); KCW1994-Kurtz, Churchwell, and Wood (1994); HL1988-Heaton and Little (1988); HM1993-Hughes and Mac Low (1993); and ZH1997-Zhang and Ho (1997). 'NFG' means the source was observed, but no radio flux was given by the authors. 'CNS' means that there was extended continuum, but no well-defined source.

describe the maser source. In the section of this chapter concerning individual sources, it was discussed that authors like Walsh et al. (1997) derived luminosities and spectral types for these sites, under the assumption that all of the IRAS far-infrared radiation comes from the maser source. These results should be considered upper limits, at best.

Table 6-3 lists the derived mid-infrared spectral types, and the radio spectral types derived from the radio flux as discussed in Chapter 4. In all cases the mid-infrared spectral type is later than the radio spectral type. It can be concluded that the mid-infrared spectral types derived for the sites where no radio emission are found, are good estimates of the latest spectral type the stellar source could be. From Table 6-3 it can be seen that all of the sources in these fields are O and B types, confirming that the water and OH masers, are indeed present where massive stars form.

CHAPTER 7
CONCLUSIONS

Conclusions from the Methanol Selected Survey

Twenty-one sites of known methanol maser emission were imaged at 10 and 18 μm. Ten of the sites contained methanol masers distributed in a linear fashion. Of those 10 sites, there were 8 detections, 3 of which have sources that are resolved and elongated in their thermal emission at the same position angle as the maser distribution. This data seems to lend credibility to the hypothesis of Norris et al. (1993) that linearly distributed methanol masers exist in, and delineate circumstellar disks. However, linear methanol masers (and methanol masers in general) do not appear to be exclusively associated with circumstellar disks, but instead trace a variety of stellar processes. Evidence was found that supports the idea that methanol masers are also associated with outflows and shocks as well.

The lower limits on the bolometric luminosity as derived from the mid-infrared flux densities imply that the stellar sources associated with methanol maser emission which do not have detectable UCHII regions are of smaller, less-ionizing masses. The sources with earlier spectral types (as derived from the mid-infrared fluxes) between B1 and B6 contain detectable UCHII regions. The sources with spectral types between B7 and A4 do not have evidence of radio continuum. It has been argued by Walsh et al. (1998) and others, that the stellar sources without UCHII regions are at an earlier stage of evolution and are too deeply embedded and have not had time to ionize their

surroundings. However, many of these sources are seen in the near-infrared as well as mid-infrared, and therefore cannot be too heavily embedded as to inhibit radio continuum emission. It was concluded that the stellar sources associated with methanol maser emission that do not have any detectable radio continuum are stars of lower mass than those that do have detectable radio continuum.

There seems to be a rough correlation between maser distribution extent and the extent of the mid-infrared sources. It was also found that the methanol masers that are coincident with mid-infrared sources are distributed in smaller areas than the mid-infrared emitting regions around these massive stars. If masers and mid-infrared emission peaks are assumed to be coincident, there is agreement with modeling by Sobolev and Deguchi (1994) and Sobolev, Cragg, and Deguchi (1997) showing that the pumping is achieved via mid-infrared photons from >150 K dust.

It was found that many of the sites of methanol maser emission have several mid-infrared sources in the 23″ x 23″ field. Since this is much smaller than the IRAS imaging beam and LRS field of view, the flux density values and spectral features observed for these sites can not be used to accurately describe or model the individual sources associated with the methanol masers.

Conclusions from the Water Selected Survey

Twenty-one sites of water maser emission were imaged at 10 μm, seven of which were also imaged at 18 μm. Because the water-maser selected sample was incomplete, there are not as many results as for the methanol maser selected survey. All results are arguments based on morphology of the mid-infrared sources and the distributions of water and OH masers.

Five sources were found that are most likely embedded massive stars coincident with water masers, and 3 sources were found where the water masers are most likely participating in outflows. These results lend credibility to the hypotheses that water masers may be excited in these two situations.

The astrometry of the IRTF was accurate enough to allow an analysis of the distribution of water and OH masers with respect to the mid-infrared source peaks. In a survey by Hofner and Churchwell (1996) of water masers near UCHII region, they found that the median separation from UCHII region peaks to water maser centers is 2.9″ or 0.091 pc (19,000 AU). Testi et al. (1998) performed a near-infrared survey towards several sites of water maser emission and were able to identify a K-band source within 5″ of the water maser components in 73% of the cases. It was found in the mid-infrared survey that the median angular separation between the water masers and the mid-infrared source peak is 1.22″, and the median physical separation is 0.042 pc (8690 AU). A similar result was found for the coincidence of OH masers with the mid-infrared sources (1.33″, 8590 AU). It was concluded that mid-infrared sources are more intimately associated with water and OH masers than near-infrared or radio continuum emission.

Like the methanol maser selected survey, many of the sites of water maser emission have IRAS fluxes that are, in some cases, magnitudes higher than that seen in the 29″ × 29″ field of view of the mid-infrared observations. These two surveys are the first-ever surveys of massive stars in the mid-infrared and at wavelengths comparable to the IRAS 12 and 20 μm passbands. Though suspected by many authors, these results show definitively for the first time that the IRAS fluxes are not a good indicator of the fluxes from the individual stellar sources associated with maser emission.

General Conclusions

As stated in Chapter 3, the general goal of this work was to determine the relationship between masers and massive stars, and in the process see what can be learned about massive star formation. Also specific questions were posed that now can be answered here.

The surveys presented in this work has confirmed that maser emission in general can trace a variety of phenomena associated with massive stars including shocks, outflows, infall and circumstellar disks. No one maser species is linked exclusively to one particular process or phenomenon. This implies that the conditions for maser excitation are not very stringent, given that each of the phenomena just mentioned would be associated with different densities, temperatures, and molecular abundances.

It was found that young massive stars can indeed have circumstellar disks, though whether or not circumstellar disks are a ubiquitous property of massive star formation remains to be seen. This limited data set implies that they are quite common, and that they indeed can be associated with methanol masers. There is also evidence from the linearly distributed water maser sources that massive stars exhibit outflow. The presence of disks and outflow implies that these massive stars formed via accretion like their low-mass stellar counterparts, or by a combination of mergers and accretion, but not by mergers alone.

Masers do not seem to be associated with different evolutionary stages of massive stars, but instead trace a variety of stellar phenomena throughout many early stages of massive stellar evolution. This conclusion is based on the fact that the maser sources

exhibit the presence or absence of emission at near-infrared, mid-infrared, submillimeter, and radio wavelengths in a variety of combinations and degrees.

Two-thirds of the fields where mid-infrared sources were detected exhibit multiple mid-infrared sources. Of the remaining third, several have nearby sources seen at other wavelengths (i.e. radio sources). It can be concluded that massive stars are in general gregarious by nature and form in a clustered way.

Interestingly, almost all the sources in the survey are stars of spectral type A or B, as derived from radio or mid-infrared measurements. Only three sources have radio derived spectral types in the O spectral class (two are O9.9, and one O9.7). Of these three sources, two (G19.61-0.23b and d) are most likely several ionizing sources given their clumpy and extended morphologies. This may mean that the conditions around the most massive O type stars are not viable for the existence of maser emission. However it could also be that massive O stars are rare, and are therefore undersampled in these surveys.

Suggestions for Future Work

One of the exciting aspects of this project and its results is that there are so many questions to answer about massive star formation and its relationship to maser activity. Furthermore, this area of astronomy is a relatively untapped resource for observations and discovery. Certainly an important future goal is to complete and expand the water maser selected mid-infrared survey. However, the results presented in this work can be augmented by many different types of observations.

The methanol maser selected survey can be expanded using newly available methanol maser/circumstellar disk candidates from Walsh et al. (1998). There are at least

30 new sites of linear distributed methanol masers in that study. The imaging of these new sites can be performed at mid-infrared wavelengths. There will be a great opportunity to discover more circumstellar disks since OSCIR will be available on the Gemini North 8 m telescope starting this fall. High-resolution mid-infrared dual-wavelength imaging from large telescopes (i.e. Gemini, Keck) would allow mapping of the temperature distributions throughout the disks, and permit evaluation of their composition.

Sub-millimeter continuum mapping would be a great asset to both surveys, allowing the detection of cold and severely embedded Class 0 sources. Of course, obtaining millimeter maps of the CO (2-1) transtition in these regions would yield crucial information for both surveys. Since CO traces outflow, the water maser survey would benefit if observations were to confirm that outflow exists at a similar position angle as the often-seen strings of water masers. CO outflow mapping would also be perfect corroborative evidence for the linearly distributed methanol maser sources. If one were to observe outflow perpendicular to the methanol maser distributions, especially for those mid-infrared sources believed to be circumstellar disks, it would be irrefutable evidence that these methanol masers delineate circumstellar disks.

Evidence for these outflows can also be gained from near-IR H_2 imaging, which is a shock indicator. Observations of several outflow sources by Davis and Eisloffel (1995) showed small-scale structure, such as cometary shaped knots of H_2 emission, extending over an average of 100,000 AU. Near-infrared cameras like NSFCAM on IRTF would have perfect fields of view to encompass the largest of outflows previously observed in H_2 at the kiloparsec distances of the targets in these surveys.

In the future, I plan on applying for HST time when NICMOS becomes available after the third servicing mission in March of 2001. Most likely, I will apply for "snapshot" time to observe a few of the more interesting mid-infrared disks in the near-IR to see if structure may be resolved (as in the case of HR4796). Around the 2003 time frame, two new observatories will be at our disposal, namely SOFIA and SIRTF. I plan on expanding the investigation to the far-infrared, which will help in characterizing the outflows and Class 0 sources in the surveys. For instance, spectra of the outflows obtained by the Airborne Infra-Red Echelle Spectrometer (AIRES) on SOFIA could be used to measure [FeII] 26 μm, [SiII] 35 μm, and [OI] 146 μm lines to determine the wind velocity, shock density, mass loss, and gas phase elemental abundances. Disk properties could also be determined using AIRES, because the spectral range of the instrument contains broad spectral features due to ices and minerals comprising circumstellar grains.

APPENDIX A
OSCIR

This section will begin with an overview of the instrument OSCIR. We will then follow the mid-infrared radiation from a source in space, through the earth's atmosphere, through the telescope and camera optics, to its final destination at the detector. Because mid-infrared radiation corresponds to the thermal radiation of terrestrial objects, special techniques are employed to extract the signal of the source in space from the overwhelming noise caused by the atmosphere, telescope, and optics.

Overview

The Observatory Spectrometer and Camera for the Infra-Red (OSCIR) is a mid-infrared camera and slit spectrometer. It was built and is operated by the University of Florida Infrared Astrophysics Group (IAG). The detector in OSCIR is a Rockwell/Boeing 128x128 pixel, arsenic doped silicon (Si:As), blocked impurity band (BIB) array.

The blocked impurity band technology was born from the Star Wars Defense program of the 1980s. It is an 'extrinsic' semiconductor, as opposed to a CCD which is an 'intrinsic' semiconductor. An intrinsic semiconductor is made from a pure semiconducting material that can interact with higher energy photons. The silicon in a CCD array interacts with an optical photon causing electrons in the semiconductor's valence band to be excited to the conduction band. The electrons in the conduction band are then free to conduct electricity, and this charge can be read out. However, silicon by itself does not effectively interact with photons of lower energy, such as mid-infrared

photons. Instead extrinsic semiconducting materials are created such as silicon or germanium that have atoms in their crystalline structure deliberately replaced with other atoms, a process referred to as 'doping'. These 'impurities', or 'dopants', are atoms that can be excited by longer wavelength photons, hence providing electrons for the conduction band. The problem with doped photoconductors is that their quantum efficiency is dependent upon the concentration of dopant. However, too much dopant causes 'tunneling' or 'hopping' across the valence band, and this can lead to large dark currents. The only other choice is to make the photoconducting material lightly doped but very thick, which leads to many operational problems. A way of overcoming this is to use a 'blocking band'. By placing a layer of pure silicon between the doped material and the read-out contact, electrons cannot hop across the material and out the contact, thus reducing the dark current. In this way, the infrared reactive material can be heavily doped to increase quantum efficiency, and the read out through the contact will only be from electrons that were excited into the conduction band by interaction with a mid-infrared photon. The arsenic doped silicon BIB array employed in OSCIR has a useful wavelength range from 5 to 25 μm.

Another fundamental difference between a BIB array and a CCD is the readout. CCDs employ a 'charge-shift' readout, whereas the BIB arrays have discrete readout amplifiers for each pixel. This allows the BIB detector to be read out at an extremely fast rate as compared to CCDs.

The Journey of a Mid-Infrared Photon

The first major obstacle for the mid-infrared light from a source to hurdle is getting through the earth's atmosphere. There are two useful 'windows' in the

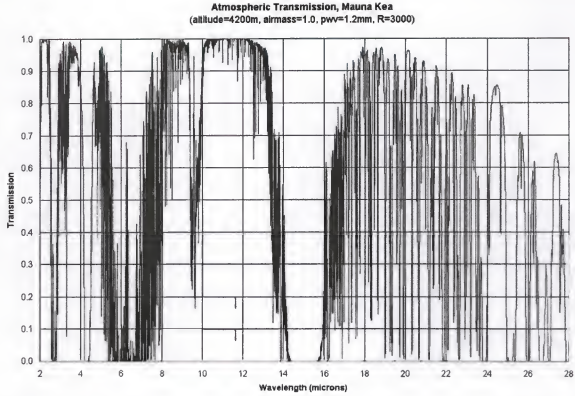

Figure A-1: Atmospheric transmission. The 7-14 micron window can be seen clearly. Longer wavelength filters take advantage of the 16-30 micron window, which has many absorption features.

atmosphere between the wavelengths of 5 to 25 μm. The first is a relatively high transmission window between 7 and 14 μm, which contains an absorption feature at 9.6 μm due to ozone. Between 14 and 16 μm, transmission drops to nil due to CO_2. However, after 16 μm is the second window, which continues until about 30 μm. This window is riddled with water vapor absorption features, but enough mid-infrared radiation can penetrate through the atmosphere at these wavelengths to be useful (Figure 1-A). After 40 μm, the atmosphere is opaque to radiation until wavelengths reach the submillimeter regime, where once again it is possible to conduct ground-based astronomy. Within these mid-infrared windows, there can be rapid variations in transmission due to atmospheric turbulence and water vapor.

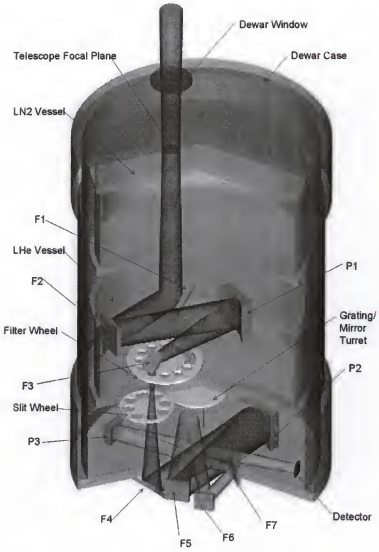

Figure A-2: A cut-away view of OSCIR. This shows the path of light (dark gray cylinder) as it passes through the system optics. Both flat ('F') mirrors and parabolic ('P') mirrors are labeled and numbered in order. The 'LN2 vessel' is the canister that holds the liquid nitrogen, and the 'LHe vessel' is lower canister that is filled with liquid helium, and is responsible for cooling the detector to temperatures near 4 K.

Once the radiation from the source penetrates the atmosphere, it is then collected by the telescope. However, the telescope optics do not just send the photons from the source to the camera. They also send many photons of their own due to the fact that they

are sources of thermal radiation as well. The same is true for the entrance window to the camera. These sources of 'background radiation' can be removed, as will be discussed in the next section.

Once the mid-infrared radiation from the astronomical source passes through the entrance window in to the camera system of OSCIR (Figure A-2), it undergoes very little attenuation before hitting the detector. This is because except for the filters and the camera entrance window, OSCIR is an entirely reflective system. All of the mirrors in the optical path of OSCIR are gold-coated, to take advantage of the low emissivity gold has in the mid-infrared. Furthermore, the entrance window is the only component in the camera that is not cryogenically cooled. By cooling the optical components in this way, they do not contribute any thermal background. The detector is also cooled to cryogenic temperatures to suppress the thermally generated dark current. Infrared cameras like OSCIR have optics that reimage the field onto the detector with a system of mirrors for two reasons. The first is to achieve the desired plate scale at the detector, and second is to create pupils within the cryostat. There are two reasons for wanting internal pupils. One reason is that the filters, which need to be placed at the pupil, can be cryogenically cooled. The second reason is that at the pupil can be placed a Lyot stop. This is done because a large background problem comes from stray light entering the camera system. In order to cut down this stray light, a circular aperture or 'stop' is placed near the pupil image of the secondary mirror where it can reject stray light from outside the beam. This stop is located internally where it can be cryogenically cooled (called a 'cold' stop) so as too not contribute any thermal emission of its own.

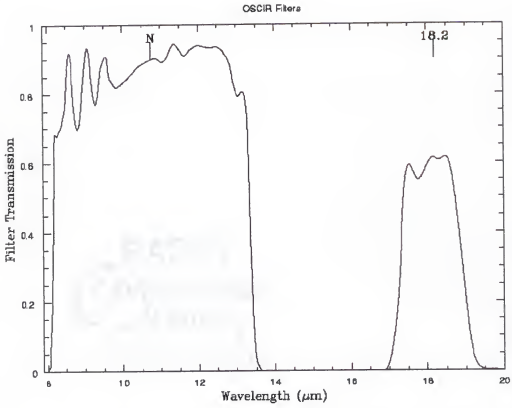

Figure A-3: OSCIR broad-band filters. The N filter takes advantage of the 10 micron atmospheric window.

The filters used in the survey are highly transmissive and have fairly broad wavelength coverage. As can be seen in Figure A-3, the N filter takes advantage of the whole 7-14 μm atmospheric window.

Once the source radiation has passed through the filters and optical path, it finally ends it journey at the detector. More will be said about the detector later.

Extracting the Source Signal

As was mentioned, the detector not only receives the mid-infrared radiation from the astronomical source, but also the highly variable radiation from the sky (i.e. sky

background), and the relatively static radiation from telescope optics and camera entrance window (i.e. radiative offset). In fact this background radiation dominates observations in the mid-infrared. For example, typical bright infrared standard stars used for flux calibration are frequently an order of magnitude fainter than the background emission. For scientifically interesting astronomical objects, which are typically much fainter than the standard stars, we may be receiving 1 source photon for every 100,000 background photons.

One consequence of such high background levels is that the detector fills its wells very quickly. For example, using OSCIR at the IRTF it was found that the background emission at N is typically ~4×10^{13} photons cm^{-2} s^{-1}. Given the high quantum efficiency of the detector, and a well depth of 22×10^{6} electrons, the wells of the detector fill to ~60% in 20 ms. Obviously, these short frame integration times requires fast electronics to handle these high data rates.

More importantly to the observer is that this extremely low ratio of source photon rate to background photon rate requires extremely precise background flux subtraction to extract the signal of interest.

The Standard Chop-Nod Technique

The requirement of precise background subtraction dictates the method by which images are acquired at a telescope. Background subtraction is effected in real time using the standard infrared astronomical "chop/nod" technique. In this technique, the telescope is pointed at an object of interest (the "program object") and a set of images is acquired by the camera. An image consists of signal from the program object superposed on the

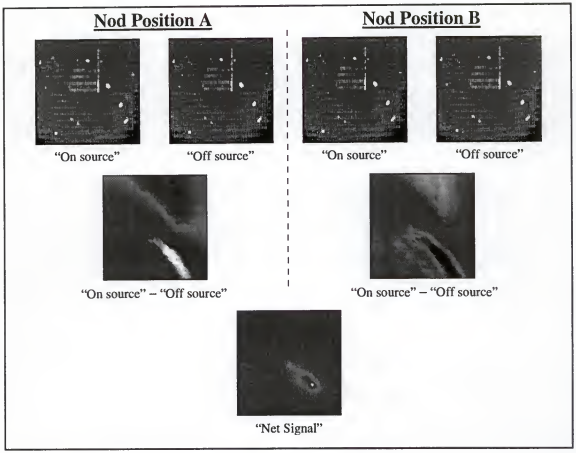

Figure A-4: A schematic of the chop/nod technique.

much larger signal from the background. The secondary mirror of the telescope is then moved slightly away from the nominal position so that the program object moves out of the field of view of the camera. Another set of images is acquired by the camera. This procedure, called a "chop" cycle, is repeated many times at typically a 5-10 Hz rate moving back and forth between "on-source" and "off-source" positions. A "chop-differenced" signal is formed by taking the difference between the on-source and off-source images.

While this rapid movement of the secondary mirror allows subtraction of a spatially uniform background that is varying in time at frequencies below the chop

frequency, it usually generates a spurious signal which may still be significantly larger than the source signal. This spurious signal, termed the "radiative offset," results from the fact that the emission pattern of the telescope, as seen by the camera, depends on the optical configuration of the telescope. Movement of the secondary mirror changes this configuration, resulting in two different emission patterns. The difference in these emission patterns shows up in the chop-differenced signal.

In order to remove the radiative offset, the entire telescope is moved after a short period of time (typically on the order of tens of seconds) so that the source now appears in what was previously the off-source position of the secondary mirror. This movement of the telescope is termed a "beam switch" or "nod". Chop-differenced frames are then formed with this new on-source and off-source configuration. A little thought shows that in this new configuration, the radiative offset will have changed sign and will cancel identically when the new chop-differenced data is added to the old chop-differenced data (provided the telescope emission has not changed in the time between beam switching).

Figure A-4 demonstrates the acquisition of data in the standard "chop/nod" mode. The images shown here were obtained with OSCIR at the IRTF. The top row of four images shows the raw data frames from the two secondary mirror positions at each of the two nod positions (called "Nod Position A" and "Nod Position B") of the telescope. These images are dominated by fixed-pattern offsets due to pixel-to-pixel variations and offsets between the 16 channels of the acquisition electronics. The background counts in these raw images correspond to 7.4×10^8 e^-/s. Each raw image consists of ~5 minutes of total integration time (i.e. 15,000 frames coadded using a 20 ms frame integration time and the N-band filter) obtained in the chop/nod sequence as described above. The second

row of two images shows the "chop-differenced" data derived from the subtraction of the on-source and off-source data in the two nod positions of the telescope. Note that the dominant pattern (principally a gradient along the diagonal connecting the lower-left to upper-right corners of the images) has changed sign between the two chop-differenced frames. However, since the subtraction is always done as "on-source minus off-source", the source signal remains positive in both chop-differenced frames. The signal levels in these differenced frames range $\pm 3.2 \times 10^6$ e^-/s, which is ~0.4% of the raw background signal. Finally, the bottom row shows the net signal obtained by adding together the two chop-differenced frames shown in the middle row (note that no other processing has been done to the data other than the additions and subtractions as described above). The detected source is the nuclear region of the starburst galaxy NGC 253. The net signal is the result of a total exposure of ~20 minutes in which half that time is actually spent imaging the off-source "reference" position. The signal level at the "tail" of this source near the middle of the frame is $\sim 6.4 \times 10^4$ e^-/s. This is about four orders of magnitude below the background level shown in the raw frame. In fact, the signal-to-noise ratio at this level in each pixel is about seven, so that the effective background subtraction is more nearly five orders of magnitude below the background.

The Detector

The detector used in OSCIR is relatively clean and flat. Figure A-5 shows an image of the detector under uniform illumination. There are approximately 10 dead pixels distributed across the array, and about the same amount of "hot" pixels that are alive, but with signifigantly different response than the others. Although there is a small amount of vignetting in the lower right corner of the array the response of the array is in general

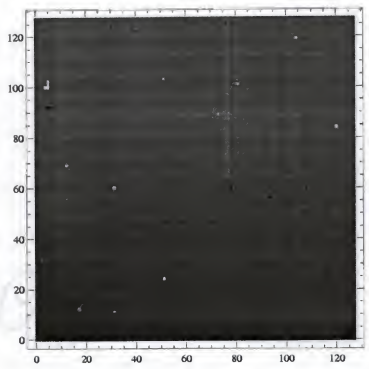

Figure A-5: Image of OSCIR detector under uniform N-band illumination. The ~10 dead pixels are the small black spots. The vignetting is in the lower right corner. The few white spots are "hot" pixels that are alive, but with signifigantly different response than the others. All of the structure here is 'fixed-pattern' and is removed in the chop/nod process.

very flat and the flat-field varies by ~ 5%. The structure seen on the array is "fixed" and is removed during the chop-nod process. Because the array is clean and flat, no flat-fielding was performed on the mid-infrared observations.

APPENDIX B
DERIVATIONS OF IMPORTANT RELATIONSHIPS

This section will show the derivations of some of the more non-obvious equations referenced with this work. They will be presented in the order that they appear in the text.

Color Correction Factor

The array employed with OSCIR is an energy counter (as opposed to a photon counter), meaning that the number of counts generated is a function of not only the number of incident photons, but their energies as well. Let the flux density from a source be given by F_ν. The number of counts, N, the detector will generate through a filter bandpass, ν_1 to ν_2, is given by

$$N = \int_{\nu_1}^{\nu_2} Q_{sys} \frac{F_\nu}{h\nu} d\nu \qquad \text{Equation A1}$$

where $h\nu$ is the photon energy at frequency ν, and Q_{sys} is the transmission through the system given by

$$Q_{sys} = T_{atm}(\nu) \cdot T_{filter}(\nu) \cdot QE(\nu)$$

However, we assume the QE to be relatively flat, so that term drops out. Flux density, F_ν, is given by the expression

$$F_\nu = \varepsilon \cdot \Omega \cdot B_\nu(T) \qquad \text{Equation A2}$$

where ε is the emissivity term which is simply

$$\varepsilon = \left(1 - e^{-\tau_\nu}\right)$$

with τ being the optical depth. Subbing Equation A2 into Equation A1 yields

$$N = \Omega \cdot \int Q_{sys} \frac{\varepsilon \cdot B_\nu(T)}{h\nu} d\nu \qquad \text{Equation A3}$$

Suppose we know a value F_{vo} at some frequency vo, with temperature T, then we can solve Equation A2 for Ω

$$\Omega = \frac{F_{vo}}{\varepsilon \cdot B_{vo}(T)}$$

Using this equation in Equation A3 yields

$$N = \frac{F_{vo}}{\varepsilon o \cdot B_{vo}(T)} \cdot \int Q_{sys} \frac{\varepsilon \cdot B_\nu(T)}{h\nu} d\nu \qquad \text{Equation A4}$$

This expression is now independent of source size Ω. Let C^p be the number of counts for a program object, and C^s be the number of counts for a calibration star, then

$$\frac{C^p}{C^s} = \frac{N^p}{N^s}$$

Therefore,

$$N^p = N^s \frac{C^p}{C^s} \qquad \text{Equation A5}$$

Substituting Equation A4 into A5 yields

$$\frac{F_{vo}{}^p}{\varepsilon o \cdot B_{vo}\left(T^p\right)} \left[\int Q_{sys} \frac{\varepsilon \cdot B_\nu\left(T^p\right)}{h\nu} d\nu\right] = \frac{C^p}{C^s} \frac{F_{vo}{}^s}{B_{vo}\left(T^s\right)} \left[\int Q_{sys} \frac{B_\nu\left(T^s\right)}{h\nu} d\nu\right]$$

Solving for $F_{vo}{}^p$ gives

$$F_{vo}{}^{p} = C^{p} \cdot \left(\frac{F_{vo}{}^{s}}{C^{s}} \right) \cdot \left[\frac{\int Q_{sys} \frac{B_{v}(T^{s})}{B_{vo}(T^{s})} \frac{1}{h\nu} d\nu}{\int Q_{sys} \frac{\varepsilon \cdot B_{v}(T^{p})}{\varepsilon o \cdot B_{vo}(T^{p})} \frac{1}{h\nu} d\nu} \right]$$

In this final expression, the first term is simply the measured counts from the source. The second is just the ratio of standard star flux (a known value) to the number of counts from the standard star. This is simply the calibration factor. The third term

$$\frac{\int \frac{B_{v}(T^{s})}{B_{vo}(T^{s})} \cdot T_{atm}(\nu) \cdot T_{filter}(\nu) \cdot \left(\frac{1}{h\nu} \right) d\nu}{\int \frac{\left(1 - e^{-\tau_{v}}\right) \cdot B_{v}(T^{p})}{\left(1 - e^{-\tau_{vo}}\right) \cdot B_{vo}(T^{p})} \cdot T_{atm}(\nu) \cdot T_{filter}(\nu) \cdot \left(\frac{1}{h\nu} \right) d\nu}$$

is the "color correction factor", which takes into account system transmission and the differences in spectral slope between the standard star and program object.

Resolution Limiting Size

The observed size (or FWHM), δ_o, of a source is equal to the real angular size of the source, δ, plus the PSF size (or beamwidth of the telescope), δ_{psf}, added in quadrature

$$\delta_o{}^{2} = \delta^{2} + \delta_{psf}{}^{2}$$

or

$$\delta^2=\delta_o{}^2-\delta_{psf}{}^2 \qquad \text{Equation A6}$$

If δ_o was greater than 2σ larger than the PSF size, it would have been resolved. So

$$\delta_o=\delta_{res}\leq\delta_{psf}+2\cdot\sigma_{psf}$$

Subbing this into Equation A6 one gets

$$\delta_{res}{}^2=\left(\delta_{psf}+2\cdot\sigma_{psf}\right)^2-\delta_{psf}{}^2$$

which after some algebra is

$$\delta_{res}=2\cdot\sigma_{psf}\cdot\left(1+\frac{\delta_{psf}}{\sigma_{psf}}\right)^{\frac{1}{2}}$$

This is the resolution limited size employed in this work.

Radio Flux Density as a Function of Lyman Continuum Photon Rate

The volume emissivity, j_ν, for thermal free-free emission is given by Spitzer (1978)

$$j_\nu=\left(3.24\times10^{-14}\right)\frac{g_{ff}\cdot Z_i{}^2\cdot n_e\cdot n_i}{T^{0.5}}\quad e^{\frac{h\cdot\nu}{kT}} \qquad \text{Equation A7}$$

where ν is the frequency in GHz, g_{ff} is the 'Gaunt factor', Z_i is the ion charge, n_e is the number density of electrons, n_i is the number density of protons, and T is temperature in units of 10^4 K. In the radio $h\nu << kT$, so this becomes

$$j_\nu=\left(3.24\times10^{-14}\right)\frac{g_{ff}\cdot n_e{}^2}{T^{0.5}}$$

under the assumption we are concerned with a charge neutral hydrogen plasma (i.e. $n_e=n_i$, $Z_i=1$). The Gaunt factor as given by from Mezger and Henderson (1967) is

$$g_{ff}=11.970\left(\frac{a}{0.9940}\right)\cdot T^{0.15}\cdot\nu^{-0.1} \qquad \text{Equation A8}$$

where a is a slowly varying parameter dependent on frequency and temperature that is close to unity. Putting Equation A8 into A7 yields

$$j_\nu=3.24\times10^{-14}\cdot\left(\frac{a}{0.9940}\right)\cdot\left(\frac{T}{10^4\cdot K}\right)^{-0.35}\cdot\left(\frac{\nu}{1\cdot GHz}\right)^{-0.1}\cdot n_e^{\,2} \qquad \text{Equation A9}$$

Luminosity is given by

$$L_\nu=4\cdot\pi\cdot\int_V j_\nu\,dV$$

and so the observed flux density is given by

$$S_\nu=\frac{L_\nu}{4\cdot\pi\cdot D^2}=\frac{1}{D^2}\cdot\int_V j_\nu\,dV$$

Substituting this into Equation A9 yields

$$S_\nu=3.24\times10^{-14}\cdot\left(\frac{a}{9940}\right)\cdot\left(\frac{T}{10^4\cdot K}\right)^{-0.35}\cdot\left(\frac{\nu}{1\cdot GHz}\right)^{-0.1}\cdot\left(\frac{1}{D^2}\cdot\int_V n_e^{\,2}\,dV\right) \qquad \text{Equation A10}$$

where S_ν is in mJy.

From recombination theory (Baker and Menzel 1938), it is known that the intensity of a spectral line, j_{nm}, caused by a transition from a level n to a level m is related to the recombination coefficient α_{nm} and the electron density by

$$4\cdot\pi\cdot j_{nm}=n_e^{\,2}\cdot\alpha_{nm}\cdot h\nu_{nm}$$

Therefore, solving for $n_e^{\,2}$

$$n_e^2 = \frac{4\cdot\pi\cdot j_{nm}}{h\nu_{nm}} \frac{1}{\alpha_{nm}}$$

Substituting this into Equation A10 yields

$$S_\nu = 3.24 \times 10^{-14} \cdot \left(\frac{a}{0.9940}\right) \cdot \left(\frac{T}{10^4 \cdot K}\right)^{-0.35} \cdot \left(\frac{\nu}{1 \cdot GHz}\right)^{-0.1} \cdot \left[\frac{1}{D^2 \cdot \alpha_{nm}} \cdot \int_V \frac{4\cdot\pi\cdot j_{nm}}{h\nu_{nm}} dV\right] \qquad \text{Equation A11}$$

Notice that this last term is just the total amount of energy per unit time divided by the energy per photon (for a given transition). In other words, this is simply the photon emission rate, N_{nm}

$$N_{nm} = \int_V \frac{4\cdot\pi\cdot j_{nm}}{h\nu_{nm}} dV \qquad \text{Equation A12}$$

When one considers the ionization balance between recombinations and ionizations by photons from a star, one does not include recombinations directly to the ground level. This is because ground-state recombinations are assumed to be balanced by immediate ionization. This is called Case B recombintaion as described by Baker and Menzel (1938). The recombination coefficient for this case in generally given by the symbol α_2.

Because the number of ionizations is believed to balance the number of recombinations, the recombination coefficient α_{nm} may be expressed in terms of the total recombination coefficient α_2, the photon emission rate N_{nm}, and the ionizing photon rate N_{lyc} as

$$\alpha_{nm} = \alpha_2 \frac{N_{nm}}{N_{lyc}} \qquad \text{Equation A13}$$

Combining Equations A11, A12, and A13 yields the relationship between radio flux, S_ν, and the Lyman continuum photon rate, N_{lyc}

$$S_\nu = 3.24 \cdot 10^{-14} \cdot \left[\left(\frac{a}{0.994} \right) \cdot \left(\frac{T_e}{10^4 \cdot K} \right)^{-0.35} \cdot \left(\frac{\nu}{GHz} \right) \cdot \left(\frac{N_{lyc}}{\alpha_2} \frac{1}{cm^{-3}} \right) \cdot \left(\frac{D}{cm} \right)^{-2} \right] \quad mJy$$

LIST OF REFERENCES

Andre, P., Ward-Thompson, D., and Barsony, M. 1993, ApJ, 406, 122

Anglada, G., Estalella, R., Pastor, J., Rodriguez, L. F., and Haschick, A. D. 1996, ApJ, 463, 205

Baart, E. E., and Cohen, R. J. 1985, MNRAS, 213, 641

Bachiller, R., Codella, C., Colomer, F., Liechti, S., and Walmsley, C.M. 1998, A&A, 335, 266

Ball, J. A., Gottlieb, C. A., Lilley, A. E., and Radford, H. E. 1970, ApJL, 162, L203

Barrett, A. H., Schwartz, P. R., and Waters, J. W. 1971, ApJL, 168, L101

Batrla, W., Matthews, H.E., Menten, K.M., and Walmsley, C.M. 1987, Nature, 326, 49

Beckwith, S.V.W., Sargent, A.I., Chini, R.S., and Gusten, R. 1990, AJ, 99, 924

Bedijn, P. J., and Tenorio-Tagle, G. 1981, A&A, 98, 85

Blaauw, A. 1991, in The Physics of Star Formation and Early Stellar Evolution, ed. C.J. Lada & N.D. Kylafis (Dordrecht:Kluwer), 125

Blitz, 1991, in The Physics of Star Formation and Early Stellar Evolution, ed. C.J. Lada & N.D. Kylafis (Dordrecht:Kluwer), 3

Bodenheimer, P., Tenorio-Tagle, G., and Yorke, H. W. 1979, ApJ, 233, 85

Bonnell, I.A. 1994, MNRAS, 269,837

Bonnell, I. A., Bate, M. R., and Zinnecker, H. 1998, MNRAS, 298, 93

Braz, M. A., and Epchtein, N. 1983, A&AS, 54, 167

Brebner, G. C., Cohen, R. J., Heaton, B., and Davies, S. R. 1987, MNRAS, 229, 679

Bronfman, L., Nyman, L., and May, J. 1996, A&AS, 115, 81

Campbell, M.F., Garland, C.A., Deutch, L.K., Hora, J.L., Fazio, G.G., Dayal, A., and Hoffman, W.F. 2000, submitted to ApJ

Carral, P., Kurtz, S.E., Rodriguez, L.F., De Pree, C., and Hofner, P. 1997, ApJ Letters, 486,103

Caswell, J.L. 1996a, MNRAS, 279, 79

Caswell, J.L. 1997, MNRAS, 289, 203

Caswell, J. L. 1998, MNRAS, 297, 215

Caswell, J.L., and Haynes, R.F. 1987, A&A, 171, 261

Caswell, J.L., Haynes, R.F., and Goss, W.M. 1980, Australian Journal of Physics, 33, 639

Caswell, J.L., and Vaile, R.A. 1995, MNRAS, 273, 328

Caswell, J.L., Vaile, R.A., Ellingsen, S.P., Whiteoak, J.B., and Norris, R.P. 1995a, MNRAS, 272, 96

Caswell, J. L., Vaile, R. A., Ellingsen, S. P., and Norris, R. P. 1995b, MNRAS, 274, 1126

Caswell, J.L., Vaile, R.A., and Forster, J.R. 1995, MNRAS, 277, 210

Cesaroni, R., Churchwell, E., Hofner, P., Walmsley, C.M., and Kurtz, S. 1994, A&A, 288, 903

Cesaroni, R., Felli, M., Jenness, T., Neri, R., Olmi, L., Robberto, M., Testi, L. and Walmsley, C.M. 1999, A&A, 345, 949

Cesaroni, R., Walmsley, C. M., and Churchwell, E. 1992, A&A, 256, 618

Chan, S.J., Henning, T., and Schreyer, K. 1996, A&A Suppl., 115, 285

Chandler, C.J. and Richer, J.S. 1999, in ASP Conf. Ser. 160: Astrophysical Discs - an EC Summer School, ed. J.A. Sellwood & J. Goodman (San Fransisco:ASP), 91

Cheung, A.C., Rank, D.M., Townes, C.H., Thorton, D.D., and Welsh, W.J. 1969, Nature, 221, 626

Churchwell, E. 1991, in The Physics of Star Formation and Early Stellar Evolution, ed. C.J. Lada & N.D. Kylafis (Dordrecht:Kluwer), 221

Churchwell, E., Walmsley, C. M., and Cesaroni, R. 1990, A&AS, 83, 119

Churchwell, E., Walmsley, C. M., and Wood, D. O. S. 1992, A&A, 253, 541

Codella, C., Testi, L., and Cesaroni, R. 1997, A&A, 325, 282

Cohen, M., Walker, R. G., Carter, B., Hammersley, P., Kidger, M., and Noguchi, K. 1999, AJ, 117, 1864

Dame, T. M., Ungerechts, H., Cohen, R. S., de Geus, E. J., Grenier, I. A., May, J., Murphy, D. C., Nyman, L.-A., Thaddeus, P. 1987, ApJ, 322, 706

de Jong, T. 1973, A&A, 26, 297

Dent, W. R. F., Little, L. T., Sato, S., Ohishi, M., and Yamashita, T. 1985, MNRAS, 217, 217

Dent, W. R. F., Sandell, G., Duncan, W. D., and Robson, E. I. 1989, MNRAS, 238, 1497

Downes, D., Wilson, T. L., Bieging, J., and Wink, J. 1980, A&AS, 40, 379

Doyon, R. 1990, Ph.D. thesis, Imperial College Univ. of London

Dyson, J. E., and Williams, D. A. 1980, The Physics of the Interstellar Medium (New York:Halsted Press)

Elitzur, M. 1992a, ARAA, 30, 75

Elitzur, M. 1992b, Astronomical Masers (London:Kluwer)

Elitzur, M., and de Jong, T. 1978, A&A, 67, 323

Elitzur, M., Hollenbach, D. J., and McKee, C. F. 1989, ApJ, 346, 983

Ellingsen, S.P., Norris, R.P., and McCulloch, P.M. 1996, MNRAS, 279, 101

Faison, M., Churchwell, E., Hofner, P., Hackwell, J., Lynch, D. K., and Russell, R. W. 1998, ApJ, 500, 280

Felli, M., Palagi, F., and Tofani, G. 1992, A&A, 255, 293

Fix, J.D., Mutel, R.L., Gaume, R.A., and Claussen, M.J. 1982, ApJ, 259, 657

Forster, J.R. 1990, A&A, 227, L37

Forster, J.R., and Caswell, J.L. 1989, A&A, 213, 339

Forster, J. R., and Caswell, J. L. 1999, A&AS, 137, 43

Forster, J. R., and Caswell, J. L. 2000, ApJ, 530, 371

Forster, J.R., Caswell, J.L., Okumura, S.K., Ishiguro, M., and Hasegawa, T. 1990, A&A, 231, 473

Frail, D.A., and Mitchell, G.F. 1998, ApJ, 508, 690

Fujiyoshi 1999, Ph.D. thesis, University of New South Wales

Garay, G., and Lizano, S. 1999, PASP, 111, 1049

Garay, G., Moran, J. M., Rodriguez, L. F., and Reid, M. J. 1998, ApJ, 492, 635

Garay, G., Reid, M. J., and Moran, J. M. 1985, ApJ, 289, 681

Garay, G., Rodriguez, L.F., Moran, J.M., and Churchwell, E. 1993, ApJ, 418, 368

Gaume, R. A., Fey, A. L., and Claussen, M. J. 1994, ApJ, 432, 648

Gaume, R. A., Johnston, K. J., and Wilson, T. L. 1993, ApJ, 417, 645

Gaume, R.A., and Mutel, R.L. 1987, ApJ Suppl. Series, 65, 193

Genzel, R., Downes, D., Schneps, M. H., Reid, M. J., Moran, J. M., Kogan, L. R., Kostenko, V. I., Matveenko, L. I., and Ronnang, B. 1981, ApJ, 247, 1039

Goebel, J.H. 1993, A&A, 278, 226

Gordon, J.P., Zeiger, H.J., and Townes, C.H., 1955, Phys. Rev., 99, 1264

Greene, T.P., Wilking, B.A., Andre, P., Young, E.T. and Lada, C.J. 1994, ApJ, 434, 614

Gwinn, C. R., Moran, J. M., and Reid, M. J. 1992, ApJ, 393, 149

Habing, H. J., and Israel, F. P. 1979, ARAA, 17, 345

Harvey, P.M., and Gatley, I. 1983, ApJ, 269, 613

Hartmann, L., 1998, Accretion Processes in Star Formation (Cambridge: Cambridge University Press)

Hatchell, J., Thompson, M. A., Millar, T. J., and MacDonald, G. H. 1998, A&AS, 133, 29

Hauschildt, H., Gusten, R., Phillips, T. G., Schilke, P., Serabyn, E., and Walker, C. K. 1993, A&A, 273, L23

Haynes, R.F., Caswell, J.L., and Simons, L.W.J. 1979, Australian J. Phys., Ap. Suppl., 48, 1

Heaton, B. D., and Little, L. T. 1988, A&A, 195, 193

Heaton, B. D., Little, L. T., and Bishop, I. S. 1989, A&A, 213, 148

Henning, T., Chan, S.J., and Assendorp, R. 1996, A&A, 312, 511

Ho, P. T. P., Das, A., and Genzel, R. 1983, ApJ, 266, 596

Hofner, P., and Churchwell, E. 1996, A&A Suppl., 120, 283

Hofner, P., Kurtz, S., Churchwell, E., Walmsley, C.M., and Cesaroni, R. 1994, ApJ Letters, 429, 85

Hofner, P., Peterson, S., and Cesaroni, R. 1999, ApJ, 514, 899

Holtz, J. Z. 1968, ApJL, 153, L117

Hrivnak, B.J., Kwok, S., Geballe, T.R., 1994, ApJ, 420, 783

Hughes, V.A., and MacLeod, G.C. 1993, AJ, 105, 1495

Hunter, T. R., Phillips, T. G., and Menten, K. M. 1997, ApJ, 478, 283

IRAS Science Team, A&A Suppl., 65, 607

Jensen, E. L. N., Donar, A. X., and Mathieu, R. D. 2000, IAU Symposia, 200, 85P

Kemball, A.J., Gaylard, M.L., and Nicolson, G.D. 1988, ApJ Letters, 331, 37

Keto, E., Proctor, D., Ball, R., Arens, J., and Jernigan, G. 1992, ApJL, 401, L113

Keto, E. R., Ho, P. T. P., and Haschick, A. D. 1987, ApJ, 318, 712

Keto, E. R., Ho, P. T. P., and Haschick, A. D. 1988, ApJ, 324, 920

Kraemer, K.E., Deutsch, L.K., Jackson, J.M., Hora, J.L., Fazio, G.G., Hoffmann, W.F., and Dayal, A. 1999, ApJ, 516, 817

Kruegel, E., and Walmsley, C. M. 1984, A&A, 130, 5

Kuchar, T. A., and Bania, T. M. 1990, ApJ, 352, 192

Kuchar, T. A., and Bania, T. M. 1994, ApJ, 436, 117

Kurtz, S., Churchwell, E., and Wood, D.O.S. 1994, ApJ Suppl. Series, 91, 659

Kurtz, S. E., Watson, A. M., Hofner, P., and Otte, B. 1999, ApJ, 514, 232

Kurucz, R.L. 1979, ApJ Suppl. Series, 40, 1

Lada, C.J. 1987, in Star Forming Regions, ed. M Peimbert & J. Jugaku (Dordrecht:Reidel), 1

Larionov, G. M., Val'tts, I. E., Winnberg, A., Johansson, L. E. B., Booth, R. S., and Golubev, V. V. 1999, A&AS, 139, 257

Larson, R. B. 1992, MNRAS, 256, 641

Leinert, C. 1986, A&A, 155, L6

Little, L. T., Brown, A. T., Riley, P. W., Matthews, N., MacDonald, G. H., Vizard, D. R., and Cohen, R. J. 1983, MNRAS, 203, 409

Little, L. T., Kelly, M. L., and Murphy, B. T. 1998, MNRAS, 294, 105

MacLeod, G.C., Gaylard, M.J., and Nicolson, G.D. 1992, MNRAS Short Communication, 254, 1P

MacLeod, G.C., Scalise, E., Saedt, S., Galt, J.A., and Gaylard, M.J. 1998, AJ, 116, 1897

Mac Low, M., Elitzur, M., Stone, J. M., and Konigl, A. 1994, ApJ, 427, 914

Martin, A. H. M. 1972, MNRAS, 157, 31

Masson, C. R., and Chernin, L. M. 1993, ApJ, 414, 230

Mathis, J.S. 1990, ARAA, 28, 37

Matthews, N., Little, L. T., MacDonald, G. H., and Nyman, L. 1984, A&A, 136, 282

Menten, K.M. 1991, ApJ Letters, 380, 75

Menten, K. M., Johnston, K. J., Wadiak, E. J., Walmsley, C. M., and Wilson, T. L. 1988, ApJL, 331, L41

Mezger, P.G., and Robinson, B.J., 1968, Nature, 220, 1107

Monin, J.-L., Menard, F., and Duchene, G. 1998, A&A, 339, 113

Neckel, T. 1978, A&A, 69, 51

Norris, R.P., Byleveld, S.E., Diamond, P.J., Ellingsen, S.P., Ferris, R.H., Gough, R.G., Kesteven, M.J., McCulloch, P.M., Phillips, C.J., Reynolds, J.E., Tzioumis, A.K., Takahashi, Y., Troup, E.R., and Wellington, K.J. 1998, ApJ, 508, 275

Norris, R.P., Caswell, J.L., Gardner, F.F., and Wellington, K.J. 1987, ApJ Letters, 321, 159

Norris, R.P., Caswell, J.L., Wellington, K.J., McCutcheon, W.H., and Reynolds, J.E. 1988, Nature, 335, 149

Norris, R.P., Whiteoak, J.B., Caswell, J.L., Wieringa, M.H., and Gough, R.G. 1993, ApJ, 412, 222

Olmi, L., and Cesaroni, R. 1999, A&A, 352, 266

Omont, A., Moseley, S.H., Cox, P., Glaccum, W., Casey, S., Forveille, T., Chan, K.W., Szczerba, R., Loewenstein, R.F., Harvey, P.M., and Kwok, S. 1995, ApJ, 454, 819

Osterloh, M. and Beckwith, S.V.W. 1995, ApJ, 439, 288

Osterloh, M., Henning, TH., and Launhardt, R. 1997, ApJ Suppl. Series, 110, 71

Panagia, N. 1973, AJ, 78, 929

Persi, P., Felli, M., Lagage, P. O., Roth, M., and Testi, L. 1997, A&A, 327, 299

Phillips, C.J., Norris, R.P., Ellingsen, S.P., and McCulloch, P.M. 1998, MNRAS, 300, 1131

Plume, R., Jaffe, D. T., and Evans, N. J. 1992, ApJS, 78, 505

Reid, M. J., and Ho, P. T. P. 1985, ApJL, 288, L17

Rodriguez, L. F. 1994, Revista Mexicana de Astronomia y Astrofisica, 29, 69

Rodriguez, L.F., Canto, J., and Moran, J.M. 1982, ApJ, 255, 103

Scott, P. F. 1978, MNRAS, 183, 435

Shu, F. H. 1977, ApJ, 214, 488

Shu, F. H., Adams, F. C., and Lizano, S. 1987, ARAA, 25, 23

Slysh, V. I., Val'tts, I. E., Migenes, V., Fomalont, E., Hirabayashi, H., Inoue, M., and Umemoto, T. 1999, ApJ, 526, 236

Sobolev, A.M., Cragg, D.M., and Godfrey, P.D. 1997, A&A, 324, 211

Sobolev, A.M., and Deguchi, S. 1994, A&A, 291, 569

Solomon, P. M., Rivolo, A. R., Barrett, J., and Yahil, A. 1987, ApJ, 319, 730

Spitzer, L. 1978, Physical Processes in the Interstellar Medium (New York: Wiley Interscience)

Stahler, S. W., Palla, F., and Ho, P. T. P. 2000, in Protostars and Planets IV, eds. Mannings, V., Boss, A.P., Russell, S. S. (Tucson: University of Arizona Press), 327

Stecklum, B., and Kaufl, H. 1998, First Circumstellar Disk around a Massive Star (ESO press release PR-08-98)

Stromgren, B. 1939, ApJ, 89, 526

Tenorio-Tagle, G. 1979, A&A, 71, 59

Tenorio-Tagle, G. T., Yorke, H. W., and Bodenheimer, P. 1979, A&A, 80, 110

Testi, L., Felli, M., Persi, P., and Roth, M. 1994, A&A, 288, 634

Testi, L., Felli, M., Persi, P., and Roth, M. 1998, A&AS, 129, 495

Tofani, G., Felli, M., Taylor, G.B., and Hunter, T.R. 1995, A&A Suppl., 112, 299

Torrelles, J. M., Gomez, J. F., Rodriguez, L. F., Curiel, S., Ho, P. T. P., and Garay, G. 1996, ApJL, 457, L107

Turner, J. L., and Welch, W. J. 1984, ApJL, 287, L81

Vallee, J. P., and MacLeod, J. M. 1990, ApJ, 358, 183

Van Buren, D., Mac Low, M., Wood, D. O. S., and Churchwell, E. 1990, ApJ, 353, 570

van der Walt, D.J., Gaylard, M.J., and MacLeod, G.C. 1995, A&A Suppl., 110, 81

Volk, K., Kwok, S., Stencel, R.E., and Brugel, E. 1991, ApJ Suppl. Series, 77, 607

Walsh, A.J., Burton. M.G., Hyland, A.R., and Robinson, G. 1998, MNRAS, 301, 640

Walsh, A.J., Burton. M.G., Hyland, A.R., and Robinson, G. 1999, MNRAS, 309, 905

Walsh, A.J., Hyland, A.R., Robinson, G., and Burton, M.G. 1997, MNRAS, 291, 261

Walther, D. M., Aspin, C., and McLean, I. S. 1990, ApJ, 356, 544

Watt, S., and Mundy, L. G. 1999, ApJS, 125, 143

Weaver, H., Williams, D.R.W., Deiter, N.H.and Lum, W.T. 1965, Nature, 208, 29

Weinreb, S., Barrett, A.H., Meeks, M.L., and Henry, J.C.1963, Nature, 200, 829

Whittet, D. C. B. 1988, in Dust in the Universe, eds. Bailey, M.E., and Williams, D.A. (Cambridge: Cambridge University Press), 25

Wink, J.E., Altenhoff, W.J., and Mezger, P.G. 1982, A&A, 108, 227

Wood, D. O. S., and Churchwell, E. 1989a, ApJS, 69, 831

Wood, D. O. S., and Churchwell, E. 1989b, ApJ, 340, 265

Wouterloot, J. G. A., and Brand, J. 1989, A&AS, 80, 149

Wynn-Williams, C. G., Becklin, E. E., and Neugebauer, G. 1972, MNRAS, 160, 1

Wyrowski, F., Schilke, P., and Walmsley, C. M. 1999, A&A, 341, 882

Yorke, H. W. 1993, in Massive Stars: Their Lives in the Interstellar Medium, eds. Cassinelli, J.P., and Churchwell, E.B. (ASP Conf. Ser. 35), 45

Yorke, H. W., Tenorio-Tagle, G., and Bodenheimer, P. 1983, A&A, 127, 313

Zeilik, M., and Lada, C. J. 1978, ApJ, 222, 896

Zhang, Q., and Ho, P. T. P. 1997, ApJ, 488, 241

Zhang, Q., Ho, P. T. P., and Ohashi, N. 1998, ApJ, 494, 636

Zhang, Q., Hunter, T.R. and Sridharan, T.K.1998, ApJL, 505, L151

Zinchenko, I., Mattila, K., and Toriseva, M. 1995, A&A Suppl., 111, 95

BIOGRAPHICAL SKETCH

I am 263 years old, and not really from Florida at all, but from a small mining planet in the vicinity of Polaris. As a baby, I was sold on the Intergalactic Black Market, where I was bought by, and lived among, a race of giant space octopi who used me as a garden decoration. I married a very attractive foot stool, and together we stowed away onboard a garbage scow headed for a harmless planet inhabited by super intelligent erasable pens, when we crash-landed on the Earth. Once here, I made the best of it. I got a low paying job as lint collector at the local laundry mat. Unfortunately, that winter was an extremely hash one, and I had to chop up my wife for firewood in order to survive. Once my feet were on stable ground, I began attending University of Florida and received my Bachelor of Science in astronomy in 1995, and my Master of Science in 1997. Amongst my hobbies are jazz, spending time with my wife-to-be, pretending I'm a lemon and growing extra limbs for fun and profit.

I certify that I have read this study and that in my opinion it conforms to acceptable standards of scholarly presentation and is fully adequate, in scope and quality, as a dissertation for the degree of Doctor of Philosophy.

Robert Piña, Chairman
Assistant Professor of Astronomy

I certify that I have read this study and that in my opinion it conforms to acceptable standards of scholarly presentation and is fully adequate, in scope and quality, as a dissertation for the degree of Doctor of Philosophy.

Charles Telesco
Professor of Astronomy

I certify that I have read this study and that in my opinion it conforms to acceptable standards of scholarly presentation and is fully adequate, in scope and quality, as a dissertation for the degree of Doctor of Philosophy.

Elizabeth Lada
Associate Professor of Astronomy

I certify that I have read this study and that in my opinion it conforms to acceptable standards of scholarly presentation and is fully adequate, in scope and quality, as a dissertation for the degree of Doctor of Philosophy.

James Hunter
Professor of Astronomy

I certify that I have read this study and that in my opinion it conforms to acceptable standards of scholarly presentation and is fully adequate, in scope and quality, as a dissertation for the degree of Doctor of Philosophy.

David Tanner
Professor of Physics

This dissertation was submitted to the Graduate Faculty of the Department of Astronomy in the College of Liberal Arts and Sciences and to the Graduate School and was accepted as partial fulfillment of the requirements for the degree of Doctor of Philosophy.

August 2000

_____

Dean, Graduate School